Ratchet dynamics in nonlinear Klein-Gordon systems

Von der Universität Bayreuth

zur Erlangung des Grades eines

Doktors der Naturwissenschaften (Dr. rer. nat.)

genehmigte Abhandlung

vorgelegt von

Luis Yansi Morales Molina

geboren in Camagüey, Kuba

1. Gutachter: Prof. Dr. F. G. Mertens

2. Gutachter: Prof. Dr. W. Pesch

Tag der Einreichung: 12.01.2005

Tag des Kolloquiums: 18.02.2005

Contents

Chapter 1

Introduction

Nowadays the study of new transport phenomena is one of the most exciting and growing areas of research. Some examples can be found in the study of biological systems where finding physical explanations for most of these phenomena has represented a challenge. Until now, the optimal mechanisms of transport are still being sought. Nevertheless, several attempts have appeared during the last years with different trends.

One emergent branch is related to a new way of producing transport, the so-called ratchet systems [1, 2]. A ratchet system is a system that is able to transport particles with nonzero macroscopic velocity although *on average* no macroscopic force is acting (see also another definition of ratchet systems in chapter 2). Precisely, the role of certain proteins with unidirectional transport in muscular contraction, cellular division, cellular traffic, and material transport along the axons of nerve cells [3, 4] has encouraged the study of systems where motion rectification processes take place as in ratchet systems

.

Consequently, during the last decade a lot of research has been devoted to the understanding of the motion of single particles, or an ensemble of particles in ratchet systems. More recently, the research has also been extended to the analysis of the propagation of nonlinear coherent localized structures in spatially extended systems. In particular, the main interest has been focused on studying certain nonlinear waves, *the solitary waves*, which conserve their identity while they propagate. Among the solitary waves, special attention has been given to the *soliton*, which has the additional property that its shape and velocity are preserved asymptotically upon collisions with other solitary waves [5, 6]. Moreover, the interest has been specifically concentrated on systems which exhibit propagation of topological solitons, i.e kinks and antikinks whose amplitudes are not affected by the dissipation. As a consequence their topological charges are conserved. This conservation, among other reasons, makes topological solitons the best candidates for the mentioned applications.

In general the investigation of these ratchet systems has been object of a continuous growing because of its potential in applied areas like nano- and micro-scale technologies [7, 8]. The main reason is the generation of directed transport from deterministic forces or random forces with zero time average. A typical example is found in extended systems for long Josephson junctions (LJJ) where instead of a direct current input a microwave generator is used as an alternating current to drive the motion of fluxons in one direction.

The main goal of the present work is to study some of the mechanisms which make the solitons move similar to a single particle in a ratchet system. Different ways of generating unidirectional transport will be the main focus

of this thesis.

In order to understand the main aspects of ratchet systems a general overview is presented in chapter 2. There an introduction is followed by a classification according to the ratchet mechanism with extension to different systems. Some of their applications are also given.

Usually, one starts from basic principles for constructing a ratchet system. Therefore the ratchet models for point particles are the best scenarios starting from which one can develop new ideas.

However, one should be careful when designing a ratchet with the same features as that for point particles. Intuitively, one tends to use models with similar structure to those for point particles. This assumption seems natural since in some approximations the dynamics of these localized structures presents a point-like particle behavior. Nevertheless, this assumption does not always lead to a correct conclusion. It is valid if one considers the same form of the ratchet potential from point particles for the substrate potential of extended systems.

There are other ways of producing directed transport in these system. First, one has to keep in mind that we are dealing with nonlinear complex systems, where the nature of motion differs from single point-particles, the dynamics being much more complicated since the nonlinearity of these systems plays the major role. The presence of many degrees of freedom that can be in principle infinite and their strong interactions are some of the essential characteristics in nonlinear extended systems. In addition the loss of symmetries and its interplay with the nonlinearity may give rise to systems with novel transport properties.

On the other hand, the assumption of regarding the solitons as point particles is only valid for some exceptional cases such as when one has an unperturbed system; or very small perturbations. In the latter case it is commonly assumed that only the center of mass motion is affected. This assumption is valid in an adiabatic approximation. Concerning this issue a lot of research has been devoted in the last years to demonstrate that this assumption fails for moderate and large perturbations.

Although such perturbations or external forces do not destroy the form of the soliton, they change its shape as a consequence. The perturbations are usually introduced by adding a driving force or impurities in the case of homogeneous systems. The most common response to such perturbations is the emission of linear waves (phonons). These phonons represent a simple case of deformation with respect to the unperturbed solitonic solution, when the system is driven by a force or when the soliton interacts with inhomogeneities. Although the phonons are damped when dissipation is taken into account, there are other features which can not be neglected which survive under perturbation even for high damping. A fundamental feature is the change of the width of the soliton when the soliton is driven by external forces or when it propagates along the chain with inhomogeneities. In such cases the width of these localized excitations becomes very important, and its consideration, as we shall show in this work, is not only crucial for describing properly the dynamics of solitons but also decisive for the occurrence of unidirectional motion. The importance of the kink width for the dynamics results from the strong interaction with the translational degree of freedom. Indeed, such an interaction has been object of research in a wide context,

and as we will show in this thesis, it leads to new ways of ratchet dynamics not observed before for single particle ratchet systems.

In order to have a deeper understanding of the soliton dynamics it is very convenient to concentrate the analysis on the fundamental degrees of freedom instead of following the soliton motion in its full details [9]. The formulation which reduces the large number of degrees of freedom of the original system (usually given by a partial differential equation (PDE) to a few "effective" degrees of freedom, is called the collective coordinate approximation. This method provides a system of ordinary differential equations (ODE) for these "effective" degrees of freedom. Such an approximation will help to unveil the ratchet mechanisms behind the dynamics of the solitons.

In chapter 3 we study the propagation of solitons under the presence of ac forces with harmonic mixing (biharmonic case). We will base our analysis on previous results concerning the appearance of a drift mechanism for kinks, where the dynamics shows a dependence on the phases of the harmonic forces. By using the collective coordinate (CC) framework, which in addition to the translational mode involves the kink width oscillations, we will explain the underlying physics behind the symmetry conditions discussed in previous works and also the consequences for the motion. Particularly, from the theoretical analysis of the collective coordinate equations a resonance condition between the driving force and the oscillation of the kink width for the occurrence of unidirectional motion is obtained. We also explain in the same CC framework different situations for which the dynamics shows a non-monotonic dependence on the damping coefficient. Specifically for relatively high damping, the average velocity decays drastically. In such a

situation we have also observed a slowing down for the oscillations of the kink width. Moreover, we see from our CC approach that, if we keep the kink width variable constant, the motion becomes purely oscillatory, a situation in which the soliton behaves like a point particle. This is a particular example where the role of the kink width is crucial for the motion. It also proves how much different the behavior of point particles is in contrast to our nonlinear excitations.

Chapter 4 is devoted to the study of a new kind of ratchet system. We present a novel design for a ratchet system which is made from a lattice of point-like inhomogeneities. The study is mainly focused on a rocking ratchet soliton behavior. Its analysis is done for the overdamped regime, albeit it is also possible to observe ratchet dynamics for a wider range of damping values.

Once again, but this time using different CC approaches, we show the importance of taking into account the kink width as a second degree of freedom. Its inclusion allows to capture the whole mechanism of motion. Furthermore, in this framework, we are able to show the similarity of our system with others, which are used for modeling molecular motors.

A similar analysis is also done in the presence of noise where unidirectional motion is observed even for cases where the motion is absent in the deterministic case. In all the cases, in spite of the possible differences with simple ratchet systems, the interplay of the two degrees of freedom leads to a ratchet behavior indistinguishable from that observed for single point particles.

Subsequently, an analysis of the dependence for the dynamics on the

damping coefficient is presented. In this case a significant unidirectional velocity in the weak underdamped regime is obtained.

Next, in order to extend our formulation to other ratchet mechanisms a brief presentation of a diffusive ratchet is shown and an analysis of the motion mechanisms is done.

At the end of this chapter different lattices of inhomogeneities for which the ratchet dynamics is possible are presented and some perspectives for this ratchet system are outlined.

Finally in chapter 5 the main results collected in the present thesis are summarized. Part of the results of this thesis have been published in [10, 11].

Chapter 2

Ratchet systems: From point particles to extended systems

A ratchet is a device which allows propagation in one direction, while it hinder the reverse motion. Based on such a mechanism, Feynman proposed a ratchet and pawl machine as a molecular gadget (Fig. 2.1). For this particular problem, when the temperature T_2 is greater than T_1, the axle will rotate due to the skewed shape of the teeth in the ratchet. The shape allows rotation clockwise but is hindering a counter-clockwise rotation. However, when the temperature T_1 is greater than T_2 the fluctuations or vibrations of the pawl dominate the motion. In this case the displacement of the teeth is greater in the counter-clockwise direction than in the clockwise direction. The main conclusion is that such a device only performs usable work in the presence of a temperature gradient, namely when we are out of the equilibrium, in

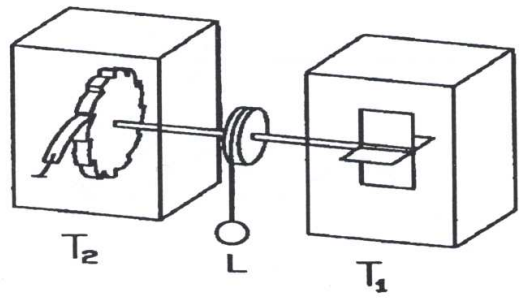

Figure 2.1: The ratchet and pawl machine: two reservoirs are connected by an axle that is attached to the ratchet in heat bath T_2 and to vanes in heat bath T_1. When $T_1 > T_2$ a small weight can be lifted.

agreement with the second law of thermodynamics [1].

More recently, such nonequilibrium ratchet systems have gained much interest in view of the possible role in describing the physical aspects that are involved in the working principles of motor proteins (the so-called molecular motors). Likewise, such devices have shown potential for novel technological applications on the nano- and micro-scale level. In order to proceed in the understanding of ratchet mechanisms, we define the term ratchet according to Leibler [21] as a system that moves the particles or conglomerates of particles with non-zero macroscopic velocity without any macroscopic forces *on average* and without field gradients . In view of this general definition we can define different types of ratchets. Some of them are exposed in this chapter as a background for understanding the results to be presented in the sequel.

[1]For a full discussion of this problem we refer the reader to the Lectures of Feynman [12] and some criticism made to the Feynman's analysis of this ratchet as an engine [13].

2.1 Ratchets for point particles

In this section we define some of the simplest examples of ratchets for point-particles and their basic principles, which take over to the ratchets in spatially extended systems.

2.1.1 Rocking ratchets

Let us consider an overdamped particle under the presence of a periodical force ($F(t) = F(t + \mathcal{T})$) with zero average over the period $\langle F(t)\rangle_{\mathcal{T}} = 0$, which additionally moves in an asymmetric periodic potential [2] like the one depicted in Fig. 2.2. In this case the equation of motion in the overdamped limit can be written as

$$\dot{x} = -\partial_x U + F(t). \tag{2.1}$$

We assume the simplest periodical force $F(t) \equiv A\sin(\omega t)$.

The asymmetry of the ratchet particularly leads to two threshold values for the amplitude A, i.e., for $|F_{max}|$. Let us analyze the case when the particle rocks the sawtooth potential shown in Fig. 2.2 back and forth between the limits

$$-min\ \ \partial_x U < |F_{max}| < max\ \ \partial_x U. \tag{2.2}$$

On one hand, the potential decreases monotonically to the left when the force is $+F_{max}$ but on the other hand, when the force is $-F_{max}$ there remain minima (signaled by arrows in Fig. 2.2) that trap a particle when it moves to

[2] In what follows we shall refer to a ratchet potential as an asymmetric periodic potential.

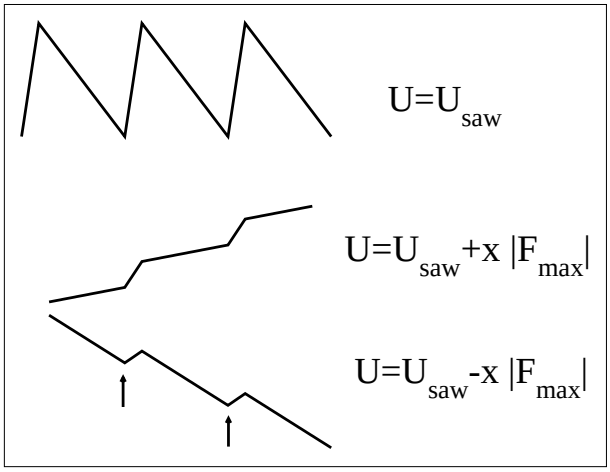

Figure 2.2: Illustrative sketch of the rectification mechanism in a *rocking ratchet*. Because of the asymmetry of the potential, starting at the bottom of any well, the force required for the particle to move to the right is greater than the force necessary to move to the left.

the right in response to the applied force. Accordingly, it will appear a net motion to the left direction that is determined by the orientation of the teeth in the sawtooth potential. Such a behavior is characteristic for overdamped systems where the inertial effects are negligible. Otherwise the particle can overcome the barrier moving to the next well and so on. In such a case the hindering mechanism does not work and therefore there is no rectification of motion.

In case when F_{max} lies below these two threshold values there will be no motion since a minimum force is required to overcome the barrier. On the contrary, when the maximum threshold value is exceeded, the ratchet is overdriven and the efficiency is reduced [66].

This mechanism persist even in the presence of small and moderate noise as we shall show in the next chapters.

2.1.2 Flashing ratchets

Let us consider the motion of a particle in a ratchet potential described by the equation

$$\dot{x} = -\zeta(t)\partial_x U + \sqrt{2D}\xi(t), \tag{2.3}$$

where $\zeta(t)$ is a periodical function $\zeta(t) = \zeta(t + \mathcal{T})$,$\mathcal{T}$ is the time period, $D = k_B T$ is the diffusion constant and $\xi(t)$ represents a Gaussian white noise with the correlation function $\langle \xi(t)\xi(t')\rangle = \delta(t - t')$.

Usually one is particularly interested in the situation when the function $\zeta(t)$ is given by

$$\zeta(t) = \begin{cases} 1, & 0 < t < \frac{\mathcal{T}}{2} \\ 0, & \frac{\mathcal{T}}{2} < t < \mathcal{T}, \end{cases}$$

i.e, when a switch between *on* and *off* takes place every half of the period (Fig. 2.3).

Particularly, for the ratchet potential depicted in Fig. 2.3, one has for the first half of the period a particle distribution localized in the minimum potential. However, during the second half of the period for which the ratchet potential is switched *off*, the distribution will spread out symmetrically by diffusion. When the potential is switched on again, a net part of the distribution will settle in the minimum towards the left. Consequently, we shall have a directed current of particles towards the left.

At a first glance, this ratchet appears as a perpetuum mobile of second type, assuming that the energy is taken from the thermal bath. However,

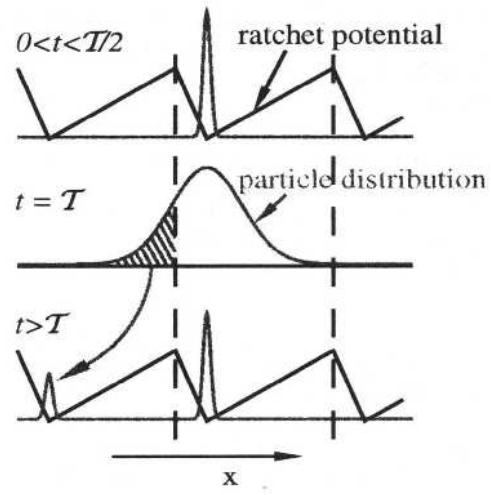

Figure 2.3: The noise induced transport mechanism in a ratchet potential that is periodically switched *on* and *off* with period $\mathcal{T}$. Sketch taken from [1].

this assumption is completely false because the energy does not come from the thermal bath but from the ratchet potential when it is switched on.

In the spirit of the second example we can realize a variety of different ratchet systems. Note that this changes not only the mechanism of motion with respect to the previous one, but also the transport takes place in opposite direction.

2.1.3 Diffusive or thermal ratchets

The diffusive ratchet which actually turns out to be closely related to the previous flashing ratchet has also been called a Brownian motor. This is because its design was inspired by the dynamics of molecular motors. In

order to explain the mechanism, let us consider Eq. 2.1 but now adding a Gaussian white noise, namely

$$\dot{x} = -\partial_x U + F + \xi(t) \tag{2.4}$$

with $\langle \xi(t)\xi(t') \rangle = 2k_B T \delta(t - t')$, where the temperature is subjected to temporally periodic modulations with period $\mathcal{T}$, i.e.

$$T(t) = T(t + \mathcal{T}).$$

Here we have chosen F as a constant external load. When this system reaches higher temperatures, the particles are able to spread without a preferential direction due to the diffusion, and when the temperature decreases the particles move to the minima of the potential. The particles in this ratchet system on average climb uphill the ratchet potential, thereby they perform work against the load force F. For the calculation of the net work and the efficiency of this system and in general for other systems, the ratchet system is usually considered as a thermodynamic motor [3].

In contrast to the previous model where the potential is switched off in order to allow the diffusive motion of particles, here the thermal noise as energy source enables the upward motion of the particles. Nevertheless, despite of such differences, it is possible to map one system into the other [18].

[3] An analysis of the efficiency of ratchet systems can be found in [19].

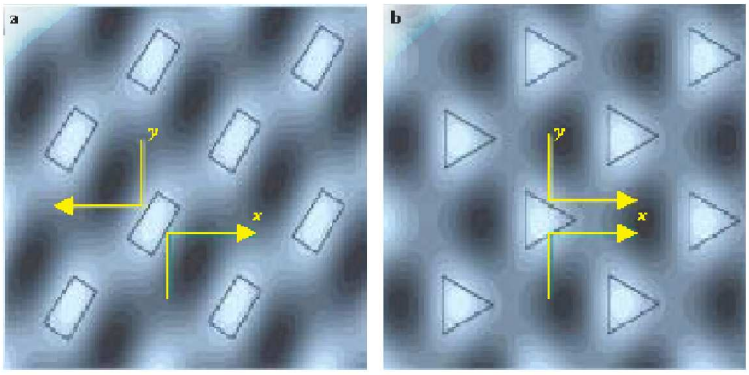

Figure 2.4: Symmetric Two-Dimensional Potentials. The figure shows contour graphs of the 2D dimensional function $V(x,y) = V_0\cos(4\pi x/L_x) + u(y)\cos(2\pi x/L_x) + \epsilon(y)\sin(2\pi x/L_x)$ with $u(y) = u_0\cos(2\pi y/L_y)$, $\epsilon(y) = \epsilon_0\cos(2\pi y/L_y + \phi)$. (a) $\phi = \pi/2$. (b) $\phi = 0$. Figure taken from [20].

2.1.4 Two-dimensional ratchets

The ratchet systems considered so far have been confined to one spatial dimension. Following the previous ideas about flashing ratchets one intuitively can develop a two-dimensional ratchet by mapping time modulated potentials into static potentials, i,e $(x,\omega t) \rightarrow (x,y)$. The modulation which was so far a function of time is now characterized by functions of the coordinate y. The nonequilibrium features are introduced by external forces in the x and y directions.

There exist two main classes of 2D ratchet potentials. In the first one proposed by Duke and Austin [22], the symmetry is broken in two directions (Fig. 2.4a). For this case a driving force in the x, y directions can cause a drift in the y, x directions where the variations in the force directions change

the resulting velocities.

A second device, suggested by Derényi and Astumian [23], possesses a broken symmetry in one direction Fig. 2.4b. This device leads to a constant drift in the x direction with zero net velocity in the y direction if one applies a driving force in the y direction with constant magnitude and periodically alternated sign. On the contrary, a force in the x direction does not produce a net flux in the y direction.

The fact that the oscillating force in the y direction can drive unidirectional motion in the x direction but not vice versa, allows to build much smaller devices, which is certainly desirable.

2.2 Ratchets in spatially extended systems

Following the previous ideas for point particles moving in asymmetric potentials and considering in a very preliminary approach the analogy of soliton-bearing excitations with point-particles in the same situation, it is expected that ratchet effects take place for solitons in asymmetric periodic on-site potentials, i.e substrate potentials with broken reflection symmetry.

This is the main reason why during the last 10 years many investigations have been devoted to the study of solitonic ratchet motions for different asymmetric on-site potentials. The first implementation of this ratchet idea for soliton-bearing systems was suggested by Marchesoni [24]. In this pioneering work he describes how time correlated noise induces current of kinks and antikinks in opposite directions for an asymmetric sine-Gordon potential. Later similar studies were carried out for asymmetric bistable potentials

[25]. Recently, in the same context a novel way of introducing the asymmetry for the on-site was developed [26]. The authors formulated the study for the generalized double sine-Gordon equation

$$\phi_{tt} + \beta\phi_t - \phi_{xx} + \sin(\phi) + \lambda\sin(2\phi + \theta) = f(t) + \eta(x,t),$$

where λ is the asymmetry parameter and θ is a constant phase. The term $f(t)$ is a sinusoidal driving force composed of one harmonic and $\eta(x,t)$ is Gaussian white noise. This system reduces for $\lambda = 0$ to the sine-Gordon equation, a system well known from the literature that does not have internal mode. For this particular situation the authors did not obtain ratchet dynamics. Therefore the authors concluded from their preliminary results that ratchet dynamics is produced because of the coupling between the driving force via a translational mode and the internal mode introduced by the second term of the double sine-Gordon potential. According to them, mainly the damping is responsible for the coupling between the translational and internal (or shape) modes of the kink. They also showed the existence of an optimal value of damping for which a maximum mean velocity is obtained.

Another way to get directed kink transport is to break the spatial symmetry using an inhomogeneous chain. As a first realization we have the study of LJJ in presence of an inhomogeneous magnetic field [27] for which an inhomogeneous junction profile is created for fluxons to propagate under an ac driver.

In chapter 4 a new proposal for the propagation of solitons in presence of point-like inhomogeneities is developed. The study is presented for Klein-Gordon systems, sG and ϕ^4. In this case the ratchet profile for the motion of solitons is created using a periodic and asymmetric lattice of point

like-inhomogeneities [11]. The study is mainly focused on rocking ratchet dynamics. Nevertheless, other type of ratchets are also proposed.

In the literature also extended ratchet systems composed of single pieces have been described [28, 29]. One example is the use of a parallel array of Josephson junctions with alternating physical properties of the junctions, such as self-inductances or the variations of critical currents. With such tools the authors have created a substrate potential with ratchet shape for the soliton propagation. The corresponding experiment was realized by Trias *et al.* [30].

So far we have made reference to ratchet systems with broken spatial symmetry. Nevertheless, it is possible to generate unidirectional motion using certain combinations of ac drivers [31, 32, 10]. In this case the net motion takes place when the time symmetry is broken. The next chapter is devoted to the analysis of the reasons and necessary conditions for the motion of topological nonlinear excitations under two mixing harmonic forces. This particular design has the advantage that we can choose the direction of the kink motion by changing the relative phase of the harmonic drivers. Recent experiments have confirmed the applicability of this idea in the context of LJJ devices [33].

2.3 Some remarkable applications of ratchet systems

As already mentioned before many works concerning ratchet systems have found various applications in different areas such as superconducting devices,

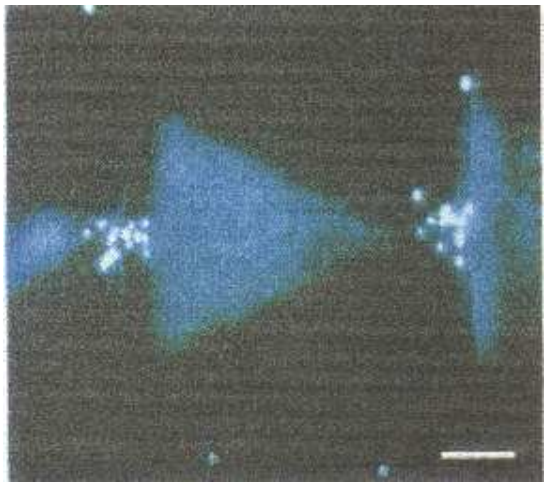

Figure 2.5: The white spots are tiny colloidal spheres trapped at the narrow necks between electrodes. Each on-off cycle of electric field produces a net particle motion from the left to right. Picture taken from [21].

separation methods, growing of surfaces, etc.

The main applications started, when an experimental pioneer work realized by Rousselet *et al.* [34] showed, beyond the pure academic interest, the great potential of such devices for moving tiny particles. They built a microelectrode system whose working principle corresponds to the flashing ratchet mechanism (see 2.1.2), where the electrodes are arranged in such a way that they produce an electrical sawtooth potential, which appears and disappears periodically following an external control. They were able to move colloidal particles with this device (Fig. 2.5). They also could prove within a certain approximation the consistency of the experimental results with theoretical models corresponding to flashing ratchet systems. A better quantitative agreement between theory and experimental results was obtained in further

works with a refined technique.

Actually, the design of such devices was inspired in the locomotion process of motor enzymes within the cell. A cascade of important investigations on ratchet systems was triggered since starting the studies of motor proteins motion. In fact, applications in biological systems have been become the most significant branches of research. Nowadays, sophisticated devices can be fabricated because of the advances in nanotechnology, such as the synthesis of molecular motors for the information processing at molecular level [35].

A practical application in this field is, for instance, the electrophoresis of DNA molecules in a submicrometer maze structure in a silicon wafer [36]. The authors constructed microlitographically obstacle arrays for studying the fractioning of large polymers of molecules with different topologies, like pieces of DNA. The improvement of such a technique might not only lead to separation of megabases pieces of DNA but also of whole cells for which the usual gel methods are inefficient. One interesting historical aspect is that such a device whose features undoubtedly fit with a ratchet device was designed even before starting the first theoretical works on ratchets.

Another area with outstanding applications is related with the design of superconductor devices. The first device proposed with ratchet dynamics was the SQUID, designed for the rectification of voltage [37]. For such a device the authors theoretically showed the appearance of Shapiro-like steps for the current-voltage characteristic with and without thermal fluctuations at large driving frequency, a typical feature of rocking ratchets. Nevertheless, only for a new variant of the design the ratchet mechanism was confirmed experimentally [38]. Other interesting devices have been built like, for in-

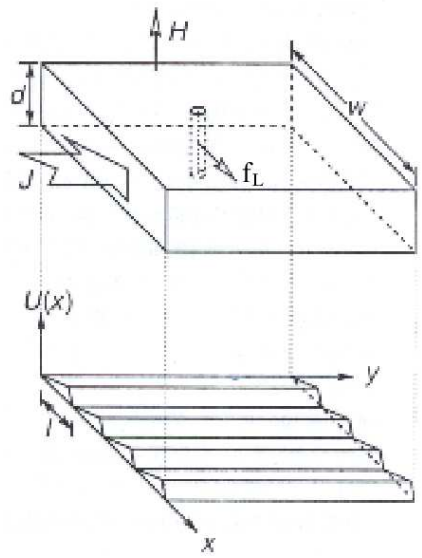

Figure 2.6: Diagram of a superconductor in the presence of an external field H. A current density J flowing along the y direction induces a Lorentz force F_L that moves the vortex in the x direction. The superconductor is patterned with a pining potential $U(x, y) = U(x)$(lower panel). The potential is periodic and asymmetric along the x direction. Picture taken from [39].

stance, the one proposed by C.S Lee *et al.* in [39], wherein a ratchet potential formed by pining sites is employed to clean the superconductor sample from vortices when an alternating current perpendicular to the magnetic field is applied (Fig. 2.6). In this case the presence of an alternating current generates a Lorentz force on the vortices which moves them in a ratchet potential created by a modulation of the pining sites density. More recently, a device in two dimension has been developed, designed again with the same goal of manipulating and controlling the vortices motion [40]. By means of the electron beam lithography technique, the authors fabricating arrays of triangular blind anti dots (Fig. 2.7). Using such device they could direct the motion

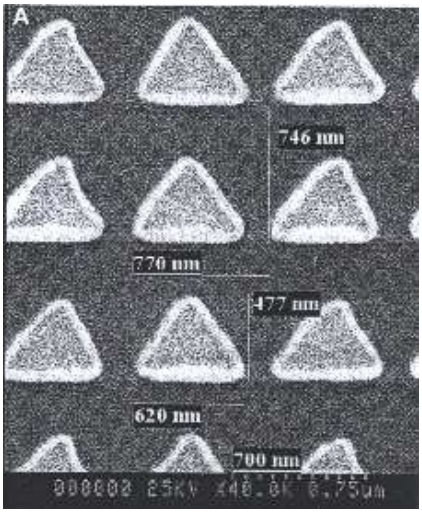

Figure 2.7: Scanning electron microscope image of an array of Ni triangles on top of Si (100) substrate. The triangle hight (Ni thickness) is typically 35 nm. Figure taken from [40].

of fluxons in a preferential direction. With this result the authors confirmed theoretical predictions obtained in preliminary studies on the rectification of vortex motion for an ac driven system with triangular blind anti dots pinning arrays [41].

These are some of the main applications of ratchet systems. There exist many more, which can be found in extensive reviews on this topic [2, 17, 42]. We have only addressed some prominent main applications of ratchet systems.

Chapter 3

Ratchet: Time symmetry-breaking

As was pointed out in the previous chapter, the appearance of ratchet-like behavior requires two ingredients: departure from thermal equilibrium (either by using correlated stochastic forces or deterministic forces) and breaking of spatial inversion symmetry [2]. This is actually the setup for the majority of ratchet models. However, it has recently been realized that the use of an *asymmetric driving* can play the same role as the spatial asymmetry. Such an effect was first proposed for one-particle systems in [43]. The analysis presented by Flach and coworkers indicated that a directed energy current appears if $f(t)$ breaks the symmetry $f(t) = -f(t + T/2)$, T being the period of the external driving. Later it was extended to the study of extended systems, both quantum [44] and classical systems [31, 32].

In [31, 32], the previous symmetry considerations were generalized to the sG model. Again, it was found that if $f(t)$ breaks the symmetry $f(t) =$

$-f(t+T/2)$, *and if the total topological charge in the system is nonzero*, a directed current should be observed whose direction and magnitude will depend on the driving and damping parameters. It is important to realize that the condition of a topological charge implies that *at least one kink or one antikink must exist*, and that the numbers of both types of nonlinear excitations should differ at least by 1. In the case when there is just one kink (or antikink) in the system, we are faced with an analogy to the point-like ratchet proposed in [43]. Indeed, as in many other instances [9], kinks behave basically as point-like particles, and the fact that their presence in the extended system is needed to have directed current reinforces this analogy. However, as we shall show in this chapter, the scenario is not that simple, and in fact the point-like particle picture is not enough to understand the general features in spatially extended systems.

From the symmetry analysis of the force one can deduce that in the case of one harmonic a directed of motion of sG kinks is not possible. This conclusion was confirmed years ago in [45, 46]. For that problem, a collective coordinate description in terms of the motion of the kink center showed a quantitative agreement with the numerical simulation results.

Let us now return to the case of a biharmonic mixing. In the first two examples for the sG system, Flach *et al.* [31] and Salerno and Zolotaryuk [32] considered $f(t) \equiv \epsilon_1 \cos(\delta t) + \epsilon_2 \cos(2\delta t + \theta)$. For this choice, they performed numerical simulations that confirmed the symmetry analysis results. In view of the fact that the system did exhibit ratchet-like behavior, i.e., it rectified ac current, as kinks moved towards one direction in space, the authors in [32] tried to implement a collective coordinate approach (see [9] for a review

on this technique), in which the kink motion was reduced to a description in terms of an ordinary differential equation for the motion of its center. However, the approach turned out to be not satisfactory [32].

In this chapter we present a complete description of the ratchet phenomenom using a new Collective Coordinate framework. This new approach considers two collective variables which represent the center and the width of kink. We also generalize the study extending the formulation to the ϕ^4 model.

For investigating the dynamics in the presence of the biharmonic force we consider a more general form for the ac driving, namely $f(t) = \epsilon_1 \sin(\delta t + \theta_1) + \epsilon_2 \sin(m\delta t + \theta_2)$ where ϵ_1 and ϵ_2 are the amplitudes of the respective harmonics with frequencies δ and $m\delta$ and phases θ_1 and θ_2. These phases can also be expressed as $\theta_1 = \delta_0$ and $\theta_2 = \delta_0 + \theta$ (see [10]). For the case $\theta_1 = 0$ and $\theta_2 = \theta$ we recover the original formulation [31]. In any case we can take this formulation to the original one, since the use of θ_1 and θ_2 is equivalent to a relative phase $\theta' = \theta_2 - m\theta_1$ with a time shift $t' = t + t_0$ where $\theta_1 = \delta t_0$. It would be a challenge in experiments to adjust the phases properly.

For the sG system the model reduces to

$$\phi_{tt} - \phi_{xx} + \sin(\phi) = -\beta\phi_t + f(t), \tag{3.1}$$

and for the ϕ^4 system we have

$$\phi_{tt} - \phi_{xx} + \phi^3 - \phi = -\beta\phi_t + f(t), \tag{3.2}$$

where β is the damping coefficient for both systems.

3.1 Collective coordinate approach

By using the variations of the energy and the momentum and taking into account the Rice *Ansatz* (see [47]) one can obtain two ODE for the collective coordinates, one for the position of the kink center, $X(t)$, and another for the width of the kink, $l(t)$, like

$$\frac{dP}{dt} = -\beta P - qf(t), \tag{3.3}$$

$$\dot{l}^2 - 2l\ddot{l} - 2\beta l\dot{l} = \Omega_R^2 l^2 \left[1 + \frac{P^2}{M_0^2}\right] - \frac{1}{\alpha}, \tag{3.4}$$

where the momentum $P(t) = M_0 l_0 \dot{X}/l(t)$ and $\Omega_R = 1/(\sqrt{\alpha} l_0)$ is the Rice's frequency. The parameters M_0, q, α and l_0 take different values according to the model, sG or ϕ^4 (see Table 3.1). The same equations can

Effective parameters	sG	ϕ^4
q	2π	2
M_0	8	$2\sqrt{2}/3$
l_0	1	$\sqrt{2}$
α	$\pi^2/12$	$(\pi^2-6)/12$

Table 3.1: Effective parameters for the sG and ϕ^4 models.

be obtained using a projection technique with a *Generalized Traveling Wave Ansatz* (GTWA) (see details in the appendix A).

Eq. (3.3) is linear and can be solved exactly, so that we can obtain the evolution of $P(t)$. Notice that, for long enough time ($t \gg 1/\beta$) the expression for the momentum becomes

$$P(t) = \frac{q\epsilon_1[\delta\cos(\delta t + \theta_1) - \beta\sin(\delta t + \theta_1)]}{(\beta^2 + \delta^2)} + \frac{q\epsilon_2[m\delta\cos(m\delta t + \theta_2) - \beta\sin(m\delta t + \theta_2)]}{(\beta^2 + m^2\delta^2)}, \tag{3.5}$$

which can be properly written as

$$P(t) = -\sqrt{\epsilon}[a_1 \sin(\delta t + \theta_1 - \chi_1) + a_2 \sin(m\delta t + \theta_2 - \chi_m)], \tag{3.6}$$

where ϵ is a rescaling parameter which can be defined as the $\min(\epsilon_1, \epsilon_2)$. The other terms read:

$$\chi_1 = \arctan\left(\frac{\delta}{\beta}\right), \quad \chi_m = \arctan\left(\frac{m\delta}{\beta}\right)$$

and

$$a_1 = \frac{q}{\sqrt{\beta^2 + \delta^2}}\frac{\epsilon_1}{\sqrt{\epsilon}}, \quad a_2 = \frac{q}{\sqrt{\beta^2 + m^2\delta^2}}\frac{\epsilon_2}{\sqrt{\epsilon}}.$$

The change of variable $g(t)^2 = l(t)$ in (3.4), leads to an Ermakov-type equation for the function $g(t)$, given by

$$\ddot{g} + \beta\dot{g} + \left[\left(\frac{\Omega_R}{2}\right)^2 + \left(\frac{\Omega_R}{2M_0}\right)^2 P^2(t)\right] g = \frac{1}{4\alpha g^3}, \tag{3.7}$$

which can only be solved analytically for $\beta = 0$ (see [47] and references therein). Therefore, in order to study Eq. (3.4) we propose an expansion of $l(t)$ around the unperturbed kink width l_0, in powers of ϵ as follows

$$l(t) = l_0 + \epsilon l_1(t) + \epsilon^2 l_2(t) + ... \ . \tag{3.8}$$

Substituting Eq. (3.8) into Eq. (3.4) we get a hierarchy of equations for different order of powers in ϵ:

For $O(\epsilon)$,

$$\ddot{l}_1(t) + \beta\dot{l}_1(t) + \Omega_R^2 l_1(t) = -\frac{\Omega_R^2}{2\epsilon M_0^2} P^2(t) l_0, \tag{3.9}$$

For $O(\epsilon^2)$,

$$\ddot{l}_2(t) + \beta\dot{l}_2(t) + \Omega_R^2 l_2(t) = -\frac{\Omega_R^2}{2\epsilon M_0^2} P^2(t) l_1 + \frac{\dot{l}_1^2}{2l_0} + \frac{\Omega_R^2 l_1^2}{2l_0}, \tag{3.10}$$

For $O(\epsilon^3)$,

$$\ddot{l}_3(t)+\beta\dot{l}_3(t)+\Omega_R^2 l_3(t) = -\frac{\Omega_R^2}{2\epsilon M_0^2}P^2(t)l_2+\frac{\dot{l}_1\dot{l}_2}{l_0}+\frac{\Omega_R^2 l_1 l_2}{l_0}-\frac{\dot{l}_1^2 l_1}{2l_0^2}-\frac{\Omega_R^2 l_1^3}{2l_0^2}. \quad (3.11)$$

These equations can be solved analytically. Let us take the first order of the expansion. In order to solve Eq. (3.9) we substitute the expression for the momentum (3.6) into (3.9), i.e.,

$$\begin{aligned}\ddot{l}_1(t) + \beta\dot{l}_1(t) + \Omega_R^2 l_1(t) = -\frac{\Omega_R}{2\epsilon\sqrt{\alpha}M_0^2}P^2(t) = A_1 + A_2\cos(2\delta t + 2\theta_1 - 2\chi_1)\\ +A_3\cos(2m\delta t + 2\theta_2 - 2\chi_m) + A_4\cos[(m-1)\delta t + \theta_2 - \theta_1 - (\chi_m - \chi_1)]\\ -A_4\cos[(m+1)\delta t + \theta_1 + \theta_2 - (\chi_m + \chi_1)], \quad (3.12)\end{aligned}$$

where

$$\begin{aligned}A_1 &= -A_2 - A_3,\\ A_2 &= \frac{\Omega_R a_1^2}{4\sqrt{\alpha}M_0^2},\\ A_3 &= \frac{\Omega_R a_2^2}{4\sqrt{\alpha}M_0^2},\\ A_4 &= -\frac{\Omega_R}{2\sqrt{\alpha}M_0^2}a_1 a_2.\end{aligned}$$

Notice in the r.h.s of the previous equation, the presence of harmonics with frequencies 2δ, $2m\delta$ and $(m\pm 1)\delta$. After transients have died out, we find

$$\begin{aligned}l_1(t) = \quad & \frac{A_1}{\Omega_R^2} + \frac{A_2\sin(2\delta t + 2\theta_1 - 2\chi_1 + \tilde{\theta}_2)}{\sqrt{(\Omega_R^2 - 4\delta^2)^2 + 4\beta^2\delta^2}} + \frac{A_3\sin(2m\delta t + 2\theta_2 - 2\chi_m + \tilde{\theta}_{2m})}{\sqrt{(\Omega_R^2 - 4m^2\delta^2)^2 + 4m^2\beta^2\delta^2}}\\ &+\frac{A_4\sin[(m-1)\delta t + \theta_2 - \theta_1 - (\chi_m - \chi_1) + \tilde{\theta}_{m-1}]}{\sqrt{(\Omega_R^2 - (m-1)^2\delta^2)^2 + \beta^2(m-1)^2\delta^2}}\\ &-\frac{A_4\sin[(m+1)\delta t + \theta_1 + \theta_2 - (\chi_m + \chi_1) + \tilde{\theta}_{m+1}]}{\sqrt{(\Omega_R^2 - (m+1)^2\delta^2)^2 + \beta^2(m+1)^2\delta^2}}, \quad (3.13)\end{aligned}$$

where

$$\tilde{\theta}_m = \arctan\left(\frac{\Omega_R^2 - m^2\delta^2}{m\beta\delta}\right).$$

As is expected we get a solution with the harmonics 2δ, $2m\delta$ and $(m \pm 1)\delta$. That means that we do not need to solve the equation in order to know the possible harmonics.

From a similar analysis for Eqs. (3.10) and (3.11), one can deduces the harmonics that appear in the second and third order of the expansion, i.e., for $l_2(t)$ and $l_3(t)$. In Table 3.2 are shown the harmonics that appear in the first order of the expansion of $l(t)$ for different values of m. In order to compute

2^{nd} harmonic(δ)	l_1	l_2
m	2δ, $2m\delta$, $(m \pm 1)\delta$	2δ, 4δ, $4m\delta$, $(m \pm 1)\delta$, $2(m \pm 1)\delta$, $(m \pm 3)\delta$, $(3m \pm 1)\delta$
2	δ, 2δ, 3δ, 4δ	δ, 2δ, 3δ, 4δ, 5δ, 6δ, 7δ, 8δ
3	2δ, 4δ, 6δ	2δ, 4δ, 6δ, 8δ, 10δ, 12δ
4	2δ, 3δ, 5δ, 8δ	δ, 2δ, 3δ, 4δ, 5δ, 7δ, 9δ, 10δ, 11δ, 13δ, 16δ

Table 3.2: Harmonic content of the first contributions to the perturbative expansion of $l(t)$. Notice that δ and $m\delta$ are the driven frequencies of the ac force (or in the momentum).

the average velocity over one period $T = 2\pi/\delta$, we use the previous expression for the momentum $P(t) = M_0 l_0 \dot{X}/l(t)$. Such an expression can be obtained by substituting the Rice's ansatz into the definition of the momentum $P(t) = -\int_{-\infty}^{\infty} dx\ \phi_t \phi_x$. Consequently, the mean velocity of the kink in the Collective

Coordinate framework can be expressed as

$$\langle \dot{X}(t) \rangle = \frac{1}{T} \int_0^T \frac{P(t) l(t)}{M_0 l_0} dt. \tag{3.14}$$

Taking into account the expansion (3.8), this expression can be written as

$$\begin{aligned} \langle \dot{X}(t) \rangle &= \frac{1}{T} \int_0^T \frac{P(t)(l_0 + \epsilon l_1(t) + \epsilon^2 l_2(t) + ...)}{M_0 l_0} dt \\ &= \langle \dot{X}_0(t) \rangle + \epsilon \langle \dot{X}_1(t) \rangle + \epsilon^2 \langle \dot{X}_2(t) \rangle + ... \end{aligned} \tag{3.15}$$

Therefore the mean velocity can be analytically calculated with some approximation taking into account the expression (3.6) for the momentum and the first terms of the expansion for the width of the kink. For $O(\epsilon^0)$, the average of the momentum is zero [see Eq. (3.6)], and therefore $\langle \dot{X}_0(t) \rangle$ vanishes. Accordingly, the net motion of the kink can only arise in next order. We proceed to solve the integral for $\epsilon \langle \dot{X}_1(t) \rangle$. By means of straightforward calculations of Eqs. (3.15) and (3.13) we get for $m = 2$:

$$\begin{aligned} \epsilon \langle \dot{X}_1 \rangle &= \frac{q^3 \Omega_R^2 \epsilon_1^2 \epsilon_2}{8 M_0^3 (\beta^2 + \delta^2) \sqrt{\beta^2 + 4\delta^2}} \left(\frac{2 \cos[2\theta_1 - \theta_2 + (\chi_2 - 2\chi_1) - \tilde{\theta}_1]}{\sqrt{(\Omega_R^2 - \delta^2)^2 + \beta^2 \delta^2}} \right. \\ &\left. - \frac{\cos[2\theta_1 - \theta_2 + (\chi_2 - 2\chi_1) + \tilde{\theta}_2]}{\sqrt{(\Omega_R^2 - 4\delta^2)^2 + 4\beta^2 \delta^2}} \right). \end{aligned} \tag{3.16}$$

This approximation describes well the behavior of the average velocity in the limit $\epsilon_i / \sqrt{\beta^2 + m_i^2 \delta^2} \ll 1, i = 1, 2$; where $m_1 = 1$ and $m_2 = m$. In the following we will refer to this case as the limiting condition for the validity of the perturbation theory.

Notice the sinusoidal dependence on θ_1 and θ_2 in $\epsilon \langle \dot{X}_1 \rangle$. Notice also, that the terms χ_n and $\tilde{\theta}_n$ with $n = 1, 2$ depend on the damping so that for some cases the damping coefficient determines the direction of the motion.

Similar analysis for $m = 4$ shows that $\epsilon\langle\dot{X}_1\rangle$ is zero. This happens because the frequencies in $l(t)$ that have contribution to the motion appear in higher order corrections. So, in order to get a nonvanishing expression for the mean velocity it is necessary to take into account the next order $\epsilon^2\langle\dot{X}_2\rangle$. After cumbersome calculations we get the expression

$$\begin{aligned}
\epsilon^2\langle\dot{X}_2\rangle \;=\; & \frac{q^5\Omega_R^4\epsilon_1^4\epsilon_2}{32M_0^5(\beta^2+\delta^2)^2\sqrt{(}\beta^2+16\delta^2)}\ \text{x} \\
& \left\{\frac{\sin(4\theta_1-\theta_2+\chi_4-4\chi_1+\tilde{\theta}_2-\tilde{\theta}_1)}{\sqrt{(\Omega_R^2-\delta^2)^2+\beta^2\delta^2}\sqrt{(\Omega_R^2-4\delta^2)^2+4\beta^2\delta^2}}\right. \\
& +\frac{(6\delta^2+\Omega_R^2)\cos(4\theta_1-\theta_2+\chi_4-4\chi_1-\tilde{\theta}_3+\tilde{\theta}_2-\tilde{\theta}_1)}{\sqrt{(\Omega_R^2-\delta^2)^2+\beta^2\delta^2}\sqrt{(\Omega_R^2-4\delta^2)^2+4\beta^2\delta^2}\sqrt{(\Omega_R^2-9\delta^2)^2+9\beta^2\delta^2}} \\
& -\frac{\sin(4\theta_1-\theta_2+\chi_4-4\chi_1-\tilde{\theta}_3-\tilde{\theta}_1)}{\sqrt{(\Omega_R^2-\delta^2)^2+\beta^2\delta^2}\sqrt{(\Omega_R^2-9\delta^2)^2+9\beta^2\delta^2}} \\
& -\frac{\sin(4\theta_1-\theta_2+\chi_4-4\chi_1+\tilde{\theta}_2+\tilde{\theta}_4)}{2\sqrt{(\Omega_R^2-4\delta^2)^2+4\beta^2\delta^2}\sqrt{(\Omega_R^2-16\delta^2)^2+16\beta^2\delta^2}} \\
& \left.-\frac{(4\delta^2-\Omega_R^2)\cos(4\theta_1-\theta_2+\chi_4-4\chi_1+2\tilde{\theta}_2+\tilde{\theta}_4)}{4[(\Omega_R^2-4\delta^2)^2+4\beta^2\delta^2]\sqrt{(\Omega_R^2-16\delta^2)^2+16\beta^2\delta^2}}\right\}. \qquad (3.17)
\end{aligned}$$

For the case $m = 3$, the calculation of the average velocity gives zero for all orders of the expansion. For this case the frequencies of the ac force (or the momentum) are "odd harmonics" of δ (δ and 3δ), whereas only "even harmonics" of δ are found in the kink width oscillations ($2n\delta$, $n \in N$). The complete selection rule for $m = 2, 3, 4$ appears in the Table 3.2. In principle the analysis can be extended to any positive integer number of the frequency for the second harmonic, i.e., for higher values of m.

We conclude from these preliminary results that the net motion occurs because of the coupling between the translation of the kink and the internal mode (oscillation of the kink width). As the most important result, we can

say that this coupling is possible only when the harmonic part of the force is able to resonate [1] with the kink width.

The previous reasoning can also cover the case $m = 1$. By looking at the expression (3.6) we realize that only the frequency 2δ can appear in the equation (3.4). In this case, for small frequencies, the oscillations of the kink width do not influence on the dynamics and therefore the collective coordinate approach for one degree of freedom (kink center) is sufficient to describe the dynamics.

Let us discuss now, why the previous theory discussed in [32] fails. The failure becomes visible when the authors tried to fit the analytical results with the numerical simulations whose parameters differ from those predicted by the theory. In this work [32] the authors considered the relativistic approximation for the CC for one degree of freedom. In this case the oscillations of the kink width are determined by the Lorentz contraction (see Eq. (12) of [32] and compare with the expression $\dot{X} = P(t)l(t)/M_0 l_0$). However, as we have observed in this chapter the dynamics is much more complicated in the presence of ac forces, needing more than one collective variable for catching the full dynamics of the system. This issue will be verified in the next section where we compare the results of CC equations with the numerical simulations.

[1] Some authors refer to this phenomenon as a synchronization between the ac force and the oscillations of the kink width, i.e., that only a directional transport occurs when the ac force locks the oscillations of the kink width.

3.2 Numerical verification

The previous results were derived within the collective coordinate approach. In order to check our predictions we have computed the numerical solution of the partial differential equations (3.1) and (3.2) by using the Strauss Vázquez scheme (see details in Appendix B), choosing a total length of $L = 100, 300$, with steps $\Delta t = 0.01$, $\Delta x = 0.1$. We have used free boundary conditions with a kink at rest as initial condition. We also implemented a fourth-order Runge-Kutta method in order to verify our results. In the following we will focus on the behavior of the ratchet dynamics and its variations with the parameters.

Concretely speaking, we will investigate the dependence of the average velocity on the harmonic phases of the biharmonic force (for different values of m) and also on the damping coefficient. In order to do so, we shall separate the analysis in two parts according to the model that we are going to deal with.

3.2.1 Sine-Gordon model

In section 3.1 we established the phenomenology for the existence of net motion. We argued that the time dependence of the kink width is not a sufficient condition for the existence of a directed motion and that the net motion appears only when at least one of the two harmonics of the ac driven force is contained in the oscillations of the kink width. We have based our arguments on the CC results (see Table 3.2 for frequencies that appear for the first order corrections in the kink width expansion).

In order to confirm these conjectures it is crucial to understand how the kink width evolves when the soliton is driven by an external force.

In this respect we proceed to the computation of the kink width dynamics. The evolution in time of the kink width obtained from the numerical simulations and from the collective coordinate equations are depicted in the left panel of Fig. 3.1.

Here for the numerical calculation of the center and width of the kink we have followed the same procedure as proposed in [50], taking into account the oscillations of the ground states due to the action of the ac driving.

There are different methods for the determination of the kink center. Here we have used the linear interpolation method. In particular, for the sG kink, this method reduces to search for each time interval, in the discrete lattice, those points x_n and x_{n+1} such that $\phi_n \leq \pi + \phi_{\text{vac}}$ and $\phi_{n+1} \geq \pi + \phi_{\text{vac}}$, where ϕ_{vac} represents the vacuum part of the sG field $\phi(\pm\infty, t)$. Then we estimate the corresponding point $\tilde{x}_n$ (the center of the kink $X(t)$) where $\phi = \pi$ by linear interpolation. Subsequently, in order to compute the kink width, we search the value of $l(t)$ that minimizes the expression $\sum_{n=1}^{N} \left| \phi_n - \left(\phi_K \left[\frac{n * \Delta x - X(t)}{l(t)} \right] + \phi_{\text{vac}} \right) \right|^2$ with $N = L/\Delta x$, where L is the length of the system, $X(t)$ is the kink center position, ϕ_n is the numerical value of the function in the nth lattice point, ϕ_K corresponds to the expression for the kink, which in the sG case is given by Eq.A.22. In this case the vacuum can be expressed as $\phi(L, t)$.

From this picture we observe an excellent agreement between simulations and the CC framework. Subsequently in order to confirm our predictions we proceed to the determination of the Fourier components for the kink width

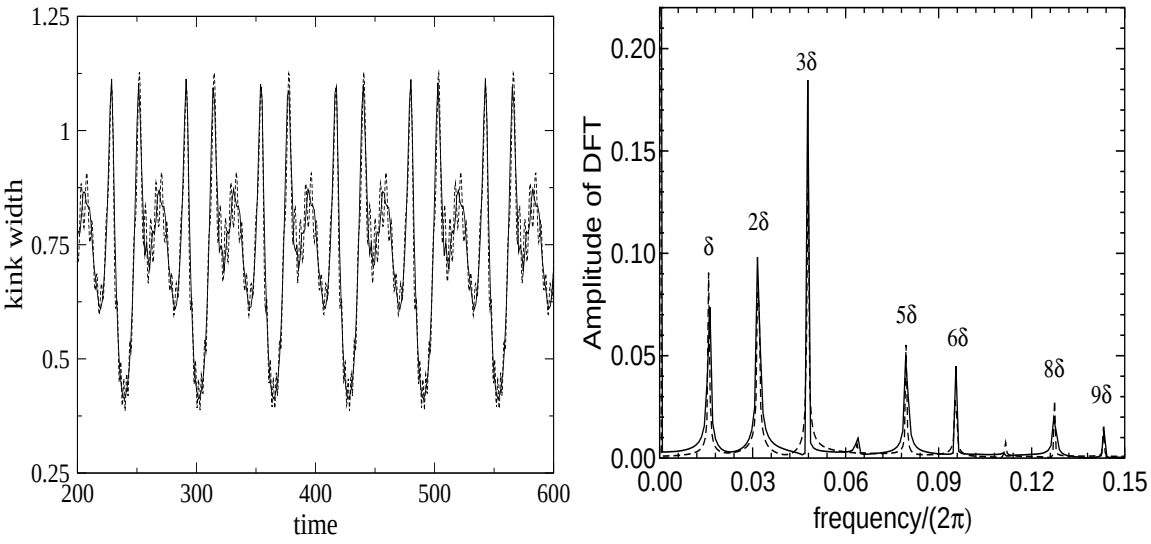

Figure 3.1: Left panel: Kink width vs time. Right panel: Discrete Fourier Transform (DFT) of the width of the kink. For both panels dashed line: numerical computation of Eqs. (3.3-3.4); solid line: Full simulation of Eq. (3.1).The parameters are $\epsilon_1 = \epsilon_2 = 0.2$, $\beta = 0.05$, $\delta = 0.1$, $\theta_1 = -2.5$ $\theta_2 = \pi/2 - 2.5$.

oscillations (see right panel of Fig. 3.1). The Discrete Fourier Transform (DFT) shows an impressive agreement between the comparison of the full simulation of Eq. (3.1) and the numerical calculus of Eqs. (3.3-3.4) validating our resonance criterion. We can observe that for $m = 2$ the frequencies δ and 2δ appear as was pointed out in the table. Consequently, because of the presence of frequencies of the harmonic driving forces in the oscillation of the kink width, one should expect a net motion of the soliton. We know in advance for this particular situation, of the existence of a directional motion for the kink center. A detailed analysis of the dynamics for $m = 2$ will be the

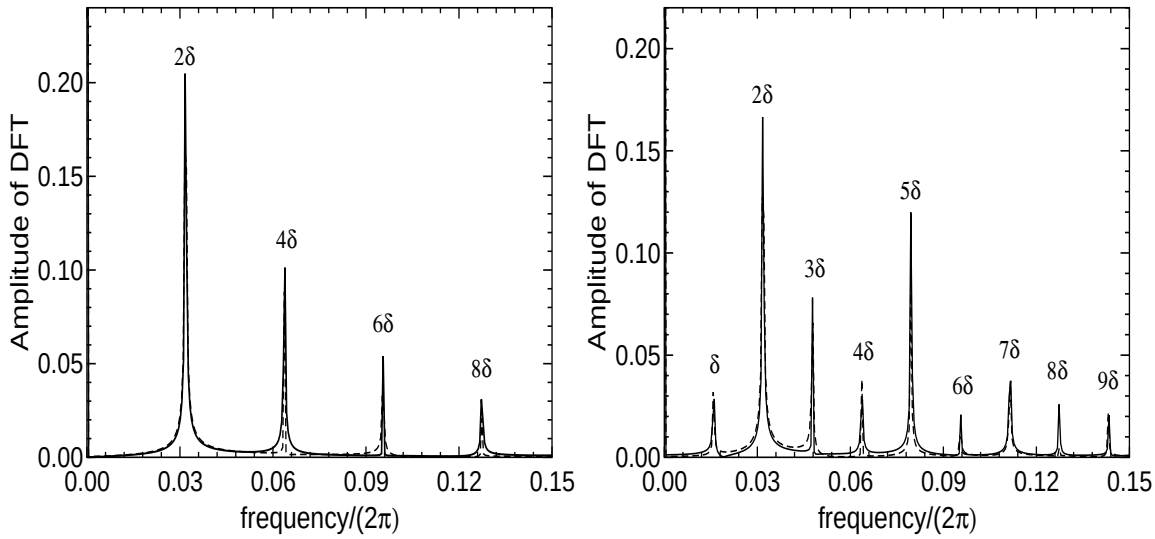

Figure 3.2: Discrete Fourier Transform of the kink width. Left panel: $m = 3$; Right panel: $m = 4$. Solid line: amplitude measured in simulations. Dashed line: numerical integration of the CC equations (3.3)-(3.4).The parameters are the same as in Fig3.1.

object of discussion below. Let us discuss what happens for other values of m. We proceed in the same way, calculating the Fourier mode of the kink width oscillations. The DFT of the kink width for $m = 3, 4$ are collected in Fig. 3.2. For $m = 4$ we observe the appearance of frequencies δ and 4δ. Therefore, the occurrence of a net motion is expected.

On the contrary, for $m = 3$ neither δ nor 3δ appear to be present in the ac driven force. In this case following our predictions we expect an oscillatory motion similar to that obtained for a force with only one harmonic component.

A definitive confirmation of our conjectures can be obtained from the

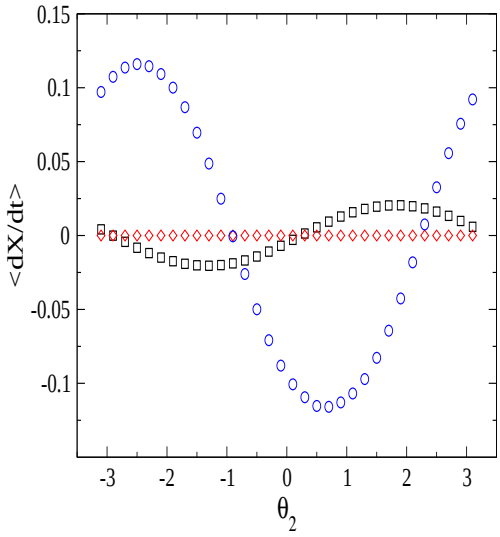

Figure 3.3: Dependence of the average velocity on θ_2 for different values of m. $m = 2$ blue circles; $m = 3$ red diamonds; $m = 4$ black squares. The parameters are $\epsilon_1 = \epsilon_2 = 0.2$, $\beta = 0.05$, $\delta = 0.1$, $\theta_1 = 0$.

motion of the kink center of the soliton. In Fig. 3.3a the results for different values of m are collected. In this picture the predictions on the existence of motion for different values of m are confirmed. Notice the sinusoidal dependence of the mean velocity function on the phases, an expected result in view of the expressions (2.16) and (2.17).

A distinct feature is the difference for the mean velocity between the cases $m = 2$ and $m = 4$. In principle such difference could be inferred from the fact that in the case $m = 4$ the contribution to the velocity appears in a higher order of the expansion than in the case $m = 2$ (see Table 3.2). However, such reasoning could lead us to a misleading conclusion.

A possible explanation can be found in the analytical expression for the

mean velocity. Taking a closer look at expressions (3.16) and (3.17) we realize that the factor ϵ_1 corresponding to the first harmonic has a power greater than one whereas the factor ϵ_2 for the second harmonic is linear. Therefore the contribution of the first harmonic is determinant for the motion of the kink.

From the comparison of the DTFs we observe that the peak corresponding to the frequency δ for $m = 2$ has a higher intensity than its counterpart for $m = 4$ (see right panel of the Figs. 3.1 and 3.2). This adjusts to our predictions and is also consistent with the results presented in Fig. 3.3.

An important feature of the motion is the dependence of the mean velocity on the phases of the harmonics of the ac force $f(t)$. For this situation a periodical behavior of the mean velocity as a function of the phases is expected from Eq. (3.16). Fig. 3.4 confirms the reliability of our theory since an excellent agreement between the numerical computation of the CC equations (3.3)-(3.4) and the full simulation of the Eq. (3.1) is obtained. We have also plotted the expression (3.16). In the left panel of Fig. 3.4, the results for the equation (3.16) are divided by a factor of 5. The factor was introduced in order to adjust it to the results of the simulations and numerical computation of CC equations. Otherwise a large deviation is obtained since for relatively large amplitudes of the ac force, outside the range of the limiting condition, the perturbation theory fails. Notwithstanding, it reproduces the sinusoidal behavior correctly, thus validating the analytical results obtained from the perturbation theory.

For very small amplitudes of the ac force in the range where our perturbation theory is valid, Eq. (3.16) fits very well to the results of the mean

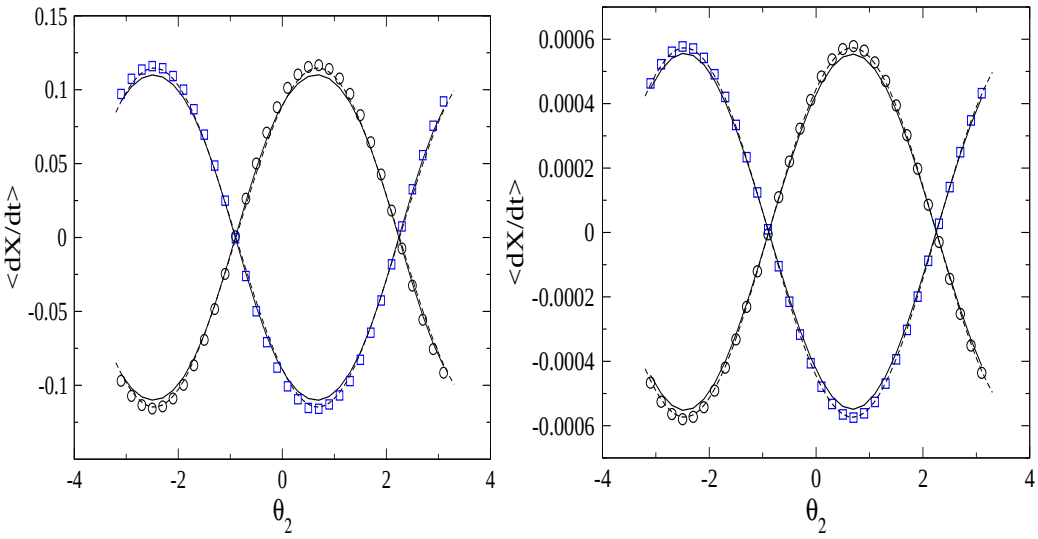

Figure 3.4: Dependence of the average velocity on θ_2 for $m = 2$. Left panel: Parameters are $\epsilon_1 = \epsilon_2 = 0.2$. Right panel: $\epsilon_1 = \epsilon_2 = 0.02$. The rest of the parameters are $\beta = 0.05$, $\delta = 0.1$. In both panels two values for θ_1 are considered. Simulations: $\theta_1 = 0$ blue squares; $\theta_1 = \pi/2$ black circles; solid line correspond to the numerical computation of the CC Eqs. (3.3)-(3.4); in left panel dashed line correspond to $\epsilon\langle\dot{X}_1\rangle/5$ and in the right panel correspond to $\epsilon\langle\dot{X}_1\rangle$ for the respective parameters of the simulations.

velocity obtained from the numerical calculus of the CC equations and of the simulations as is shown in the right panel of the same Fig. 3.4.

For the case $m = 4$ again a very good agreement between the results of the collective coordinates equations and the simulations is obtained (see Fig. 3.5). In this figure the dependence of the mean velocity on the phases of the force is plotted. The left and right panels show the behavior of the mean velocity on θ_2 and θ_1 respectively. Notice the increasing number of

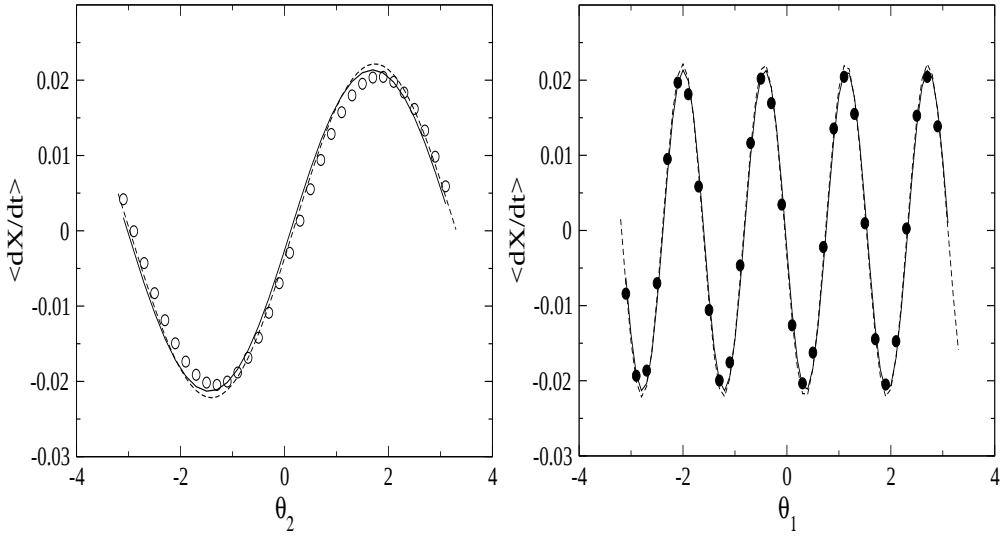

Figure 3.5: Dependence of the average velocity on the harmonic phases for $m = 4$. Left panel shows the dependence on θ_2 for $\theta_1 = 0$; Right panel shows the dependence on θ_1 for $\theta_2 = 0$. In both cases circles are simulations; solid line, numerical computation of CC Eqs. (3.3)-(3.4); dashed line, $\epsilon^2\langle\dot{X}_2\rangle/9$. The parameters taken are $\epsilon_1 = \epsilon_2 = 0.2$, $\beta = 0.05$, $\delta = 0.1$.

oscillations from one situation to the other. This result can be deduced from the dependence of the mean velocity on θ_2 and θ_1 in the analytical expression (3.17). In Fig. 3.5 the analytical results of Eq. (3.17) are also plotted. Although the results are obtained in a range of parameters where the perturbation theory is outside the range of validity (the limiting condition is not fulfilled), in both cases the sinusoidal behavior for the mean velocity is correctly reproduced.

Dependence on the damping: Harmonic Mixing

Another feature predicted by the CC theory is the dependence of the mean velocity on the damping coefficients. According to the standard behavior of point particles under friction, one should expect a monotonic dependence for the velocity as a function of the damping coefficient. However, abnormal behaviors like the existence of an optimal damping for the occurrence of net motion have been observed in some works related to the motion of soliton ratchets [26]. In this respect the authors of [31] have also pointed out the sharp contrast to other results [32] concerning the behavior of the mean velocity when the damping is changed.

Our expression for the mean velocity Eq. (3.16), deduced for the case $m = 2$, sheds light on the dependence of the dynamics with the damping. The dependence on the damping coefficient occurs in such a way that for some cases the damping coefficient β determines the direction of motion. In Fig. 3.6 are depicted three different situations where the velocity varies as a function of the damping. The first case depicted in Fig. 3.6a corresponds to the situation in which the velocity drastically decreases as β increases. Typically, this is the expected behavior. The second situation corresponds to the case when we can reverse the average velocity direction by changing the damping; as was pointed out in [32]. This can be deduced from Eq. (3.16) in which for certain relations between the phases one can change the sign of the velocity by varying the damping coefficient. Finally, for some cases there exist an optimal damping for the net motion (see Fig. 3.6c), i.e., there exist a damping for which the kink center moves with the largest possible absolute value of the mean velocity. It is also possible to find a value of the parameter

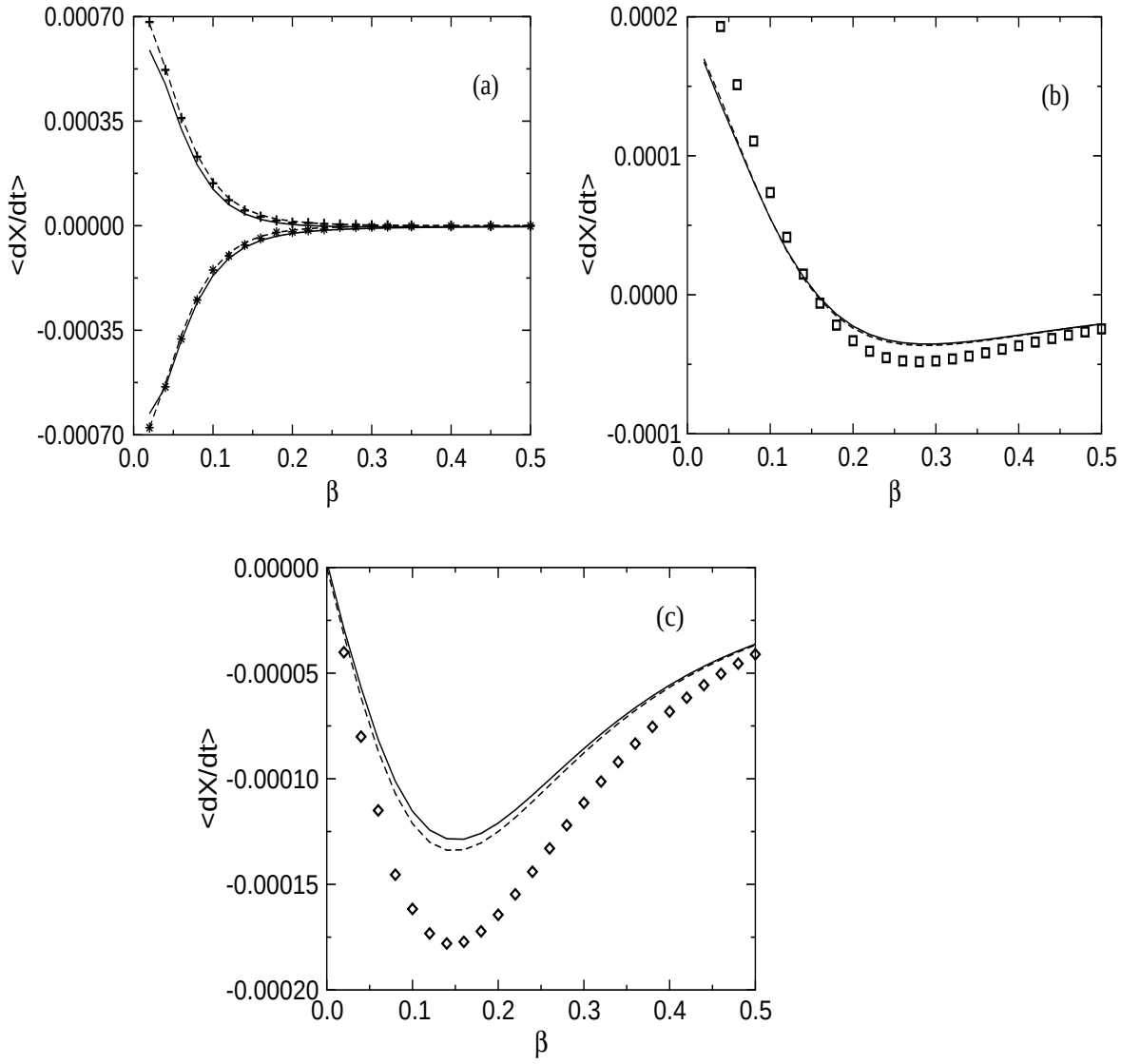

Figure 3.6: The average velocity as a function of damping. Panel (a):$\epsilon_1 = \epsilon_2 = 0.02$, $\delta = 0.1$, $\theta_1 = \pi/2$; Simulations: $\theta_2 = \pi$ $(*)$; $\theta_2 = 0$ $(+)$. Panel (b): $\epsilon_1 = 0.04$, $\epsilon_2 = 0.026$, $\delta = 0.25$, $\theta_1 = -\pi/2$, $\theta_2 = -\pi/2 + 0.8$; Simulations: $(\square)$. Panel (c): $\epsilon_1 = 0.04$, $\epsilon_2 = 0.026$, $\delta = 0.25$, $\theta_1 = -\pi/2$, $\theta_2 = -\pi/2$; Simulations: $(\Diamond)$. In all cases the solid line show results obtained from the numerical solution of Eqs. (3.3)-(3.4) and the dashed line correspond to the plot of Eq. (3.16) for the respective parameters of the simulations.

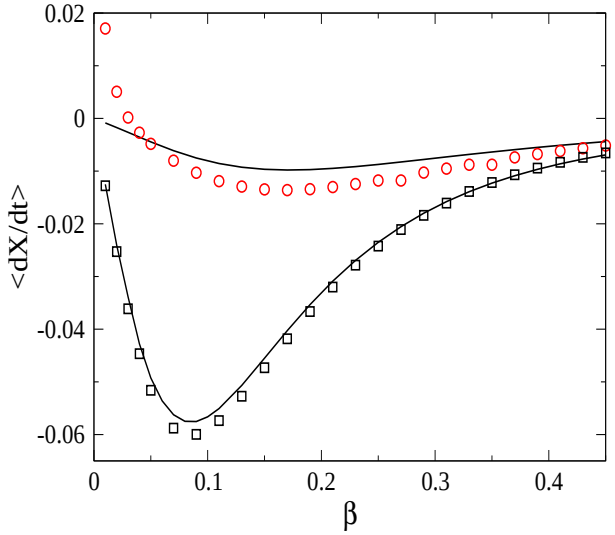

Figure 3.7: The average velocity as a function of damping for two different frequencies. $\delta = 0.1$ squares; $\delta = 0.25$ circles. The other parameters are $\epsilon_1 = 0.2$, $\epsilon_2 = 0.12$, $\theta_1 = -\pi/2$, $\theta_2 = -\pi/2$. In both cases the solid line show the results obtained from the numerical solution of Eqs. (3.3)-(3.4).

β that minimizes the expression (3.16) for a specific set of parameters.

Notice that we have taken small values for the amplitude of the force in order to compare our numerical results with the analytical expression, where very small values of the velocity are obtained. Our results may lead to an interpretation that the strong variations with β are characteristic for small values of the external force. In order to prove that such effect appears as an *intrinsic* characteristic feature of our models we have plotted in Fig. 3.7 the situation corresponding to the third case, for two different frequencies and higher amplitudes of the forces, because of the interest and connection with analogous problems discussed in the literature [26].

We observe from the picture that the agreement is still good and the behavior remains basically the same as in the smaller amplitude case. However, one notices that for a special situation, i.e., when the frequency is higher and for small damping, the simulation results disagree with the numerical computation of the CC equations. In fact, we observe that a reverse of current takes place in the simulations, contrary to the CC results.

In order to understand such a behavior it is necessary to analyze the action of the force on the system. The force contains δ and 2δ harmonics. For the sake of simplicity let us to analyze separately the action of the harmonics of the force. According to the expression (3.7) (see also previous studies [47, 48]) the kink width will sense the action of $P^2(t)$[2] with harmonics of frequencies 2δ and 4δ for the respective harmonics δ and 2δ of the force, i.e., that for a value of $\delta = 0.25$ we will have in $P^2(t)$ the harmonics with $2\delta = 0.5$ and $4\delta = 1$. Notice that the latter harmonic frequency coincides with the bottom of the phonons band. Moreover, according to our DFT diagrams, where a joint action of the harmonics takes place, one expects to find even higher harmonics, already inside the phonons band. Therefore for large enough force amplitude at small damping a strong excitation of phonons is expected. Accordingly the phonons dynamics can reverse the direction of motion. In this case our CC approach fails since it does not take into account the phonons contribution to the motion. Nevertheless, for very small values of the force, the phonons contribution is very small and therefore we obtain a behavior like that depicted in Fig. 3.6c where a good agreement with the

[2]Here it is important to remind that the momentum $P(t)$ contains the same harmonics as the force $f(t)$.

CC is observed.

On the other hand, for small frequencies of the harmonic components of the force like $\delta = 0.1$ and $2\delta = 0.2$, following our previous reasoning, the kink width will oscillate with the harmonics $2\delta = 0.1$ and $4\delta = 0.4$ which are far from the frequency range of the phonons band, even if we regard the next higher harmonics. Therefore the excitation of phonons is not significant which explains the nice agreement between the CC approach and the results from the simulations even for relatively large amplitudes of the forces.

In both cases we notice a decay of the absolute value of the average velocity for a high damping. Correspondingly, we have observed a decay of the kink width oscillations. This confirms the importance of the oscillations of the width in the translational motion of the kink.

Experimental confirmation

One of the areas where the sG equation presents a practical application is in the description of the propagation of fluxons along LJJ.

Recently, the motion of fluxons (a well known example of a topological kink) under two harmonic drivers was realized by Ustinov *et al.* [33]. The motion of fluxons gives rise to a dc voltage V across the junction, which is proportional to the fluxon mean velocity. In general an external dc current causes the fluxons to move with a certain velocity, which produces a dc voltage. However, even in the absence of dc bias is possible to find a non-zero voltage state, which clearly indicates the ratchet effect.

The ratchet-like effect induced by a biharmonic in the context of Josephson junctions is reflected in the non-zero voltage state in the absence of dc

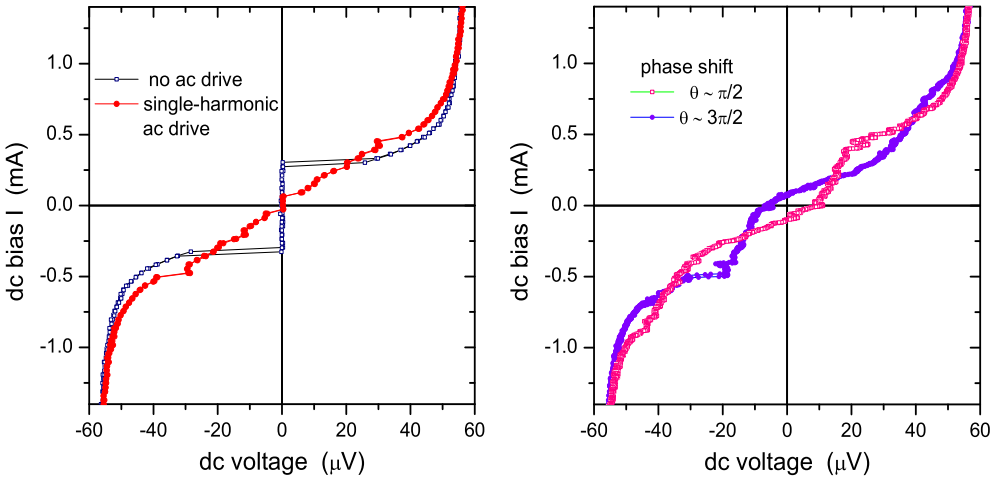

Figure 3.8: Left panel: Current-voltage characteristics of a single fluxon in annular Josephson junction with no ac drive (open symbols) and with single-harmonic ac drive (solid symbols) having the frequency $f_1 = 4.8$ GHz. Right Panel: A single-fluxon current-voltage characteristics. The fluxon is driven by bi-harmonic ac drive having the frequencies $f_2 = 2f_1 = 2.4$ GHz and power $P_2 = +4$ dB. The phase shift θ between the two harmonics is fixed to $\pi/2$ (open symbols) and $3\pi/2$ (solid symbols). Figure taken from [33].

bias.

In the sequel, we want to sketch the most important results obtained in this experimental work, without going into the experimental details (for details we refer to the original paper [33]). In order to confirm previous theoretical predictions the authors of Ref.[33] performed several experiments for different situations. They first measured the current-voltage characteristic of a fluxon in the junction with and without a microwave source. Subsequently,

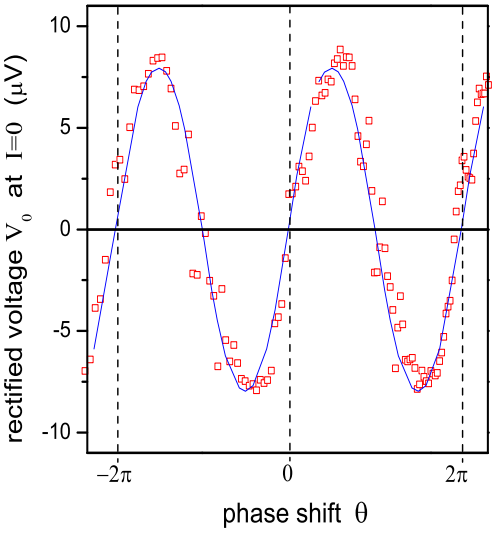

Figure 3.9: A dependence of the rectified dc voltage measured at zero dc bias current on the phase shift θ between the two harmonics of ac drive. $f_1 = 1.2\,\mathrm{GHz}$ and $f_2 = 2.4\,\mathrm{GHz}$ and power $P_2 = +4\,\mathrm{dB}$. Solid line shows results of numerical computation of the voltage for the dimensionless ac bias amplitudes $E_1 = E_2 = 0.1$. Figure taken from [33].

they measured the current-voltage characteristic of the fluxons under the influence of two microwave sources with 1 : 2 ratio for the frequencies. In this case, the authors electronically controlled the phase shift between the sources. The results of the two measurements are depicted in Fig. 3.8.
Two important features of this figure deserve to be highlighted. First from the left panel one observes that in the presence of only one harmonic, the voltage vanishes for a zero dc current. This confirms previous results about the nonexistence of net motion of a kink for this situation. On the other hand, in the right panel, a dc voltage at zero value of the dc current is ob-

served. This result reveals the occurrence of a directional motion of fluxons in the presence of harmonics driving with two frequencies, thus confirming previous theoretical results.

Later, in order to corroborate previous theoretical predictions about the dependence on the relative phase of the force harmonics, they measured the voltage varying the relative phases. They also performed numerical simulations in order to compare with the experimental results. For that purpose they used a dimensionless sG equation, like Eq. (3.1) with the biharmonic force $f(t) = \epsilon_1 \sin(\delta t) + \epsilon_2 \sin(m\delta t + \theta)$ as ac drivers for the description of the fluxons propagation. Here $\delta = f/f_p$ and $\epsilon_i \sim \sqrt{P_i}$ with $i = 1, 2$; $f_p = 120$ GHz being the plasma frequency and P_i the respective ac power levels for the sources. This representation of the force is equivalent to the choice $\theta_1 = 0$ and $\theta_2 = \theta$ in our notation. For the dimensionless equation with the parameters $\epsilon_1 = \epsilon_2 = 0.1$, $\beta = 0.05$ and $\delta = 0.01$, they obtained the picture depicted in Fig. 3.9. Notice the sinusoidal dependence of the voltage on the relative phase, in line with our previous results.

3.2.2 ϕ^4 model

The phenomenology for the existence of a directed motion of kinks in the ϕ^4 model is the same as in the sG model. We observe in Fig. 3.10 the same spectrum of frequencies as was in the sG model (see Figs. 3.1 and 3.2) obtained for the different values of m. We also performed additional numerical simulations in order to support the results on the kink dynamics. As before, we found in the case $m = 2$ and $m = 4$ unidirectional motion, in contrast to $m = 3$ where an oscillatory motion takes place. Also the phase

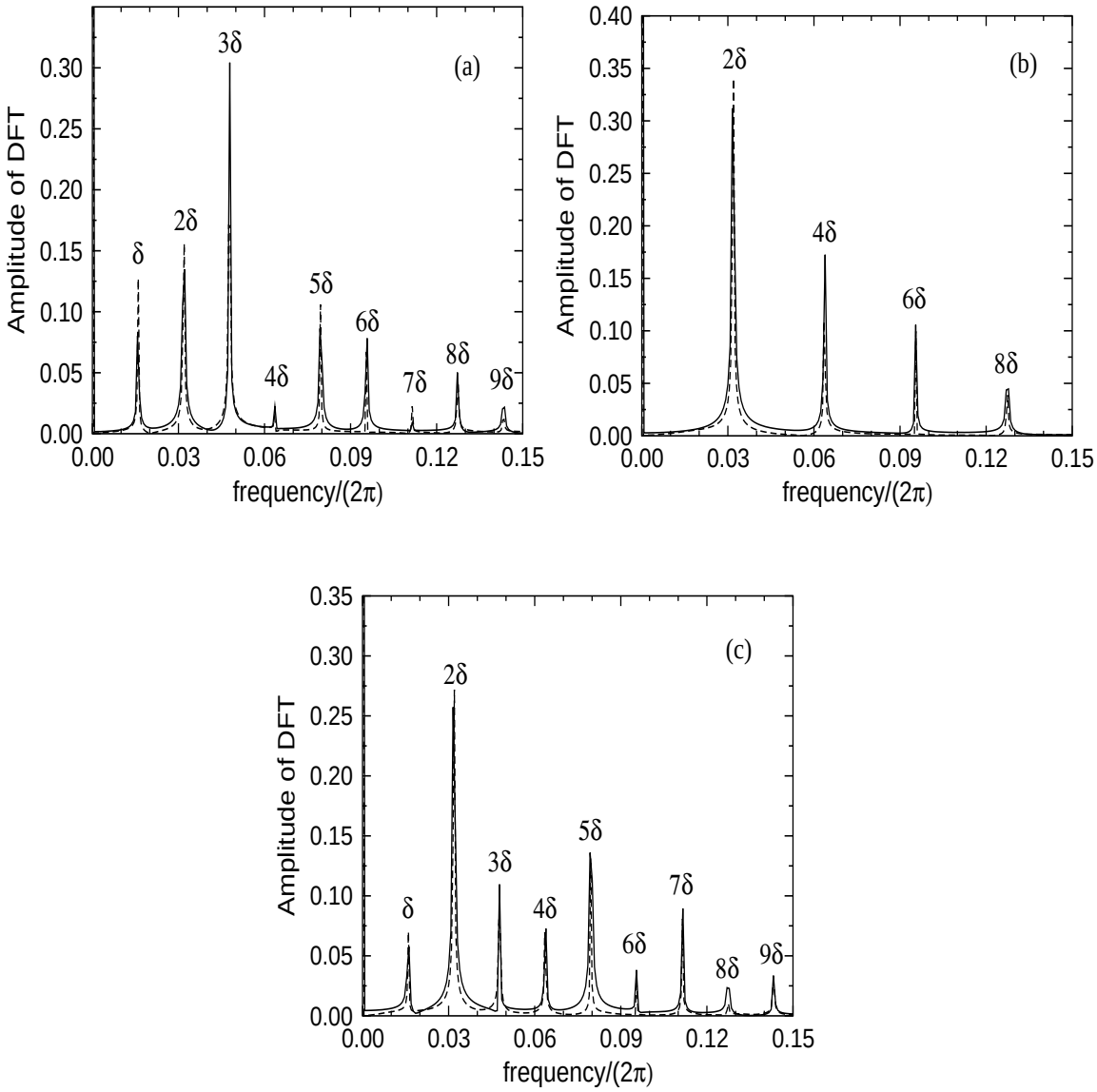

Figure 3.10: Discrete Fourier Transform of the kink width. Panel (a): $m = 2$; Panel (b): $m = 3$; Panel (c): $m = 4$. Solid line: Simulations of Eq. (3.2). Dashed line: numerical integration of the CC equations.

dependence of the mean velocity was similar to the sG case.

However, for the ϕ^4 model higher velocities compare to the sG system are obtained, i.e., the mobility is enhanced. This is observed in Fig. 3.11, where the values for the mean velocity are greater than their counterparts depicted in Fig. 3.6 for the same parameters. Such a behavior can be deduced from the relation between the effective parameters for the collective coordinate equation (3.3), specifically from the relation between the normalized effective amplitudes[3] for the sG and ϕ^4 models. These amplitudes depend on the topological charge and the effective mass as $A_{ef}^{sG} = q^{sG}A^{sG}/M_0^{sG}$ and $A_{ef}^{\phi^4} = q^{\phi^4}A^{\phi^4}/M_0^{\phi^4}$, for the respective systems. Because of the inequality $q^{sG}/M_0^{sG} < q^{\phi^4}/M_0^{\phi^4}$ (see Table 3.1) we conclude consequently that for the same amplitude of the ac force, i.e., $A^{\phi^4} = A^{sG}$, a higher mobility for the ϕ^4 should takes place. Moreover, we have observed that for $m = 2$ such differences in the mobility become more accentuated at low damping values. This behavior finds an explanation in the possible phonons contribution to the dynamics of the system, especially if we take into account the fact that according to our previous analysis of the amplitude of the forces in the ϕ^4 case a larger energy is deposited into the system than in the sG case.

[3]The normalization is realized by dividing Eq. (3.3) by the effective mass.

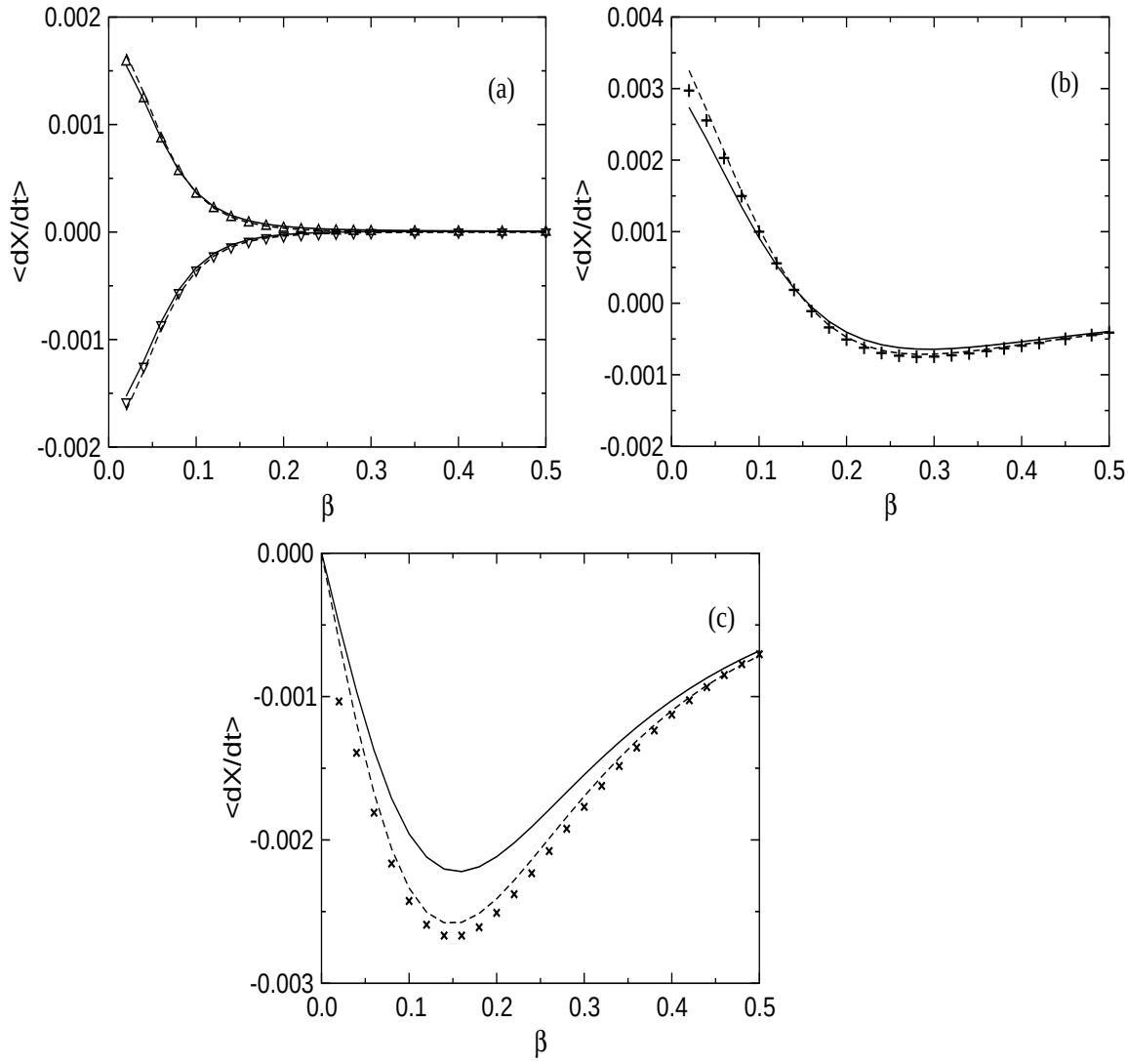

Figure 3.11: The averaged kink velocity as a function of damping. Panel (a):$\epsilon_1 = \epsilon_2 = 0.02$, $\delta = 0.1$, $\theta_1 = \pi/2$. Simulations: $\theta_2 = \pi$ ($\triangledown$); $\theta_2 = 0$ ($\triangle$). Panel (b): $\epsilon_1 = 0.04$, $\epsilon_2 = 0.026$, $\delta = 0.25$, $\theta_1 = -\pi/2$, $\theta_2 = -\pi/2 + 0.8$. Simulations: (+). Panel (c): $\epsilon_1 = 0.04$, $\epsilon_2 = 0.026$, $\delta = 0.25$, $\theta_1 = -\pi/2$, $\theta_2 = -\pi/2$; Simulations: (x). In all cases the solid lines show results obtained from the numerical solution of Eqs. (3.3)-(3.4) and the dashed lines correspond to the plot of the Eq. (3.16) for the respective parameters of the simulations.

Chapter 4

Ratchet: Spatial symmetry-breaking (inhomogeneities)

In this chapter, we present a simple design for a spatially extended ratchet. The new design implies a ratchet device consisting of a lattice of *point-like inhomogeneities*. For this system net motion of solitons arises from the interplay between disorder[1] and nonlinearity of the nonlinear spatially extended system [49]. This makes the model more realistic for the description of different phenomena and at the same time suitable for the study of different ratchet mechanisms.

The study is mainly devoted to the analysis of a rocking ratchet since we consider a system driven by an ac force. Nevertheless, at the end of the chapter, a diffusive ratchet is implemented in order to demonstrate the

[1] By disorder we refer here to defects across the lattice.

possible applicability of other ratchet mechanisms. In all cases the dynamic, as we will show, is very similar to that exhibited by point particles.
Concerning the rocking ratchet system we would like to emphasize that, in contrast to the previous ratchet model, this ratchet system works irrespective of the symmetry of the ac force. We chose one harmonic driver for the study of the rocking ratchet mechanism.

We focus our analysis specifically on nonlinear Klein-Gordon systems like sine-Gordon (sG) and ϕ^4 models because of their important applications. In the case of the sG model the study is motivated from its potential application in superconducting devices such as long Josephson Junctions (LJJ). For the ϕ^4 model, the motivation stems from research on models of energy propagation along microtubule filaments inside a cell [51]. This application is specially interesting in view of the possible connection to the dynamics of transport in molecular motors in biological systems, with features similar to those of solitons as extended objects.

The mechanism, we will present, is very general and it can be also applied to other soliton-bearing systems where the interaction of kinks with point-like inhomogeneities is similar to that occurring in the sG [52, 53, 54], to mentioning an example.

4.1 Ratchet model and transport

Kink dynamics in the presence of inhomogeneities exhibits interesting and qualitatively different behaviors compared to the homogeneous case, depending among other factors on the interplay between the inhomogeneities and the

nonlinearity [52, 53]. The generation of net motion using a lattice of point-like inhomogeneities is a good example of such a non-trivial phenomenon. The model can be defined in principle for any nonlinear Klein-Gordon type system. In order to be specific, for our analysis we formulate the model as follows:

$$\phi_{tt} + \beta\phi_t - \phi_{xx} + \frac{\partial \widetilde{U}}{\partial \phi}[1 + V(x)] = A\sin(\omega t + \delta_0), \tag{4.1}$$

where $\widetilde{U}(\phi)$ is the potential for the nonlinear Klein-Gordon equations and $A\sin(\omega t + \delta_0) \equiv f(t)$ is an external ac force with the parameters A, ω and δ_0 representing the amplitude, frequency and phase of the periodic force, respectively. In particular, for the ϕ^4 and sG models the corresponding nonlinear potentials are $\widetilde{U}(\phi) = \frac{1}{4}(\phi^2 - 1)^2$ and $\widetilde{U}(\phi) = [1 - \cos(\phi)]$.
We choose $V(x)$ to be spatially periodic, where the unit cell contains as a basis an asymmetric array of delta function peaks (inhomogeneities) in order to produce a ratchet-like phenomenon. The unit cell, of length L, is defined by three inhomogeneities with the same intensity, the first one located at the beginning of the cell, the second one at a distance a from the first one, and the third one at a distance b from the second one as sketched in Fig. 4.1. However, different configurations to that shown in Fig. 4.1, can be implemented in order to break the spatial symmetry, as to be discussed at the end of this chapter.

The mathematical expression corresponding to the array of delta peaks depicted in Fig. 4.1 is given as:

$$V(x) = \epsilon \sum_n [\delta(x - x_1 - nL) + \delta(x - x_2 - nL) + \delta(x - x_3 - nL)], \tag{4.2}$$

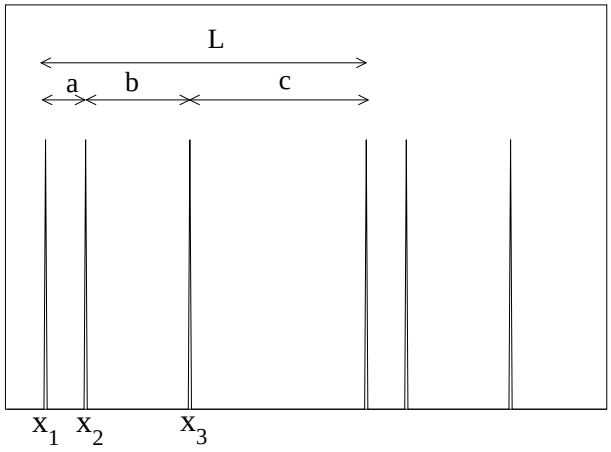

Figure 4.1: Schematical representation of an asymmetric array of point-like inhomogeneities, that repeats periodically with period L.

where the parameters (a, b, c) are chosen to be comparable to the static kink width in absence of inhomogeneities l_0. In addition the parameters should fulfill the conditions $a, b < c$ with $a \neq b$, where $L = a + b + c$, $a = x_2 - x_1$, $b = x_3 - x_2$ and $c = L + x_1 - x_3$, with $x_1 < x_2 < x_3$. For our study we have taken $\epsilon > 0$, where in the case of sG, specifically for LJJ the point-like inhomogeneities represent microshorts [55, 56]. However, the case $\epsilon < 0$ deserves attention as well, to which particularly for the sG model many investigations have been devoted [57].

The choice of three inhomogeneities in the unit cell is motivated by biological polymers like DNA where the existence of three bases per codon seems to be the ideal configuration for the occurrence of net transport [58]. In principle it is possible to get unidirectional motion by using an array whose configuration presents more than three inhomogeneities per period L if the distances between the delta functions are of the same length scale as the kink‘s width (otherwise a qualitatively different behavior could arise as demonstrated e.g. in [53]). However, the inclusion of more inhomogeneities per unit cell diminishes the efficiency of the transport in terms of the speed

as we will demonstrate later.

In contrast to the case of point particles, where a motion through point-like inhomogeneities (delta functions) is physically meaningless, we deal with kinks (extended objects) with a well determined width. The width is an intrinsic characteristic feature of these nonlinear excitations and correspondingly the competition between the width and the distance between the inhomogeneities is crucial for the kink motion. Interference effects induced by the inhomogeneities [54] create an effective potential for the motion of the kink center, where the locations of the inhomogeneities determine the direction of motion. For the particular configuration of three inhomogeneities per unit cell, directional motion takes place only under the condition $a \neq b$. This is demonstrated in the top panel of Fig. 4.2, where results of simulations of Eq. (4.1) in the sG case with different values of a and b are depicted. This picture shows clearly that our ratchet device is a generic rectifier. The rectification process results from the interaction of the kink with the inhomogeneities similar to what occurs for single particles in a ratchet potential. In addition, as in ratchet systems for point particles, the directional motion of the kink center takes place only for certain values of the amplitude of the ac force (see bottom panel of Fig. 4.2), a behavior that depends on the ac force frequency. A detailed picture of the dynamics of the mean velocity[2] for the kink center as a function of the ac force amplitude for different frequencies can be observed in Fig. 4.3. Another distinctive feature of this ratchet

[2]The $\langle dX/dt \rangle$ means the average of the velocities over one period of time. In order to be accurate, it is very convenient to make the average over many time periods instead of averaging the velocities over one period. Another easy way and that we have mainly used is by means of the computation of the slope for the curve trajectory versus time.

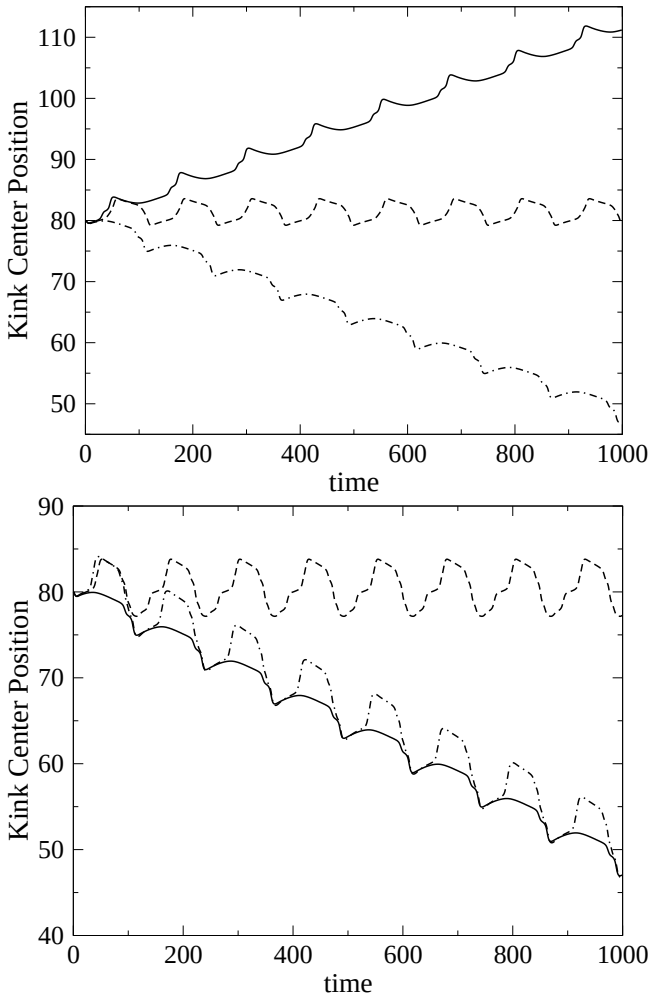

Figure 4.2: Simulations of Eq. (4.1) for sG case: Position of kink center vs time: Top panel: Different arrays with the same amplitude of the force $A = 0.35$. $x_1 = 0.5$, $x_2 = 1.8$, $x_3 = 2.3$ ($a > b$) (solid line); $x_1 = 0.5$, $x_2 = 1.4$, $x_3 = 2.3$ ($a = b$) (dashed line); $x_1 = 0.5$, $x_2 = 1$, $x_3 = 2.3$ ($a < b$) (dashed-dotted line). Bottom panel: For different amplitudes of the ac force: $A = 0.35$ (solid line); $A = 0.45$ (dashed line); $A = 0.50$ (dashed-dotted line) with the array $x_1 = 0.5$, $x_2 = 1$, $x_3 = 2.3$. The other parameters used are $\beta = 1$, $\omega = 0.05$, $\epsilon = 0.8$, $\delta_0 = \pi$ and period $L = 4$.

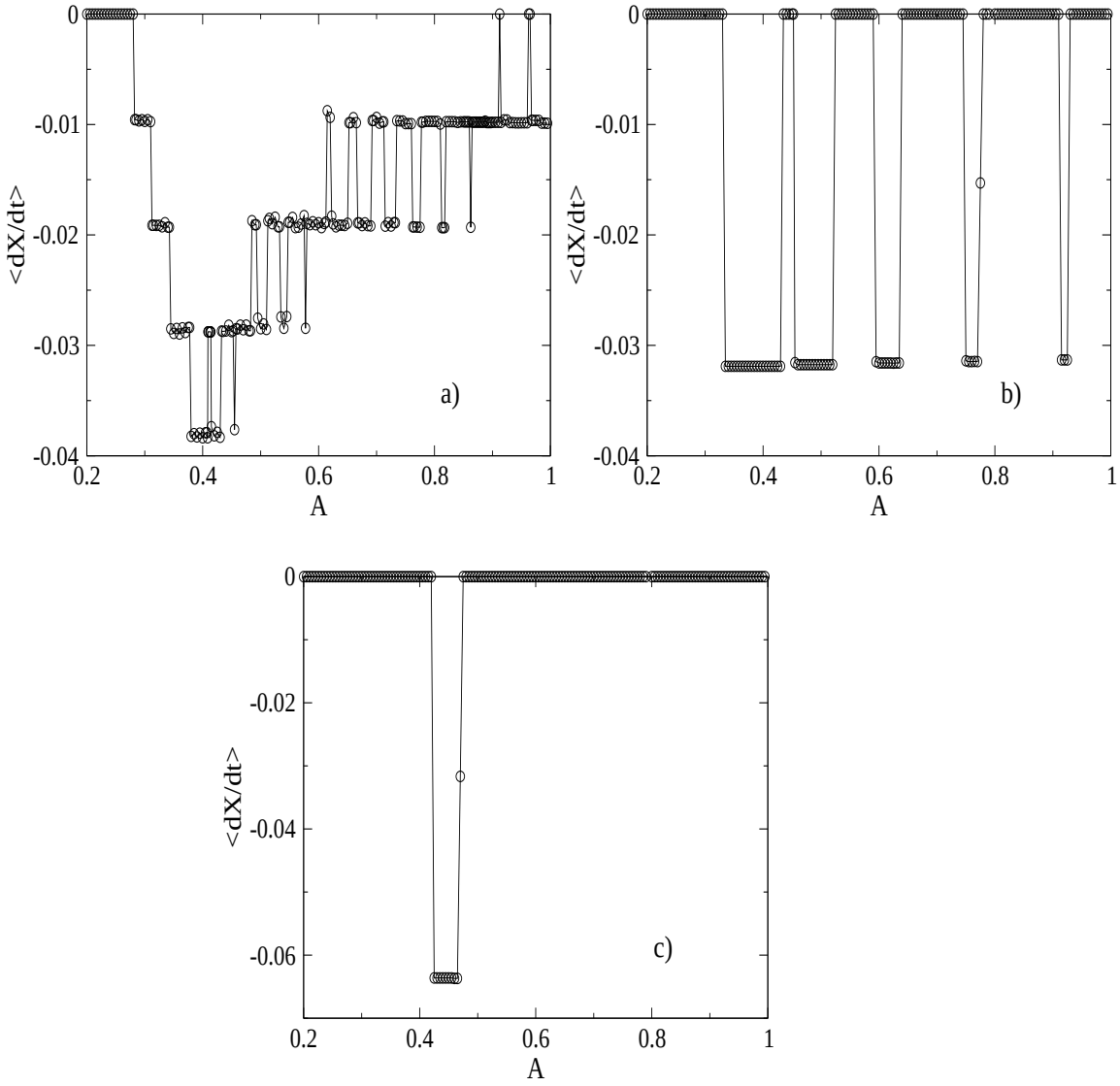

Figure 4.3: sG: Mean kink velocity $\langle dX/dt \rangle$ vs driving amplitude A for different frequencies: a) $\omega = 0.015$, b) $\omega = 0.05$, c) $\omega = 0.1$. The other parameters are $x_1 = 0.5$, $x_2 = 1$, $x_3 = 2.3$, $\epsilon = 0.8$, $\beta = 1$ and period $L = 4$. Circles: direct numerical simulation of Eq. (4.1), with the sG potential. The line is a guide to the eye.

system is the stair-step structure that shows the mean velocity as a function of the amplitude of the ac force for relatively low frequencies close to the adiabatic limit, i.e. for $\omega \ll 1$ (see e.g. Fig. 4.3a). The peak observed in the figure 4.3a indicates the amplitude of the driving force for which our ratchet reaches a maximum efficiency.

A similar behavior for the ϕ^4 case is observed in Fig. 4.4. In this case the motion takes place in a different range of amplitudes of the ac force. A discussion of the scaling relation between sG and ϕ^4 systems will be given further below. In addition, for the smallest frequency an increment of the absolute value of the mean velocity with respect to sG system is noticed.

We have restricted ourselves to the overdamped case by taking $\beta = 1$, where the inertial effects are small, thus reducing the generation and propagation of phonons. The kink center moves then on a tilted effective potential due to the external ac force. In this regime transients due to the initial conditions quickly die out, contrary to what happens in the underdamped regimen where the initial conditions can determine the motion [59]. However, the overdamped regime is not always suitable for applications. Concerning applicability, a brief analysis of the dynamics when varying the damping coefficient will be shown later on. For the integration of Eq. (4.1) we have used a Strauss-Vázquez numerical scheme (see details in Appendix B) with free boundary conditions and spatial and temporal steps $\Delta x = 0.1$ and $\Delta t = 0.01$ respectively. We have validated our results with two different spatial steps $\Delta x = 0.05$ and $\Delta x = 0.02$. The spatial interval for the simulations was done for $[-30, 150]$ with inhomogeneities arranged periodically according to our unit cell in $[0, 120]$. We have used the following step representation for the

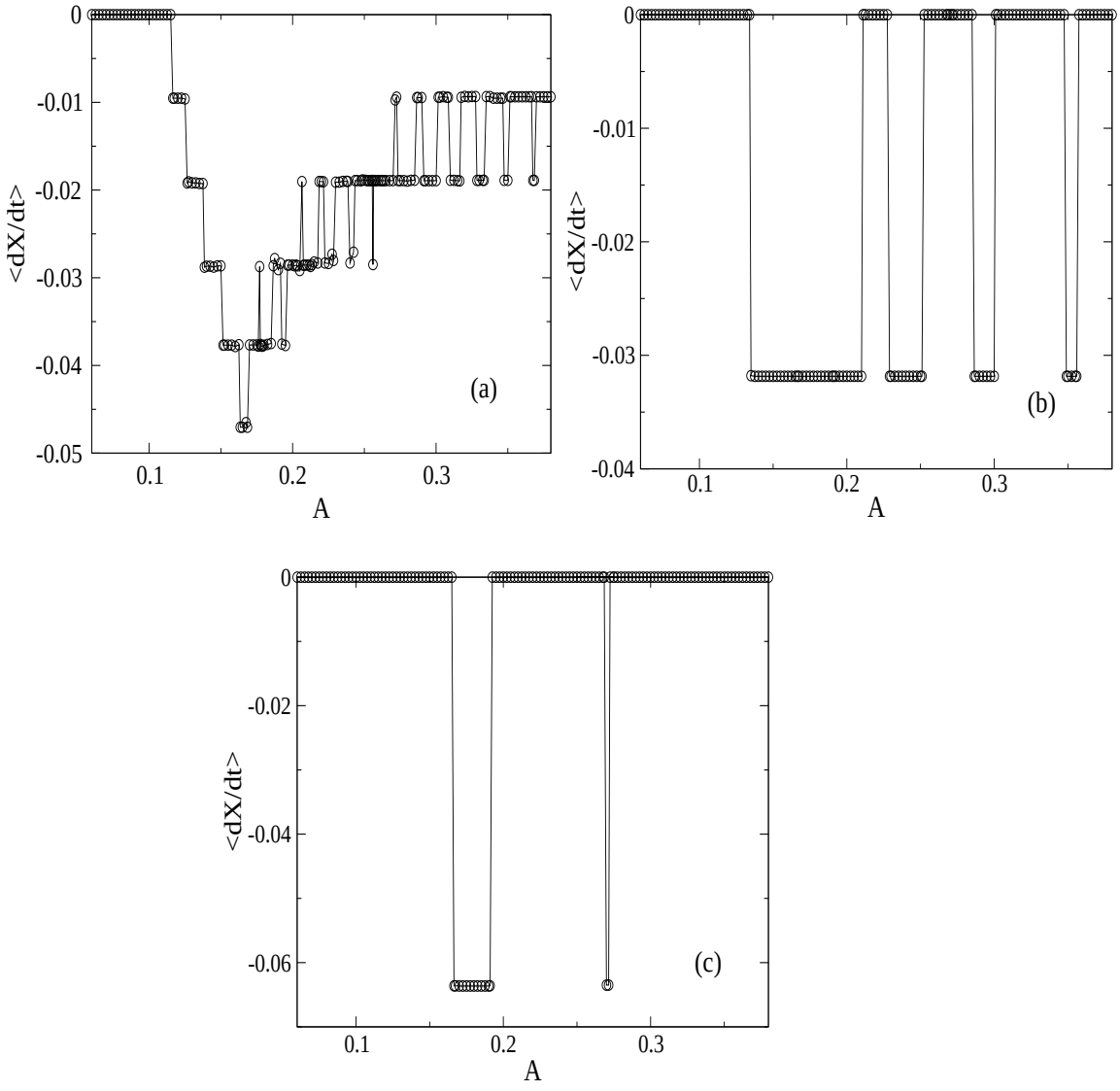

Figure 4.4: ϕ^4: Mean kink velocity $\langle dX/dt \rangle$ vs driving amplitude A for different frequencies: a) $\omega = 0.015$, b) $\omega = 0.05$, c) $\omega = 0.1$. Other parameters are the same as in Fig. 4.3. Circles: direct numerical simulation of Eq. (4.1), with the corresponding potential. The line is a guide to the eye.

delta function

$$\delta(x - x_c) \to \begin{cases} 1/\Delta x, & |x - x_c| < \Delta x/2 \\ 0, & \text{otherwise.} \end{cases} \tag{4.3}$$

This representation is not unique but is presumably the simplest form to implement in numerics (see e.g. [52, 54]). A simple derivation of the discrete part of the PDE using the method of finite elements (see Appendix B) shows that it is the suitable discrete representation for the delta function.

4.1.1 Collective coordinate approach

As a first step to justify our choice of the perturbative term $V(x)$, we present a simple collective-coordinate analysis of its effect on the soliton dynamics. The idea of this well-known approximate technique for treating soliton-bearing equations is to assume that perturbations affect mostly the motion of the soliton center (and/or other parameters, as we will see below). This leads to a drastic reduction of the number of degrees of freedom by deriving an effective equation for the corresponding collective coordinate (see e.g. [9] for a recent review and further references). One of the simplest procedures to derive equations for the collective coordinate is by means of the conservations laws, making use of the so-called adiabatic approach, first proposed by McLaughlin and Scott [55].

For obtaining the equation of motion we exploit the close relation between the calculus of variations and conservation laws. In order to do so we rewrite Eq. 4.1 in a more general way as

$$\phi_{tt} - \phi_{xx} + \frac{\partial \widetilde{U}}{\partial \phi} = F(x, t, \phi, \phi_t, \phi_x), \tag{4.4}$$

where the perturbations are contained in the r.h.s term of the equation.

Starting with the total momentum expression

$$P(t) = -\int_{-\infty}^{\infty} dx \;\; \phi_t \phi_x, \tag{4.5}$$

we arrive immediately to

$$\frac{dP}{dt} = -\int_{-\infty}^{\infty} dx \;\; (\phi_{tt}\phi_x + \phi_t \phi_{xt})\,. \tag{4.6}$$

Then substituting Eq. (4.4) into Eq. (4.6) we obtain the expression

$$\frac{dP}{dt} = -\int_{-\infty}^{\infty} dx \;\; \left[\phi_{xx}\phi_x - \frac{\partial \widetilde{U}}{\partial \phi}\phi_x + \phi_t \phi_{xt} + F(x,t,\phi,\phi_t,\phi_x)\phi_x\right]. \tag{4.7}$$

After suitable rearrangement, the latter expression can be reformulated as

$$\frac{dP}{dt} = -\int_{-\infty}^{\infty} dx \, \frac{\partial}{\partial x}[\frac{1}{2}\phi_t^2 + \frac{1}{2}\phi_x^2 - \widetilde{U}(\phi)] - \int_{-\infty}^{\infty} dx \;\; F(x,t,\phi,\phi_t,\phi_x)\phi_x. \tag{4.8}$$

Here we have exploited the interchangeability of the derivatives, i.e., $\phi_{xt} = \phi_{tx}$, which is not true in the case of considering delta functions as inhomogeneities due to the singularities introduced. However, in our approximation, we will use only the undistorted kink-like shape as solution so that this problem is circumvented.

Under the same assumption it is straightforwardly derived that the first integral of the r.h.s of Eq. (4.8) vanishes, taking into account that the function $\widetilde{U}(\phi)$ is zero in the ground states. Consequently the equation of motion can be expressed as:

$$\frac{dP}{dt} = -\int_{-\infty}^{\infty} dx \;\; F(x,t,\phi,\phi_t,\phi_x)\phi_x. \tag{4.9}$$

For obtaining the equation of motion in terms of the kink center coordinate we introduce the *Ansatz*

$$\phi(x,t) = \phi^{(0)}[\gamma(x - X(t))] = 4\arctan\left(\exp\left[\gamma(x - X(t))\right]\right), \tag{4.10}$$

as solitonic solution of the Eq. (4.4) with $\gamma = 1/\sqrt{1-\dot{X}^2}$. Notice that our ansatz corresponds to an undistorted kink[3] whose variables position and velocity are the quantities which pick up the effects of the external perturbations.

Then inserting the ansatz into Eq. 4.9 and taking into account the expression for the momentum given by

$$P(t) = -\int_{-\infty}^{\infty} dx \;\; \phi_t \phi_x = \gamma M_0 \dot{X}, \tag{4.11}$$

we finally obtain the equation of motion

$$\gamma^3 M_0 \ddot{X} = -\int_{-\infty}^{\infty} dx \;\; F(x,t,\phi^{(0)},\phi_t^{(0)},\phi_x^{(0)}) \;\; \phi_x^{(0)}, \tag{4.12}$$

where $M_0 = 8$ is the mass or the energy of the kink at rest.

Then Eq. 4.12 with the perturbation $F(x,t,\phi,\phi_t,\phi_x) = -\beta\phi_t - \dfrac{\partial\widetilde{U}}{\partial\phi}V(x) + f(t)$ becomes

$$\gamma^3 M_0 \ddot{X} + \gamma M_0 \dot{X} = -qf(t) + \int_{-\infty}^{\infty} dx \;\; \frac{\partial\widetilde{U}}{\partial\phi} V(x)\phi_x^{(0)}. \tag{4.13}$$

By the use of $\phi_x^{(0)} = -\phi_X^{(0)}$ we get the expression

$$\gamma^3 M_0 \ddot{X} + \gamma M_0 \dot{X} = -qf(t) - \int_{-\infty}^{\infty} dx \;\; \frac{\partial\widetilde{U}}{\partial\phi} V(x)\phi_X^{(0)}. \tag{4.14}$$

[3]The only deformation of the kink is a Lorentz contraction due to the relativistic effects.

Then taking into account the expression for $V(x)$ from Eq. 4.2 and after some manipulations Eq. 4.14 transforms into

$$\gamma^3 M_0 \ddot{X} + \beta\gamma M_0 \dot{X} = -qf(t) - \frac{\partial U}{\partial X}. \tag{4.15}$$

We can see that this result is identical to that obtained in the Appendix A for $D = 0$ using the GTWA method. The latter method has the advantage that it allows to get directly the expression for the effective potential avoiding some assumptions made in the above procedure.

For the non-relativistic approximation $\dot{X}^2 \ll 1$ we get the equation

$$M_0 \ddot{X} + \beta M_0 \dot{X} = -qf(t) - \frac{\partial U}{\partial X}, \tag{4.16}$$

where the effective potential is given by

$$U(X) = 2\epsilon \sum_n \left[\frac{1}{\cosh^2(X - x_1 - nL)} + \frac{1}{\cosh^2(X - x_2 - nL)} + \frac{1}{\cosh^2(X - x_3 - nL)} \right]. \tag{4.17}$$

The expression (4.17) is depicted in Fig. 4.5a for the perturbation $V(x)$ defined in Eq. (4.2) with the three delta peaks introduced in the previous section, with positions at $x_1 = 0.5$, $x_2 = 1$, $x_3 = 2.3$ and with period $L = 4$. This corresponds to an asymmetric potential characteristic for ratchet systems as it can be observed from the figure 4.5a. In fact, equation (4.15) is the same as that for a point particle in a rocking ratchet. As in the simulations we restrict ourselves to the overdamped case where there is no dependence on the initial conditions in the dynamics.

Due to the tilt of this ratchet potential, one expects a soliton movement towards the left side, in agreement with the simulations results. We can also

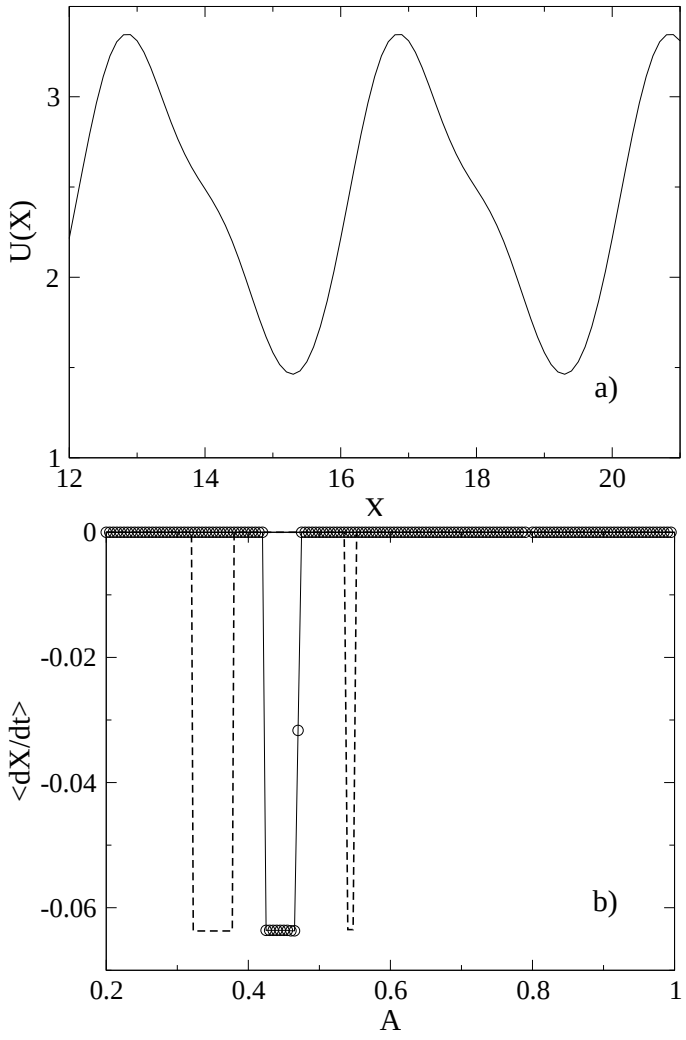

Figure 4.5: sG: a) Effective potential for the kink center within the adiabatic approach, originating from the perturbation $V(x)$ defined in Eq. (4.2) with $\epsilon = 0.8$, $x_1 = 0.5$, $x_2 = 1.$, $x_3 = 2.3$ and period $L = 4$. b) Mean kink velocity $\langle dX/dt \rangle$ vs driving amplitude A for the frequency $\omega = 0.1$. Circles: direct numerical simulation of Eq. (4.1), the line being only a guide to the eye; dashed line: adiabatic approach.

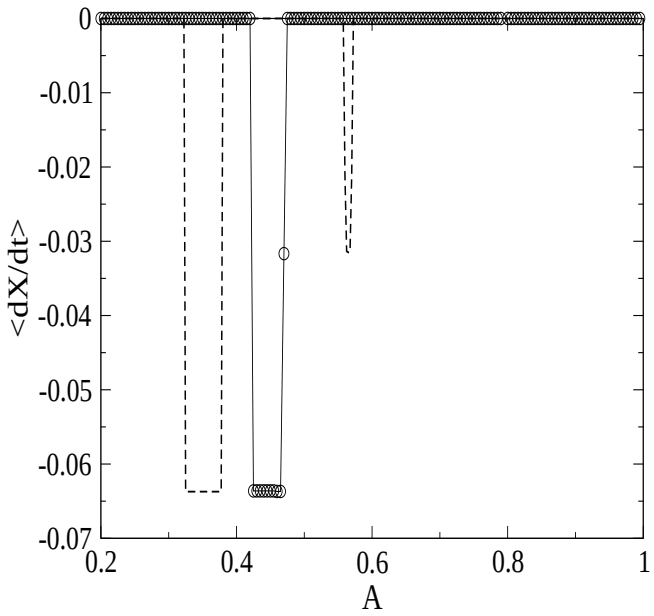

Figure 4.6: sG: Mean velocity vs driving amplitude A for the frequency $\omega = 0.1$ Circles: direct numerical simulation of Eq. (4.1) (sG case), the line being only a guide to the eye; dashed line: 1- collective variable, relativistic approach, Eq.4.15. We have used the same parameters as in Fig. 4.5.

estimate from the slopes of the potential the amplitude range of the force for which the motion reaches a maximum efficiency. With such elements one can understand the underlying physics of this ratchet system in the simplest way, connecting it to the known rocking ratchet for point particles.

However, the agreement with the collective coordinate theory presented above is not quite satisfactory because neither the number of windows nor their locations are correctly predicted, see Fig. 4.5b. Such a result is expected taking into account that our first proposal for the CC does not consider the deformation of the kink under relatively strong perturbations. Even the inclusion of the possible relativistic effects for high values of the ac force does not change the previous situation (see Fig. 4.6).

A deeper look at the simulations explain the main reason for this discrep-

ancy, that the soliton shape changes during its motion in the inhomogeneities array (namely, its width is oscillating with a dynamics determined by the interaction with the inhomogeneities). This feature can not be accounted for within the framework of our theory above and therefore we set out to improve our scheme in the following.

A good candidate for explaining the interaction of the kink with the inhomogeneities is the formulation of the CC introduced in the previous chapter, which considers a coupling between the translational mode and the kink width dynamics. In the present case the deformation of the kink is mainly caused by the interaction with the inhomogeneities rather than with the ac-field.

The new approach whose collective variable equations describe the dynamics of the two main degrees of freedom of the system 4.1 (see Appendix A for details) take the form

$$M_0 l_0 \frac{\ddot{X}}{l} + \beta M_0 l_0 \frac{\dot{X}}{l} - M_0 l_0 \frac{\dot{X}\dot{l}}{l^2} = -\frac{\partial U}{\partial X} - qf(t), \tag{4.18}$$

$$\alpha M_0 l_0 \frac{\ddot{l}}{l} + \beta\alpha M_0 l_0 \frac{\dot{l}}{l} + \frac{1}{2} M_0 l_0 \frac{\dot{X}^2}{l^2} - \frac{1}{2}\alpha M_0 l_0 \frac{\dot{l}^2}{l^2} = -\frac{\partial U^{int}}{\partial l} - \frac{\partial U}{\partial l}, \tag{4.19}$$

where the internal potential energy of the kink is

$$U^{int} = \frac{1}{2} M_0 \left(\frac{l_0}{l} + \frac{l}{l_0} \right). \tag{4.20}$$

In particular for the sG case $M_0 = 8$, $l_0 = 1$, $\alpha = \pi^2/12$, $q = 2\pi$ and the

effective potential is given by

$$U(X,l) = 2\epsilon \sum_n \left[\frac{1}{\cosh^2[(X - x_1 - nL)/l]} + \frac{1}{\cosh^2[(X - x_2 - nL)/l]} + \frac{1}{\cosh^2[(X - x_3 - nL)/l]} \right]. \quad (4.21)$$

As we can see from the previous equations the kink width dynamics is coupled to the motion of the center of the kink. Therefore, changes in the kink width directly affect the translational motion. It is possible to observe, for instance, that decreasing the kink width decreases the effective ac force, making necessary to increase the amplitude of the ac force in order to compensate such an effect. This is an important factor that explains in part the shift observed in the locations of the windows of motion of the simulations with respect to those obtained from the 1-CC approach. Another relevant conclusion is the feedback between the effective potential landscape and the kink width, determined in turn by the potential. In this fashion, the 2-CC approach reflects the non-trivial interaction of the kink with the inhomogeneities, which is otherwise known to exhibit many counterintuitive phenomena [54].

In fact, the picture observed in Fig. 4.7, shows that the comparison between our improved collective coordinate theory and the simulations is quite satisfactory, as the window numbers and locations are correctly estimated, thus confirming our previous analysis.

We thus see that although the point particle approximation (collective coordinate $X(t)$) is sufficient to predict the appearance of a ratchet phenomenon, the detailed dynamics requires the inclusion of an additional degree of freedom $l(t)$ arising from the fact that we have a spatially extended

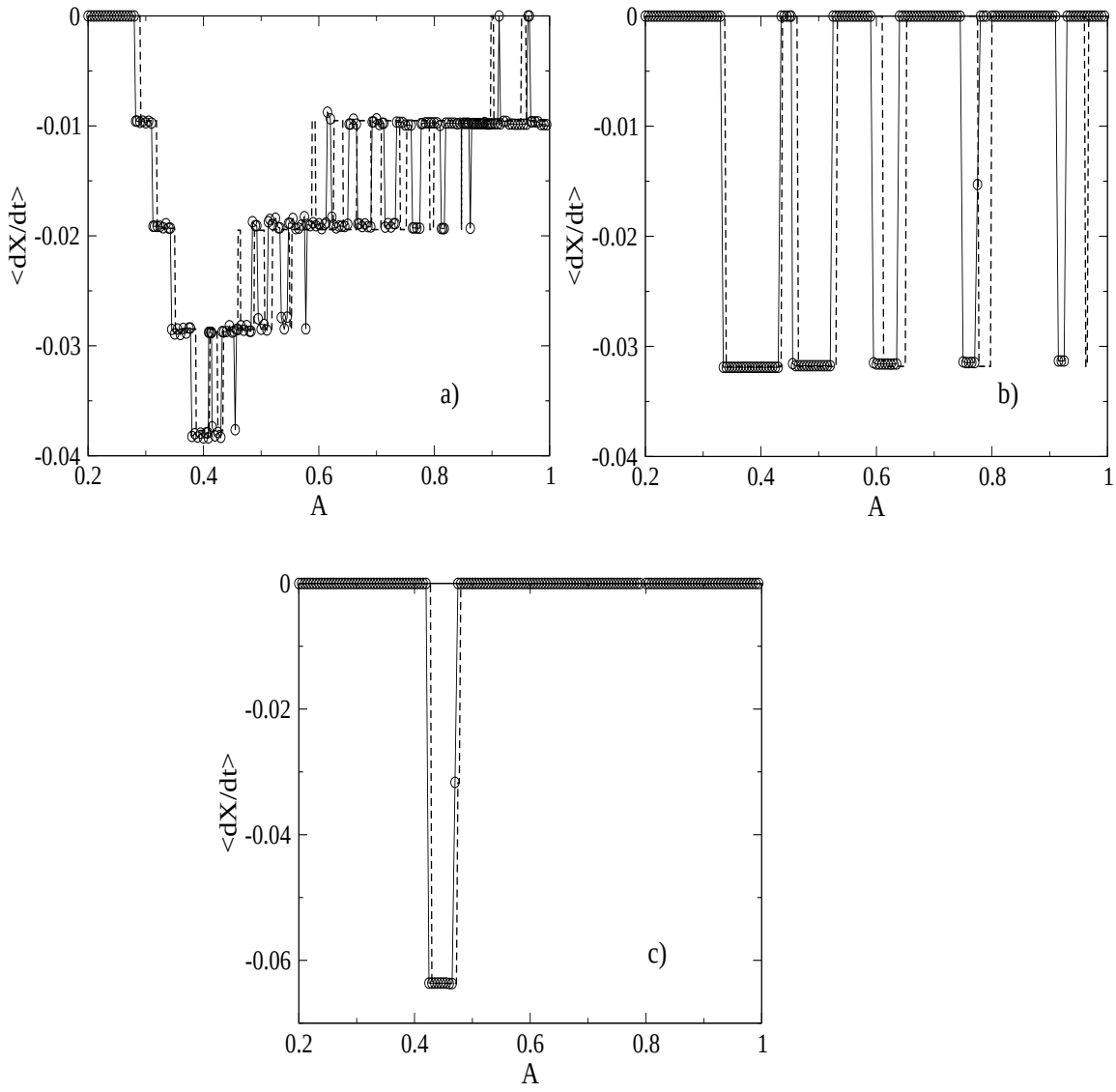

Figure 4.7: Mean kink velocity $\langle dX/dt \rangle$ vs driving amplitude A for different frequencies: a) $\omega = 0.015$, b) $\omega = 0.05$, c) $\omega = 0.1$. Other parameters are the same as in Fig. 4.3. Circles: direct numerical simulation of Eq. (4.1), the line being only a guide to the eye; dashed line: improved collective coordinate theory.

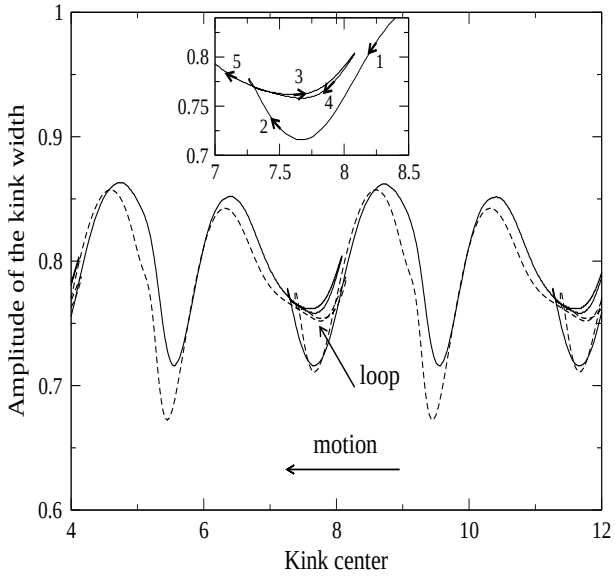

Figure 4.8: sG: Amplitude of the kink width versus kink center. Simulation (solid line); 2-CC Approach Eqs. (4.18-4.19) (dashed line). The parameters are $\omega = 0.1$, $A = 0.44$, for the array $x_1 = 0.5$, $x_2 = 1$, $x_3 = 2.3$, period $L = 4$ and $\epsilon = 0.8$. See text for a discussion of the loop. Inset: enlargement of the loop indicated by an arrow in the main figure. The motion of the kink center is indicated by numbered arrows.

system. Even then, the interplay of the two degrees of freedom, lead eventually to a behavior truly indistinguishable from a rocking ratchet mechanism for point-particles.

To deepen our understanding of the dynamics, let us look into the oscillations of the kink width. As in the case of simulations we restrict ourselves to the overdamped case (taking $\beta = 1$). A picture of the kink width oscillations versus the kink center position is shown in Fig. 4.8. As we can

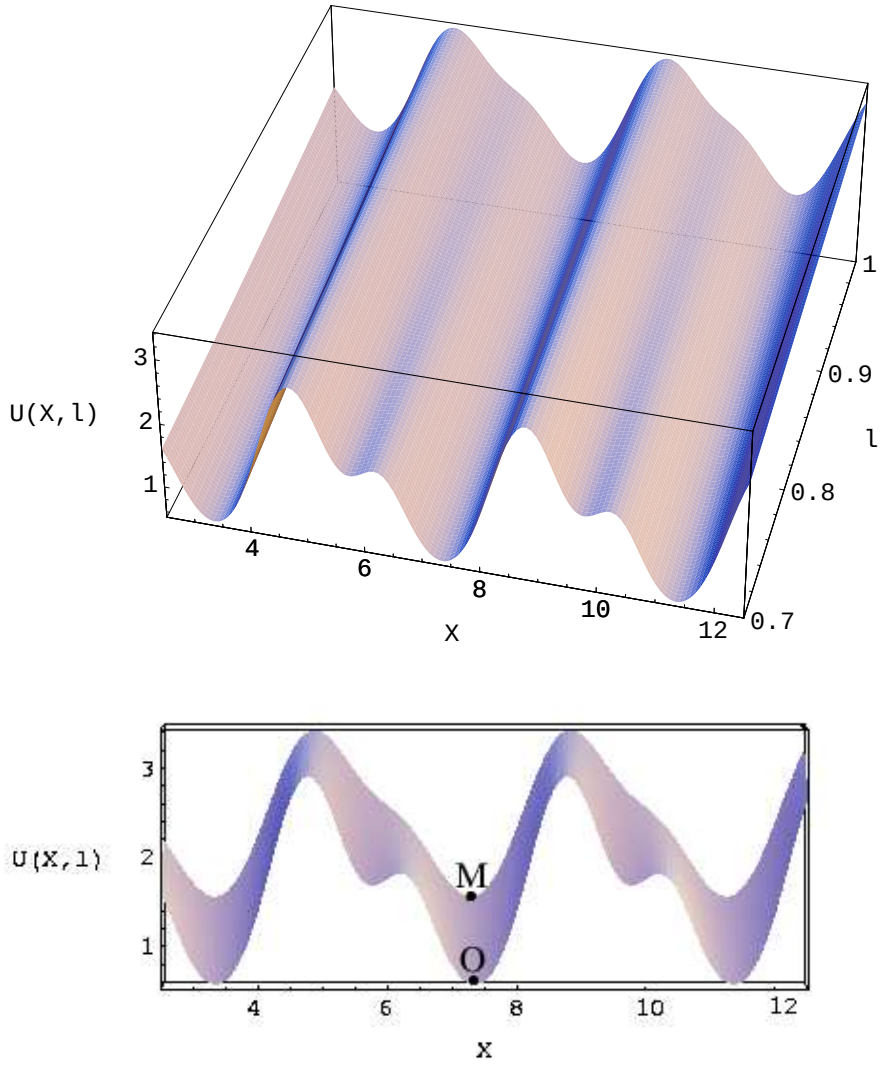

Figure 4.9: Top panel: Landscape of the effective potential Eq.4.21. Bottom panel: Frontal view of the landscape rotated with a small angle. The array used is the same as in Fig. 4.8.

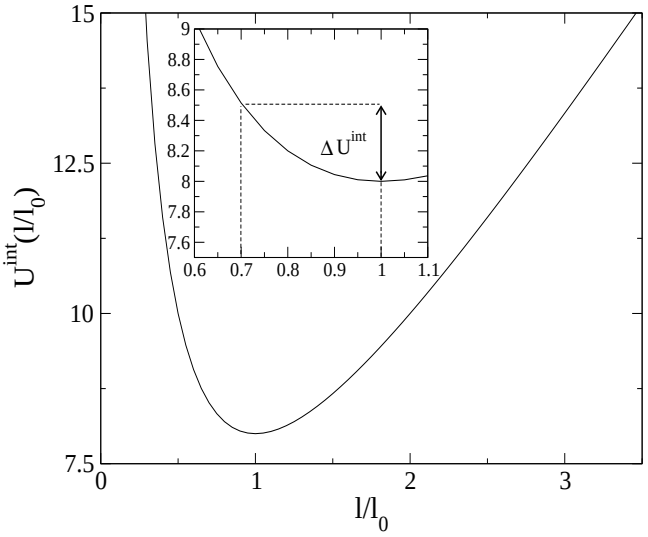

Figure 4.10: Internal Potential energy vs normalized kink width (4.20) (sG case). The inset shows a part of curve where the oscillations of the kink width take place.

see, the agreement with the CC approach is excellent, confirming the validity of our predictions. The existence of loops is particularly interesting, which arises as a consequence of the kink center motion rocking back and forth in the wells of the effective potential (see Fig. 4.9), which takes roughly half an oscillation before overcoming the barrier.

Interestingly, another feature that stands out clearly is that the oscillations are around a value different from $l_0 = 1$, the width of the unperturbed kink. Figure 4.8 shows that they take place around $\bar{l} \approx 0.8$ and, furthermore, that l_0 is not even included in the range of oscillations.

This phenomenon is the result of the balance between two opposite effects. a) On one hand, the inclusion of inhomogeneities increases the potential energy of the system. This fact is reflected in the effective potential energy landscape Fig. 4.9. Such picture shows that when the kink width decreases, the potential energy decreases as well. Taking two points with the same value for X but with different kink widths l, for example M and O in the bottom

panel of Fig. 4.9, we see clearly this difference in potential energy, i.e., $U_M > U_O$ where $l_M > l_O$. Therefore, as the system tends to move to the minimum of the potential energy, the kink width would decrease. b) On the other hand, the kink internal potential energy, Eq. (4.20), has a minimum at l_0, and hence the energy increases when the kink width decreases (see Fig. 4.10 for $l < l_0$); notice that the first term of this equation accounts for a repulsive interaction while the second is for an attractive interaction. As a result of the balance between a) and b), a new minimum will appear for the oscillations of the kink width. It is important to note that the difference ΔU^{int} of the internal potential energy for the kink width $l = 0.7$ with respect to the value $l_0 = 1$ (inset of Fig. 4.10) is of the same order as the energy difference $U_M - U_O$ between the points mentioned before for the effective potential introduced by the inhomogeneities, in agreement with this discussion.

4.1.2 Related point particle models.

A problem closely related to our 2-CC approach, given by a point particle ratchet with two degrees of freedom, has been studied in [61]. This model was designed for describing molecular motor dynamics consist of two particles joined by a spring moving in a ratchet potential. The corresponding equations of motion are given by

$$\dot{u_1} = -\frac{\partial V(u_1)}{\partial u_1} - \frac{\partial W(u_2 - u_1)}{\partial u_1} + A\sin(\omega t) + \xi_1(t), \tag{4.22}$$

$$\dot{u_2} = -\frac{\partial V(u_2)}{\partial u_2} - \frac{\partial W(u_2 - u_1)}{\partial u_2} + A\sin(\omega t) + \xi_2(t), \tag{4.23}$$

where V is a sawtooth potential and W is the internal potential energy. Here ξ_i with $i = 1, 2$ are Gaussian white noises. Ignoring the noise terms

and their influence on the net motion, we see that the change of variables $X = \frac{1}{2}(u_1 + u_2)$ and $l = u_2 - u_1$ casts the system into a similar shape as Eqs. (4.18-4.19) in the overdamped case, where in good approximation the inertial terms could be neglected. In this new context the variables X, l can be interpreted as the center of mass and the elongation (distance between the particles), respectively, and obviously resemble to the center of mass and width of the kink variables in our system.

Notice that in both models we have an asymmetric potential. In our case it is given by Eq. (4.21), which is asymmetric at the CC level if the already mentioned conditions for the distances between the inhomogeneities are satisfied. In both systems, there are internal potential energies that characterize their elastic properties. In the model in [61], the internal potential is expressed via a harmonic function (in the original variables):

$$W(u_1, u_2) = \frac{1}{2}k[(u_2 - u_1) - l_0]^2, \tag{4.24}$$

which in our collective coordinates can be rewritten as

$$W(l) = \frac{1}{2}k[l(t) - l_0]^2. \tag{4.25}$$

where k is the elasticity constant. The links between the two models can be made more explicit by using a value for l_0 close to the minimum around which the kink width oscillates in our simulations (cf. the discussion in the preceding subsection). However, what the quantity l actually means is the distance at which the kink shape approaches its asymptotic values, measured from the center. This means that l in our notation is half the "real kink width". Consequently the ratio (real kink width)/(period of the effective

potential) becomes $2\bar{l}_0/L \approx 0.4$ for which a very interesting dynamics for point particles dynamics has been reported in related 2-particle model [63].

This comparison between our model and that in [61] allows to point out their main differences as well. It is particularly important that in our framework, the internal energy can describe satisfactorily the repulsive interaction between real molecules where a wan-der-Waals like-force prevents their overlap. This is very close to what occurs in molecular motors: if we take again the motion of kinesin as an example, this molecule has two dimer heads that act as 'feet', allowing the molecule to 'walk' along a microtubule [60]. The repulsion would then appear when the two dimer heads are too close. Such a repulsive interaction can not be naturally accounted for within the model of two particles. For solving this problem the authors of [61] resort to fix arbitrary values for l_0 which in our case is not necessary. Note, however, that in spite of the technical differences between both models, phenomenologically they are very similar: both of them try to understand how the motion of molecular motors, which proceeds in steps accompanied by deformations (in the case of kinesin, when one step advances in front of the other) can arise. The common conclusion is that a point particle ratchet would not be a good model because the second degree of freedom is needed to capture the whole mechanism of the motion. The advantage in our approach is that this second degree of freedom arises by its own, without a priori constructions, as an emergent property of the nonlinear excitation. Recent studies [62, 63] show similar phenomena for the two degrees of freedom point particle ratchet of [61] when the ratchet is of flashing type. The close relationship of the model of [61] to ours suggests that nonlinear Klein-Gordon models not

only can exhibit rectification working as flashing ratchets but also as diffusive ratchets. This last ratchet mechanism will be discussed in a section of this chapter.

4.1.3 Length scales and quantization of transport

It should be clear from the results discussed so far that in order to obtain a ratchet device for extended nonlinear systems with topological nonlinear excitations, the configuration of the inhomogeneities should be designed in such a way that the distance between the inhomogeneities is of the order of the kink width. However, this picture is somewhat too simple, and as we will see below, another important factor to be taken into account is the existence of interference effects.This is borne out clearly by considering the ϕ^4 model.

Naively, one may try to design a similar ratchet system for the ϕ^4 equation. Considering only the kink width factor, it would seem that enlarging the sG array by a factor of $\sqrt{2}$ (the ratio between the kink widths in both models) similar phenomena would be observed. Let us make a more specific comparison between both models. To this end, we use the 1-CC framework in the nonrelativistic approach, where the equation of motion for the center of mass coordinate X can be written as

$$\ddot{X} + \beta\dot{X} = -\frac{du}{dX} - \frac{qA}{M_0}\sin(\omega t + \delta_0), \tag{4.26}$$

where $u = U/M_0$ is the normalized effective potential. For the sG case we have the following expression

$$u(X) = \frac{2\epsilon}{M_0}\sum_n \sum_{i=1}^{3} \frac{1}{\cosh^2[(X - x_i - nL)/l_0]} \tag{4.27}$$

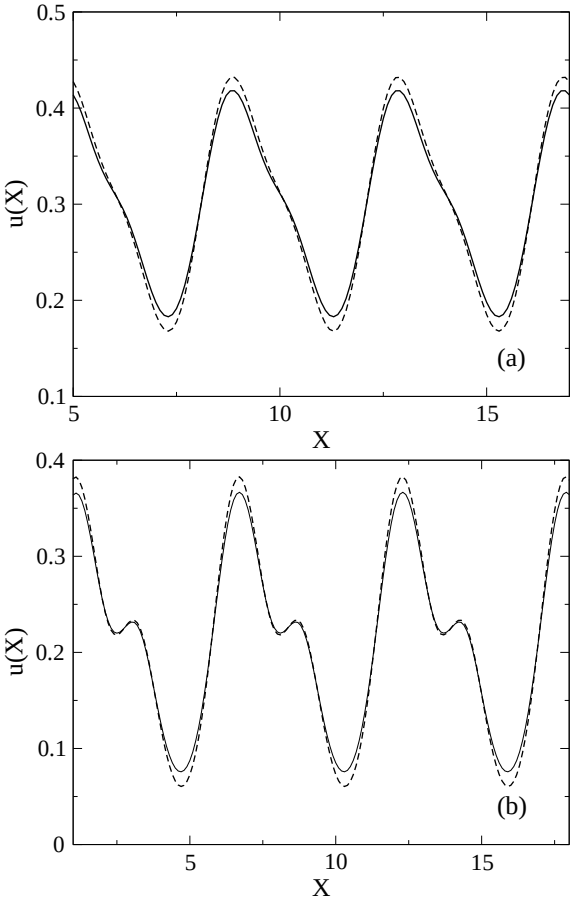

Figure 4.11: Normalized effective potential for the kink center coordinate within the CC approach, Eq. (4.27-4.28), for two different delta peak arrays with $\epsilon = 0.8$. (a): $x_1 = 0.5$, $x_2 = 1.$, $x_3 = 2.3$ and $L = 4$. (b): $x_1 = 0.7$, $x_2 = 1.4$, $x_3 = 3.2$, $L = 5.6$. In both panels sG (solid line); ϕ^4 (dashed line).

with $l_0 = 1$ and $M_0 = 8$, whereas for the case of ϕ^4 we have

$$u(X) = \frac{\epsilon}{4M_0} \sum_n \sum_{i=1}^{3} \frac{1}{\cosh^4[(X - x_i - nL)/l_0]} \tag{4.28}$$

with $l_0 = \sqrt{2}$ and $M_0 = 2\sqrt{2}/3$. The normalized effective potential for two different arrays of inhomogeneities are depicted in Fig. 4.11. Panel a) shows standard asymmetric potentials for rachet systems obtained with an array that satisfies the conditions mentioned above for the location of the inhomogeneities in the sG case. However, in case b) the effective potentials obtained for an array approximately given by the multiplication of the factor

$\sqrt{2}$ of the first one, shows a local minimum similar to an array of asymmetric double-well traps. This potential has been used for studying the motion of vortices in superconductor materials [64].

According to the our previous arguments based on the important role of the kink width, a similar picture is expected for the normalized effective potential of ϕ^4 and sG if the arrays verify the same length scale ratio as the full systems. Strikingly, Fig. 4.11 shows that the normalized effective potentials are almost the same *but for the same array length*. This apparent discrepancy can be explained if we take a detailed look at the potential given by Eqs. (4.27-4.28) for both cases (sG and ϕ^4). It is clear from those expressions that, while in the case of ϕ^4 we have a $\cosh^4$ factor in the denominator, sG has a $\cosh^2$ factor. Therefore, the peaks and valleys in the effective potential for the ϕ^4 system are much narrower than for sG, thus compensating for the increment in length scale. In addition, as in the sG model, we will have dynamical changes of the effective potential due to the kink width variations, making the dynamics of motion more complicated. In any case, the effective potentials obtained in the simple approach highlight the importance of interference effects (see also [53, 54]) and make it clear that the kink width is not the only quantity to take into account.

The consequences of choosing either the original or the rescaled one for the kink dynamics are revealed in Fig. 4.12. We have chosen for the analysis the ϕ^4 model with a relative low frequency of the ac force, for which the mean velocity as a function of the ac force amplitude shows a staircase structure. The range of the amplitude values were taken from the following rescaling expression: $q^{\phi^4}A^{\phi^4}/M_0^{\phi^4} = q^{sG}A^{sG}/M_0^{sG}$. This relation is deduced from the

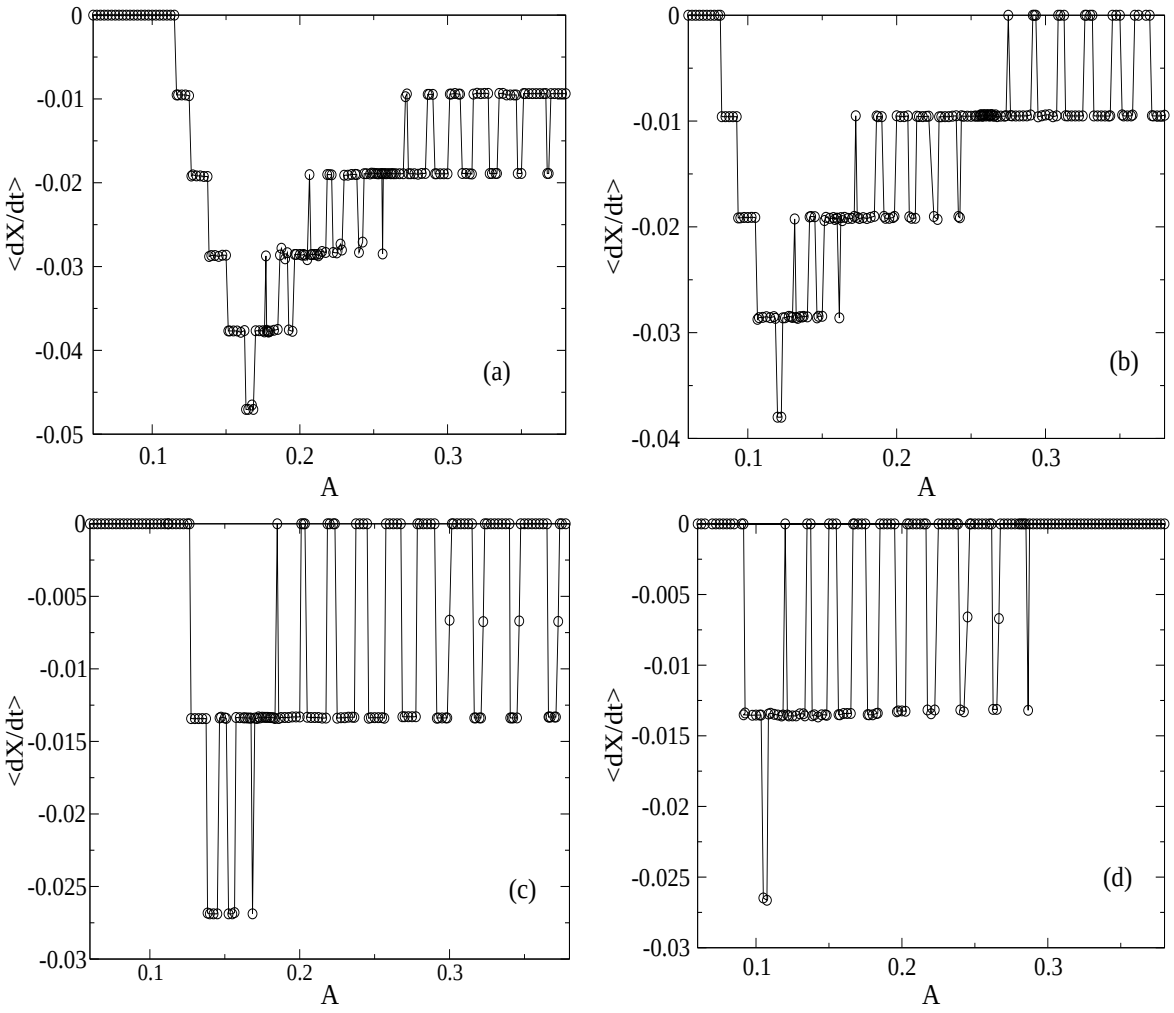

Figure 4.12: ϕ^4: Mean velocity vs driving amplitude A for the frequency $\omega = 0.015$.(a) $\epsilon = 0.8$, $x_1 = 0.5$, $x_2 = 1$, $x_3 = 2.3$, $L = 4$.(b) $\epsilon = 0.6$, $x_1 = 0.5$, $x_2 = 1$, $x_3 = 2.3$, $L = 4$. (c) $\epsilon = 0.8$, $x_1 = 0.7$, $x_2 = 1.4$, $x_3 = 3.2$, $L = 5.6$. (d) $\epsilon = 0.6$, $x_1 = 0.7$, $x_2 = 1.4$, $x_3 = 3.2$, $L = 5.6$. The thin lines connecting the points serve as guides for the eye.

comparison between the 1-CC approaches for sG and ϕ^4 models, considering the similarity of the normalized potentials discussed above. Fig. 4.12 shows the dependence of the kink mean velocity as a function of the amplitude for two different arrays and heights of the perturbations introduced by the inhomogeneities. As we can see, the motion is quantized as in standard ratchet systems [16, 15] and is characterized by the existence of gaps for which the net motion is absent (i.e., pure oscillating states). The absolute value of the mean velocity can be expressed as $|\langle dX/dt\rangle| \equiv |\langle V\rangle| = \frac{L\omega}{2\pi}\frac{m}{n}$ as usual [65], where the indexes m, $n \in \mathbb{N}$ quantize the motion.

Using the expression for $|\langle V\rangle|$ we can characterize the motion for each frequency and period of the array. Comparing the values obtained from the simulations with the results derived from the expression for $|\langle V\rangle|$ with corresponding parameters L and ω, we find that m and n can take the following values: For panel a), $m = 1, 2, 3, 4, 5$ and $n = 1$; for panel b), $m = 1, 2, 3, 4$ and $n = 1$; for panel c), $m = 1, 2$ with $n = 1$ and $n = 2$, and for panel d), $m = 1, 2$ with $n = 1$ and $n = 2$. Although the absolute value of the mean velocity increases with the spatial period, the index m significantly decreases, leading to a global decrease of the velocity. These results prove that the inclusion of more inhomogeneities per unit cell, which obviously enhances the period L, is not a good option if we want to reach high velocities. Furthermore, a very low frequency would be required to obtain windows of motion. In the case of the dependence on the inhomogeneities height, the starting point of the stair-steps structure shows a shift towards greater amplitude of the ac force when increases the height, which is a natural trend in order to overcome the barrier. Nevertheless, a higher speed is found,

arising from a higher m and observable also as a broadening in the windows of motion.

4.2 Dynamics under the influence of noise

So far, we have analyzed the ratchet-like behavior of our system in the deterministic case. However, it is clear that for our model to be more realistic, for instance, in the context of LJJ, the effect of the temperature has to be taken into account. The behavior of ratchet systems for nonzero temperature has been extensively studied both for point particles [15, 1, 66, 67, 68, 69] and for nonlinear extended systems [24, 29]. However no investigation concerning ratchet-like phenomena in the presence of spatial inhomogeneities has been performed. Therefore, to address this issue here is of considerable importance. In the present thesis, we will focus on the robustness of our rocking ratchet mechanism under the influence of thermal fluctuations. Another relevant issue would be the possibility of activation, resonances or modifications of the transport features induced by noise, but this topic deserves a further detailed analysis and will be the subject of a future work.

4.2.1 The model

For the sake of definiteness, we consider the sG model under the influence of a Gaussian white noise; the results for the ϕ^4 equation are similar. Introducing the effect of the temperature through the fluctuation-dissipation relationship and considering the overdamped case as before, ($\beta = 1$), we start with the

following equation:

$$\phi_{tt} + \phi_t - \phi_{xx} + \sin(\phi)[1 + V(x)] = f(t) + \eta(x,t), \tag{4.29}$$

where

$$\begin{aligned} \langle \eta(x,t) \rangle &= 0, \\ \langle \eta(x,t)\eta(x',t') \rangle &= D\delta(x-x')\delta(t-t'). \end{aligned} \tag{4.30}$$

with $f(t) \equiv A\sin(\omega t + \delta_0)$ and the noise intensity $D = 2k_BT$.

For the numerical simulations of the full partial differential equation as well as for the numerical solution of the collective variables approximation (to be discussed in the next subsection), we have used the Heun method with the Box-Muller-Wiener algorithm for generating Gaussian random numbers of mean zero and variance one [70]. In Fig. 4.13 we show the behavior of the kink center dynamics under thermal fluctuations. Hereafter, we have set the array parameters to be $x_1 = 0.5$, $x_2 = 1.$, $x_3 = 2.3$, $L = 4$ and $\epsilon = 0.8$ for our study (see Fig. 4.1). The mean velocity was calculated using the expression in [2], namely

$$\langle \dot{X} \rangle = \lim_{t\to\infty} \frac{\langle X(t) - X(0) \rangle}{t}, \tag{4.31}$$

where the average is to be understood over many realizations of the noise. From Fig. 4.13 we see that the steps of the deterministic case are now smoothed, a typical feature for the dynamics under noise. It is important to realize that this smoothing affects the regions between the windows, which become minima of the absolute value of the mean velocity $|\langle \dot{X} \rangle|$ instead of gaps with zero mean velocity (see Fig. 4.13a). This phenomenon is directly related to the strength of noise, i.e., when the noise increases the absolute

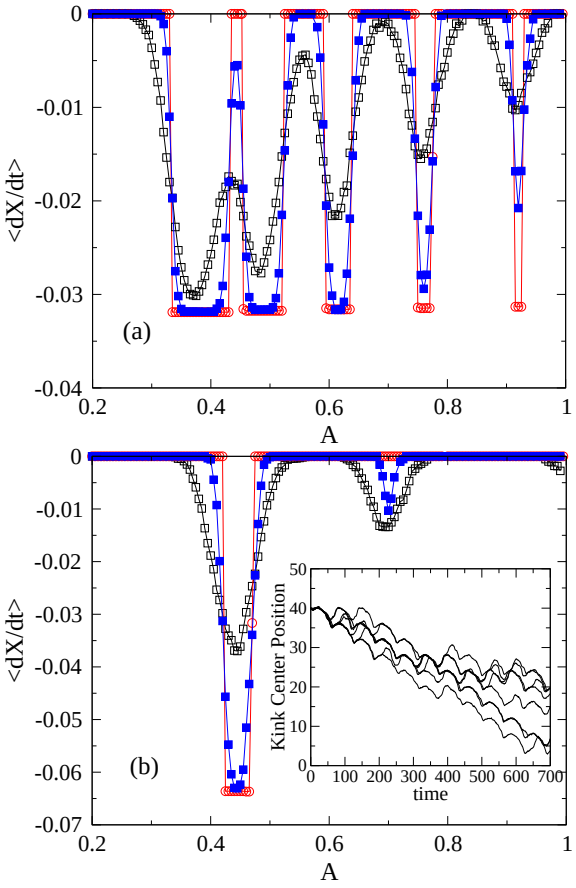

Figure 4.13: Mean kink velocity $\langle dX/dt \rangle$ vs driving amplitude A for different intensities of the noise. (a) $\omega = 0.05$. (b) $\omega = 0.1$. In both cases red circles correspond to $D = 0$; blue filled squares to $D = 0.005$; black squares to $D = 0.05$. The lines serve as guides for the eye. The inset in (b) shows several realizations for the motion of the kink center with $A = 0.43$, $\delta_0 = \pi$ and $D = 0.05$ as function of time.

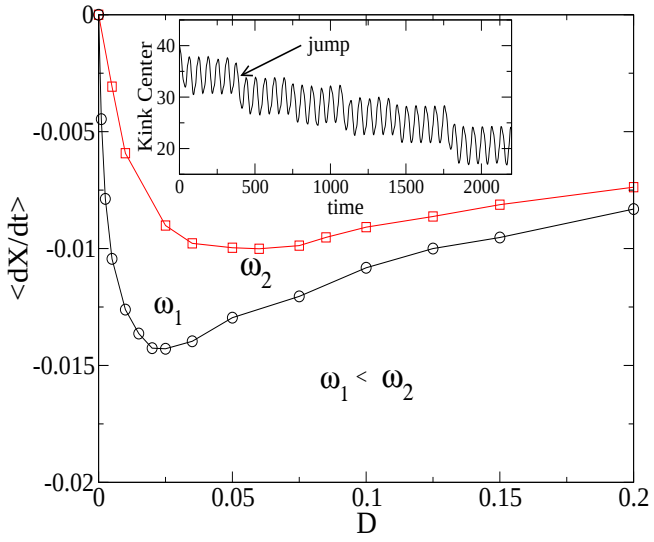

Figure 4.14: Mean kink velocity $\langle dX/dt \rangle$ vs intensity of noise D. Circles: $\omega = 0.1$ and $A = 0.70$; squares: $\omega = 0.11$ and $A = 0.75$. Inset shows one realization for the motion of the kink center for $\omega = 0.1$, $A = 0.70$, $\delta_0 = 0$ and $D = 0.005$.

value for the mean velocity decreases but simultaneously the connection between the windows becomes more evident and the windows of motion become less pronounced.

As in most other ratchet systems, in our model the stochastic fluctuations due to temperature assist the jumps of the kink center from one well to the next one, allowing in some cases jumps in the direction opposite to the rectification (see the inset graph in Fig. 4.14) which is not possible in the absence of noise. Accordingly, the thermal fluctuations affect the mechanism of rectification whereas, on the other hand, they destabilize the dynamics of the pure oscillating states of the kink center (i.e., they destabilize the regions with locked directional motion at zero temperature). The combined action of both effects leads to the smoothing of the windows and the connection of the deterministic gaps. For relatively high temperatures the thermal kink energy is sufficient to overcome the barriers of the effective potential, and the

kink dynamics is practically diffusive, the influence of the barriers becoming negligible. For this reason the rectification of motion takes place only for not too large values of the noise intensity (see discussion in [71]).

A remarkable feature observed in the simulations is shown in Fig. 4.13b for frequency $\omega = 0.1$, where new windows (absent in the deterministic case) appear. This scenario is very similar to the one reported in [29] where a similar surprising and intriguing phenomenon was reported. There, the authors discussed that these new windows arose due to jumps of the fluxons between stable and unstable pinned fixed points of the deterministic dynamics. Considering the interest for this purely stochastic phenomenon, we carried out a careful analysis of the corresponding zone. To summarize this investigation, in Fig. 4.14 we have plotted the mean velocity as a function of the noise intensity for different values of the frequency, showing the existence of an optimal value for the intensity of the noise for which a maximum absolute value of the mean velocity is obtained. The inset in Fig. 4.14 makes clear that, as expected and suggested in [29], the mechanism of activation occurs through jumps between multistable states (states of the kink center which in absence of noise are purely oscillating). Therefore, a higher velocity is obtained when the residence time in these multistates is reduced or, in other words, when the intervals between consecutive jumps decrease. Once again, this process of activation becomes more effective when the noise intensity increases, but above a certain value of the noise intensity the kink center starts to jump in the direction opposite to that of the rectification, leading to a global loss in efficiency. This explains the existence of an optimal value for the noise intensity for which the modulus of the mean velocity reaches a

maximum value.

On the contrary, for the ϕ^4 model with the corresponding value of frequency, a second window of motion appears for the deterministic case (see Fig. 4.4c). In this case only a decay of the modulus of mean velocity was observed when the intensity of the noise increased.

Another interesting characteristic observed in Fig. 4.14 is the dependence of the maximal mean velocity on the frequency. Specifically, for a frequency value slightly larger than $\omega = 0.1$, the absolute value of $\langle \dot{X} \rangle$ decreases, the peak moving towards greater values of the noise strength and the corresponding window of motion moving towards greater values of the ac force. Accordingly, for relatively large values of the frequency, above $\omega = 0.11$, the window of motion induced by noise disappears. On the other hand, for frequencies slightly smaller than $\omega = 0.1$, a new window in absence of noise is obtained. With all these results, it is clearly established that the unidirectional motion induced by noise occurs only for a narrow window of frequency values.

We will show in the next subsection that this phenomenon seems to be a general feature, since at the CC level the system behaves very much like the dynamics of point particles.

4.2.2 Collective coordinates in presence of noise

In order to understand the behavior observed in the previous section we resort again to the CC approach. As a first step, we take only into account the fundamental degree of freedom. Although, as discussed above, this framework is inaccurate for describing quantitatively the kink motion on a lattice

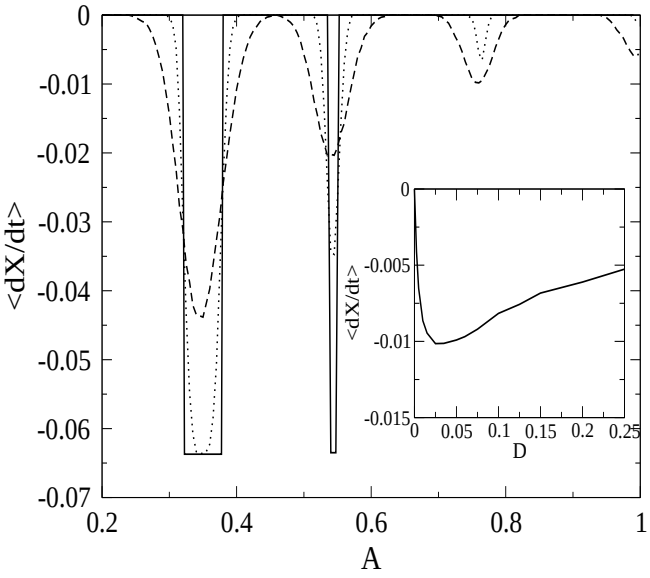

Figure 4.15: CC approach: Mean kink velocity $\langle dX/dt\rangle$ vs driving amplitude A for different intensities of the noise and frequency $\omega = 0.1$. Solid line: $D = 0$, dotted line: $D = 0.005$, dashed line: $D = 0.05$. Inset: Mean kink velocity $\langle dX/dt\rangle$ vs intensity of noise D for $A = 0.7625$.

of inhomogeneities, it does help understand qualitatively most of the features observed in the simulations, without unnecessary analytical complications. After some algebra (see Appendix A for details), with $\beta = 1$, we find the following stochastic equation for the kink center coordinate X:

$$M_0\ddot{X} + M_0\dot{X} = -\frac{d\,U}{dX} - qf(t) + \sqrt{DM_0}\;\xi(t) \tag{4.32}$$

with $\langle\xi(t)\rangle = 0$, $\langle\xi(t)\xi(t')\rangle = \delta(t-t')$. For sake of simplicity we have taken the nonrelativistic approach $\dot{X}^2 \ll 1$, for which the noise contributes additively.

Figure 4.15 presents the results of the numerical integration of Eq. (4.32). Much as we did in the simulations, we calculate the mean velocity using Eq. (4.31), taking up to 500 realizations. From this plot two main features also observed in the simulations can be seen. First, smooth curves are obtained for the mean velocity as a function of the amplitude of the ac force, with values

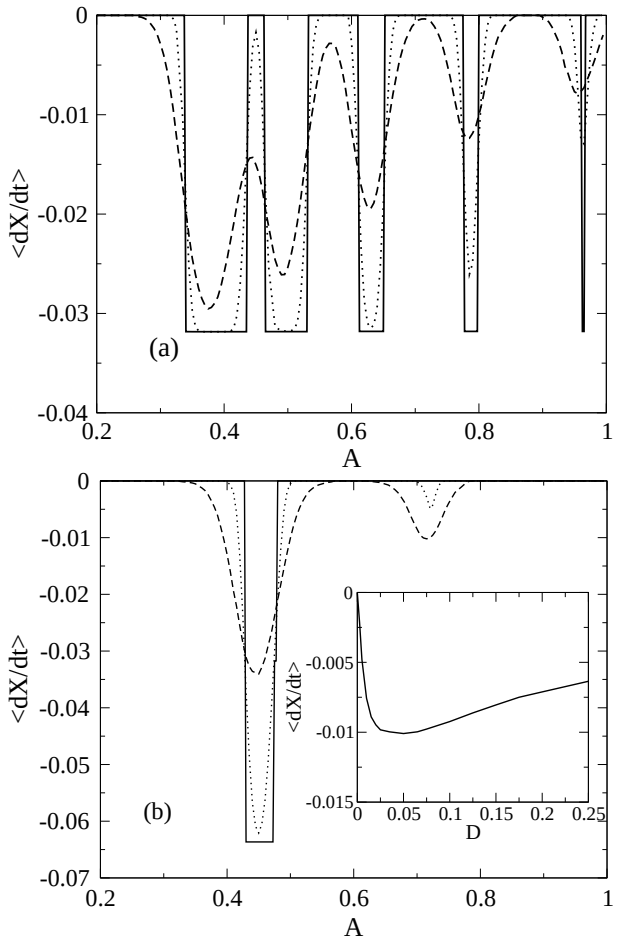

Figure 4.16: CC Approach for two degrees of freedom (Eqs. (A.36)-(A.37) of the appendix). Mean kink velocity $\langle dX/dt \rangle$ vs driving amplitude A for different intensities of the noise. (a) $\omega = 0.05$. (b) $\omega = 0.1$. In both cases solid line: $D = 0$; dotted line: $D = 0.005$; dashed line: $D = 0.05$. Inset in (b) shows the mean kink velocity $\langle dX/dt \rangle$ vs noise intensity D for $A = 0.72$ and $\omega = 0.1$.

that decrease when the noise strength is increased. Second, new windows appear, and inside them there is a value of the noise intensity for which the module of the mean velocity reaches a maximum value (inset in Fig. 4.15). It is thus evident that, in spite of the quantitative differences with the simulations, this simple approach does predict correctly the qualitative behavior of the full system.

In order to improve the results presented so far, we have extended the framework to two collective variables. By doing so (see Appendix B) we arrive at Eqs. (A.36)-(A.37) with two uncorrelated *multiplicative* white noise, which mean that the stochastic driving terms depend on the kink width dynamics.

The results for this improved approach are collected in Fig. 4.16. Comparing with the simulations (Fig. 4.13), we can observe the excellent agreement, with the locations of the windows correctly predicted. As expected the curves are again smooth, a feature correctly accounted for already in the 1-CC framework. For the frequency $\omega = 0.1$, a new window is predicted, whose location is also in very good agreement with its corresponding window in the simulations. These results confirm the importance of considering the kink width dynamics in the framework of the collective coordinates in order to achieve correct quantitative results as compared to the simulations.

On the other hand, this 2-CC approach can be used in a wide context. For instance, the results derived of our system as a diffusive ratchet can be correctly interpreted since the framework of 2- CC (see below). Concerning the role of the width kink for the motion we can say that is becoming more and more evident the crucial contribution of internal degrees of freedom in the functioning of molecular motors [60]. In this respect, our framework can

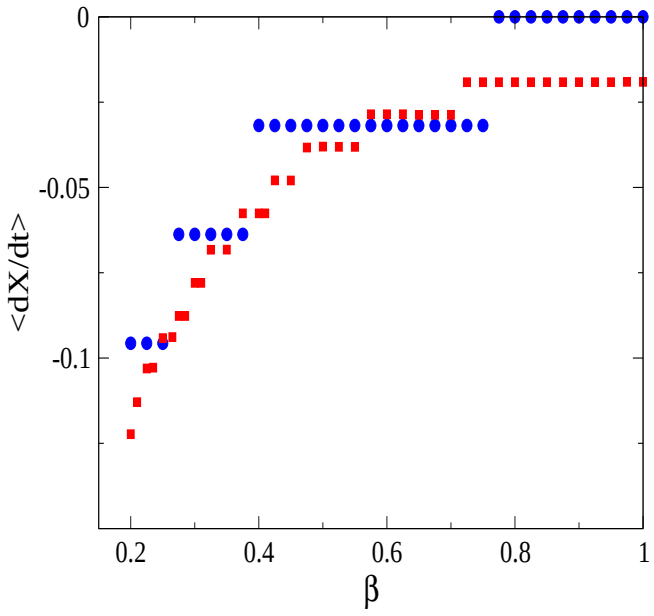

Figure 4.17: Mean velocity vs damping coefficient β for different frequencies. red squares: $\omega = 0.015$; blue circles: $\omega = 0.05$. The parameters used are $\epsilon = 0.5$, $A = 0.2$, $x_1 = 0.5$, $x_2 = 1$, $x_3 = 2.3$ and $L = 4$.

be very useful for describing the transport of proteins assisted by a thermal bath provoked by ATP molecules hydrolization.

4.3 Ratchet behavior: Dependence on damping

Throughout this chapter we have taken $\beta = 1$ in order to show the functioning of ratchet mechanisms for this system, i.e., we have done our study over the basis of an overdamped system. The main reason is that the motion for small damping may result in chaotic dynamics. Nevertheless, ratchet dynamics for this system is also possible in the weakly underdamped regime. It is very important in view of covering a wide range of applications.

Certainly, the overdamped regime is not suitable for some applications.

For instance standard Josephson junctions work usually for small damping. The reason is the following: If one has to work in the overdamped or in the weakly underdamped regime and we use conventional technology to fabricate LJJ, it means that the working temperature should be close to T_c (critical temperature). As an alternative variant one can use junctions with intrinsically high damping such as superconductor insulator normal-conductor insulator-superconductor LJJ or high-T_c LJJ technology, like for instance $YBa_2Cu_3O_{7-\delta}$(YBCO, $T_c = 90$K) junctions [72]. The first experimental investigation of ratchet effects with the mentioned materials was carried out in asymmetric dc SQUIDS [38]. The authors achieved to fabricate such a device for the overdamped regime. They also studied the transition from strong to intermediate damping.

Here, with a similar purpose we proceed to the computation of the mean velocity, varying the damping coefficient. The results of the numerical simulation of Eq.4.1 are collected in Fig. 4.17. This figure shows the dependence of the mean velocity on the damping coefficient for different frequencies. As expected, the module of mean velocity values are quantized, reaching their highest values for a lower frequency. We can also observe from the Fig. 4.17, a significant increase of the module of the mean soliton velocity as the damping coefficient decreases. The dynamics depicted in Fig. 4.18, shows how the center of mass of the soliton moves. As we can observe during one part of the period of the ac force, the soliton moves in one direction but during the other part the soliton does not move, behaving as if it would be trapped. This is because of the rectification mechanism, that hinder the motion in the opposite direction. With the presentation of these results we have extended

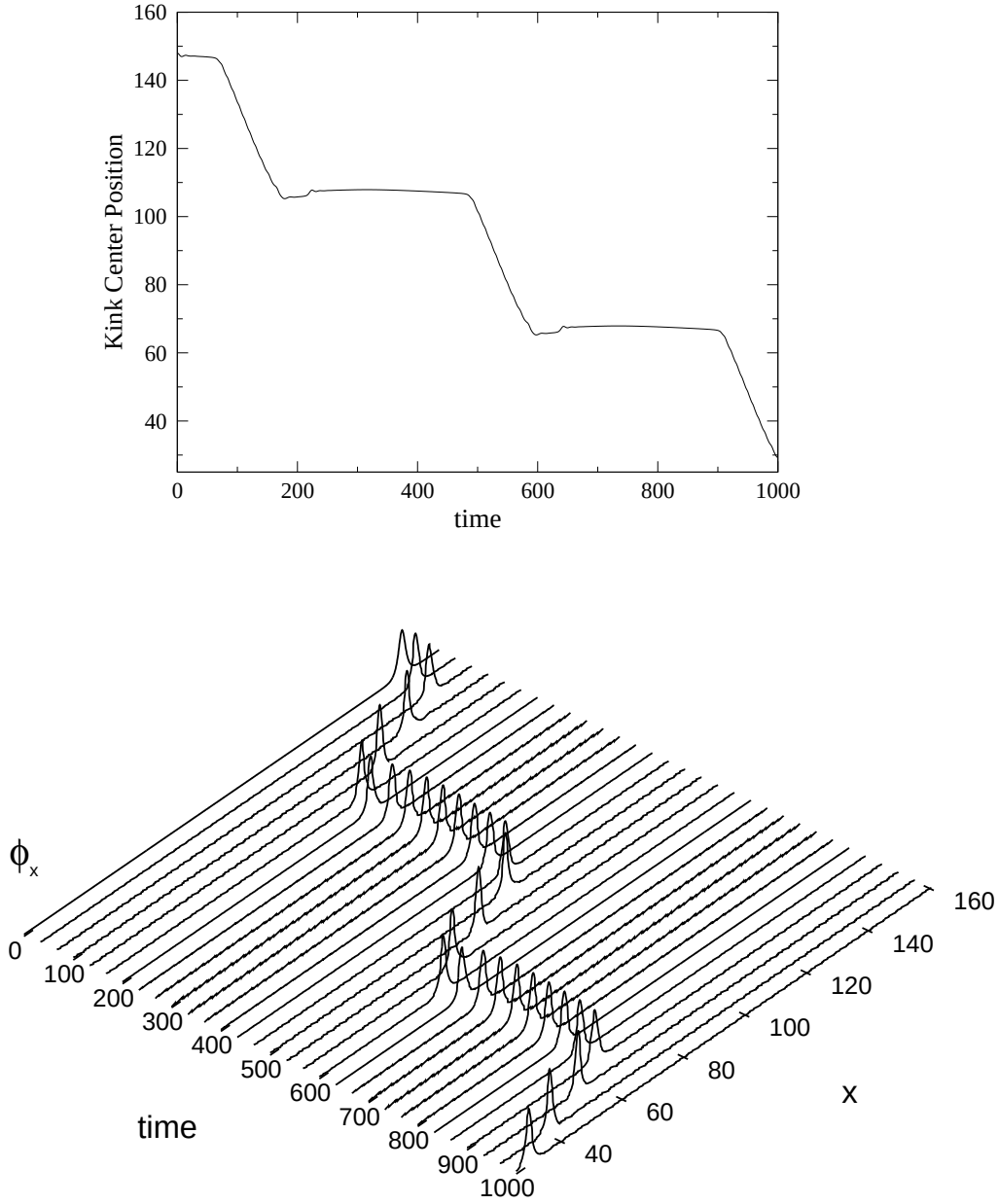

Figure 4.18: Top panel: Plot of the kink center position versus time. Bottom panel: Evolution of the derivative of the kink profile: The parameters are $\omega = 0.015$ $\beta = 0.25$, $\delta_0 = 0$, $A = 0.2$, $x_1 = 0.5$, $x_2 = 1$, $x_3 = 2.3$, $\epsilon = 0.5$ and $L = 4$.

our framework to the weak underdamped regime, where a higher efficiency is obtained.

4.4 Diffusive ratchets

So far we have studied the motion dynamics of solitons for a rocking ratchet. Nevertheless, the same framework can be extended to diffusive ratchets or even flashing ratchets. In this section we show a simple realization for a diffusive ratchet. We retake the Eq.4.1, but this time, instead of using an alternating force we consider a periodic behavior for the temperature. Such an equation can be written as

$$\phi_{tt} + \phi_t - \phi_{xx} + \sin(\phi)[1 + V(x)] = \eta(x,t), \tag{4.33}$$

with

$$\begin{aligned} \langle \eta(x,t) \rangle &= 0, \\ \langle \eta(x,t)\eta(x',t') \rangle &= D\delta(x-x')\delta(t-t'), \end{aligned} \tag{4.34}$$

where $D(t)$ is a periodic function of the time given by $D(t) = D_0[1 + q\sin(\omega t)]^2$. We consider for the function $V(x)$ a similar asymmetric configuration as that represented in Fig. 4.3 with additional inhomogeneities per unit cell. We take four inhomogeneities per period, whose configuration fulfills the condition $x_2 - x_1 < x_3 - x_2 < x_4 - x_3$ in order to preserve the asymmetric profile for the effective potential.

The Fig. 4.19 shows the existence of a net motion towards the right side. In this figure one can observe the existence of points where the soliton spends

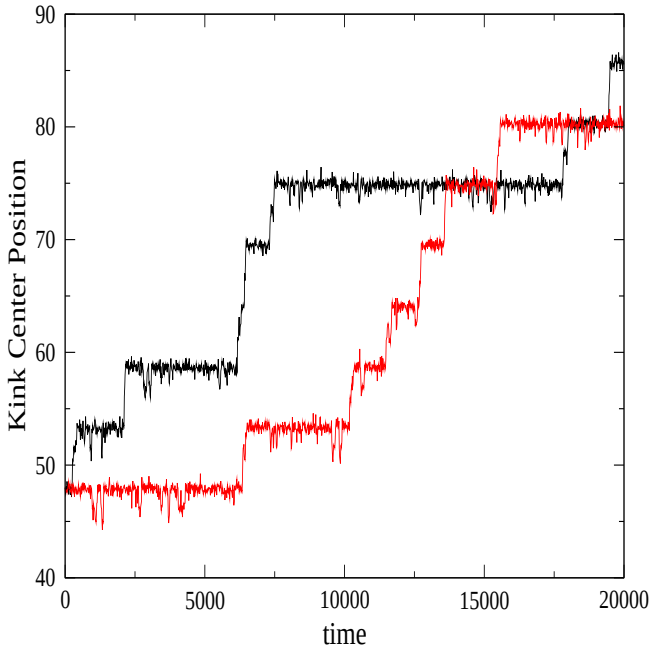

Figure 4.19: Simulations of Eq. 4.33: Two realizations for the motion of the kink center. The parameters are $x_1 = 0.5$, $x_2 = 1.1$, $x_3 = 2.3$, $x_4 = 3.6$. The other parameters used are $D = 0.4$, $\omega = 0.12$, $q = 0.5$, $\epsilon = 0.6$ and period $L = 5.4$.

some time before jumping over the barrier and moving to the next well. They correspond to the minima of the asymmetric potential. This motion is closely related with the relaxation time, i.e., the necessary time for the soliton motion towards the minima, after jumping over the barriers. Therefore it is strongly dependent on the frequency of the temporal fluctuations of the temperature ω and also of the intensity of the thermal fluctuations D_0 and q.

Let us make a simple analysis for the motion dynamics of solitons in terms of the probabilities for overcoming the barriers. In order to do so we resort to the Kramer expression given by $P \sim \exp(-\Delta U/k_bT)$, where ΔU is the necessary energy for overcoming the barrier [73]. This expression quantifies the probability for jumping over the barrier. The question is how to proceed for the soliton framework.

From previous works on kink diffusion, there is controversy about the

tendency of an increment of the kink width while the time passes [74, 75]. As regards our system, rather than an increment, a diminution of the kink width is expected because of the presence of inhomogeneities (see end of section 4.1.1 for noiseless case). On the other hand, we know from the 2-CC framework, that the soliton energy not only depends on its position but also on its width (see Eqs. (4.20-4.21)). Therefore, one should expect the influence of this factor on the dynamics.

Following the previous arguments and considering an energy landscape for the motion of the kink center like the ratchet potential depicted in Fig. 4.9, one should expect for the kink jumps over the barriers a dependence on the width. Therefore the probability for overcoming the barrier has to be expressed in terms on the kink width. In order to quantify such a value we propose as a first approximation, the modified Kramer expression $P \sim \exp(-[U_2(l_2) - U_1(l_1)]/k_bT)$. According to this expression the probability for overcoming the barrier depends on the kink width at the beginning and at the end of the jump event. A similar analysis can be done for two particles coupled by one spring.

We conclude from this preliminary study the existence of a diffusive ratchet motion. Such a dynamics shows features indistinguishable from a diffusive ratchet behavior for point particles like the one presented in chapter 2. Nevertheless, an influence of the kink width to the dynamics is expected.

4.5 Asymmetrical configurations

In contrast to the previous configuration with three inhomogeneities per unit cell, we have chosen two, i.e.,

$$V(x) = \sum_n \left[\epsilon_1\, \delta(x - x_1 - nL) + \epsilon_2\, \delta(x - x_2 - nL)\right] \tag{4.35}$$

where $\epsilon_1 \neq \epsilon_2$ and $x_2 - x_1 \neq L - x_2$.

The possibility of breaking the symmetry with two instead of three inhomogeneities per unit cell is mainly determined by the difference between the strengths of the inhomogeneities. In the framework of Eq. (4.35) one can design different configurations. In Fig. 4.20 two different variants for the lattice configuration are depicted. The combination of such configurations gives rise to a new configuration. Likewise from the combination of the new configuration with other configurations new complex asymmetric arrays are obtained and so forth. Therefore a transition from a periodical to a disorder array of inhomogeneities is expected.

It is also possible to design an asymmetric array with random intensities of the inhomogeneities. A detailed analysis of disorder supported by an analytic study was done for a single particle ratchet system [76]. In this work it is proved that disorder quenches the rectifying power of the ratchet system, as expected. However, some remarkable transport properties were detectable. In this respect, our system can serve as a benchmark for understanding realistic problems like the dynamics of motor proteins. In particular it could help to understand the transport of polymerase along the DNA backbone.

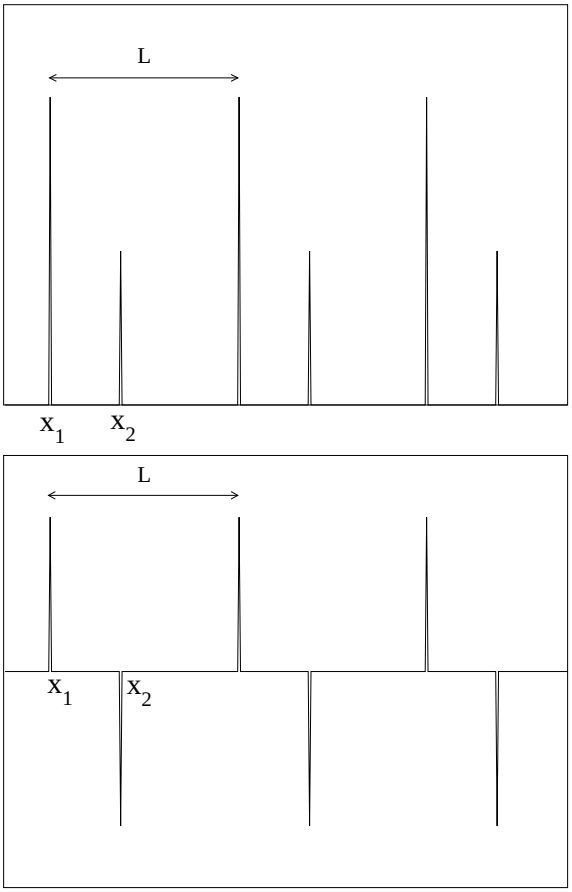

Figure 4.20: Schematical representation for a periodic and asymmetric arrray of point-like inhomogeneities. Top panel: $\epsilon_1 > \epsilon_2$. Bottom panel: $\epsilon_1 = -\epsilon_2$. In both cases $x_2 - x_1 < L - x_2$.

4.6 Perspectives

We have pointed out several issues in this chapter. However, the discussion was far from being completed. There is the case of our rocking ratchet when it is influenced by the action of more than one harmonic component in the external force. We know from the results for one harmonic obtained in this chapter that the direction of the net motion is determined by the spatial arrangement of the inhomogeneities. Therefore only changes in the position of the inhomogeneities can reverse the direction of motion.

This represent a drawback compared to the first ratchet model, where by changing the phases one can reverse the direction of motion. However, recently, theoretical predictions in ratchet systems for point particles have shown the possibility of obtaining a current reversal with the use of a biharmonic force [77] irrespectively of its symmetry. We have tested that this is also possible in our system. Furthermore, in the overdamped regime we have observed that such a ratchet system exhibits a greater efficiency in terms of the mean velocity compared to previous one. Recall that the directed motion in the previous ratchet systems is determined by the resonant coupling between the external force and the kink width oscillations. Consequently the mean velocity decays as the oscillations are damped. The previous arguments lead us to propose this ratchet system as a candidate for ratchet devices constructed of materials with intrinsic high damping like the one mentioned above. This will be object of a future report.

On the other hand, the investigation reported here, opens new perspectives in the design of ratchet devices for more complicated extended nonlinear systems, such as general coupled chains [78]. Of particular interest in this class are stacked LJJ [79], apart from many other systems with potential applications in different areas.

Chapter 5

Summary

In this work we have investigated the ratchet dynamics of topological solitons for some Klein-Gordon systems. The study was realized taking into account different symmetry-breaking mechanisms.

In Chapter 3 we have reported the results of a study of the dynamics of solitons in the presence of a biharmonic force. The analysis was based on previous studies on sG systems in the presence of an asymmetric biharmonic force. We explained the reasons for the breaking of symmetry and especially the ratchet motion in the sG system using a collective coordinate approach which regards two main degrees of freedom, the translational mode and the kink width dynamics (internal mode).

As an important result, our study has shown that unidirectional motion only takes place when the external force resonates with the harmonics contained in the kink width oscillations. This was first predicted by an analytic expression obtained from a multiscale perturbative expansion and was verified later by the numerical results of the CC equations and by the full

simulations of the PDE equation. The analysis of the harmonic modes of the oscillations of the kink width was based on the results obtained from the DFT of CC equations and from the simulations. The agreement obtained between both results was impressive, validating our resonant CC criterion.

Such a behavior was proven for asymmetric and symmetric biharmonic forces, in particular for biharmonic forces composed by two harmonics with a frequency δ for the first harmonic and frequencies $m\delta$ with $m = 2, 3, 4$ for the second harmonic.

As a main conclusion we have shown that net motion occurs when an effective coupling between the translation and the internal mode (oscillations of the kink width) takes place.

Another important observation was the sinusoidal dependence of the kink center motion on the independent phases of the harmonics of the force, generalizing previous results about the dependence on the relative phase. In all the cases our theory predicted the correct behavior of the ratchet dynamics. This was supported by numerical solutions of CC equations and by the simulations of the full system.

We also emphasized on the motion dependence on the damping. Particularly, using the analytical results we could explain the apparent contradictions in former studies about the dependence of the mean velocity on the damping coefficient. Three different situations were analyzed. First the appearance of a current reversal; second the existence of an optimal value for the damping coefficient for which a maximum for the absolute value of mean velocity takes place and third the decaying monotonic behavior of the mean velocity takes place as the damping increases. In all the cases a decay of the maximum

velocity for higher values of the damping was observed. The explanation was found in the oscillations of the kink width, which decay as the damping increases.

We also extended the analysis to the ϕ^4 model where a similar dynamics to the sG model was obtained. As regards the mobility, a higher mean velocity in the ϕ^4 model compared to the sG model was observed. The explanation of such effect was based on the relation between the effective parameters for the CC equations of both systems. All the previous results were supported by numerical simulations.

In Chapter 4 we conceived a new form of ratchet systems by means of a lattice of point-like inhomogeneities. With a particular design of a periodic and asymmetric array of the inhomogeneities we could rectify the motion dynamics of the kink center where we showed that the undirectional motion depends on the locations of the inhomogeneities. An interesting result derived from the previous rectification dynamics were the discrete values obtained for the absolute value of the mean velocity, whose values can be computed by the expression $|\langle dX/dt\rangle| \equiv |\langle V\rangle| = \frac{L\omega}{2\pi}\frac{m}{n}$ where the indexes m, $n \in \mathbb{N}$ quantize the motion. Particularly, for small frequencies close to the adiabatic limit, the dynamics showed shapiro-like steps, contrary to the much higher frequencies situation where windows of motion separated by gaps were obtained. These previous features, characteristics of a rocking ratchet for single particles allowed us to infer that the ratchet dynamics observed here for spatially extended systems corresponds to the analogous of a rocking ratchet for point particles. The study was focused on the sG and ϕ^4 models. Also a comparative analysis between both systems was realized.

Later, in order to support this study, we implemented different collective coordinate approaches, taking as a benchmark the sG model. With a first approach that regards the center mass as the only degree of freedom we were able to account for the physical reasons for the occurrence of ratchet motion. The main success of this approach resided in the fact that it allowed us to connect the behavior of our rocking ratchet with the basic rocking ratchet dynamics for single particles, thus confirming our previous inference. Consequently, we were able to predict the direction of the motion, as well as to estimate the regime of the force amplitude for which the kink motion reaches the highest efficiency. Nevertheless, a quantitative agreement was not found. The explanation for such a discrepancy we found in the deformation of the kink solution, which changes its shape during its motion along the inhomogeneities. Later, we implemented a second approach which included the oscillation of the kink width and the motion of the kink center mass. With such formulation we achieved to describe most of the features of the dynamics.

We also extended the analysis to the case when the motion is affected by the thermal fluctuations. As a consequence of the noise a reduction of the mean velocity was observed and the sharp boundaries for the windows of motion obtained for the noiseless case became smooth. Also for this situation new windows of motion arose from the thermal fluctuations. This process of activation of motion became enhanced for an optimal value of the noise intensity, for which a maximum value for the mean velocity modulus was found. The location of the new windows as well as the maximum value obtained for the absolute value of the mean velocity turned out to be dependent on the

frequency.

A similar study as in the noiseless case was carried out, using the two previous CC approaches in presence of a Gaussian white noise. In both cases we got smooth curves for dependence of the mean velocity on the amplitude of the force. Also in both cases the CC equations predicted the appearance of new windows of motion. Furthermore, the theory showed the same behavior for the dependence of mean velocity on the noise intensity. An excellent prediction for the location of the new window of motion was obtained in the CC framework which regards the kink width as second degree of freedom.

We also extended the functioning of our ratchet system to other damping regimes. An important result obtained from this study was the significant increment of the mean velocity for small damping.

Subsequently, we pointed out the possibility of implementation of different ratchet mechanisms in our framework. Specifically, we showed the use of our framework for describing the dynamics of the kink motion as a diffusive ratchet.

Finally, at the end of the chapter 4, forthcoming investigations were outlined.

Appendix A

Collective coordinates: Generalized traveling wave ansatz

In this appendix we present a detailed explanation of how to obtain the collective coordinate equations. In order to do so, we appeal to the use of a well known projection technique called *Generalized Traveling Wave Ansatz*. It has been used in a wide context of solitons bearing systems. A first proposal, in order to explain the motion of magnetic vortices, was introduced by Mertens *et al.* [85]. Later, it was extended to unidimensional systems for the study of solitons motion in nonlinear Klein-Gordon (NKG) systems. Essentially such a technique rest on variational principles. A recent work, using a Lagrangian formulation, has shown the equivalence with this technique [86].

A.1 Collective coordinates, first approach

In order to show the projection technique we take for the analysis, the Eq.(4.1) in addition of Gaussian white noise. This represent a general model that regards all the perturbations contained in the thesis. By proceeding as in [85] we rewrite the full system as

$$\dot{\phi} = \frac{\delta H}{\delta \psi}, \tag{A.1}$$

$$\dot{\psi} = -\frac{\delta H}{\delta \phi} - \beta\dot{\phi} - \frac{\partial \widetilde{U}}{\partial \phi}V(x) + f(t) + \eta(x,t) \tag{A.2}$$

with

$$\begin{aligned} \langle \eta(x,t) \rangle &= 0, \\ \langle \eta(x,t)\eta(x',t') \rangle &= D\delta(x-x')\delta(t-t'), \end{aligned} \tag{A.3}$$

where $\psi = \dot{\phi}$, $f(t) \equiv A\sin(\omega t + \delta_0)$, $D = 2\beta k_B T$ and H is the Hamiltonian corresponding to the unperturbed form of Eq. (4.1) given by

$$H = \int_{-\infty}^{+\infty} dx \Big\{ \frac{1}{2}\psi^2 + \frac{1}{2}\phi_x^2 + U(\phi) \Big\}. \tag{A.4}$$

As starting point we assume that the solution has the form

$$\phi(x,t) = \phi_K[x - X(t), \dot{X}], \tag{A.5}$$

and therefore by definition of ψ we have that

$$\psi(x,t) = \psi_K[x - X(t), \dot{X}, \ddot{X}]. \tag{A.6}$$

The index K refers to the kink shape, but in the following we will omit it for simplicity.

Following the procedure in [85], inserting $\dot{\phi}$, $\dot{\psi}$ into Eqs. (A.1)-(A.2) we get the expressions

$$\frac{\partial\phi}{\partial X}\dot{X} + \frac{\partial\phi}{\partial\dot{X}}\ddot{X} = \frac{\delta H}{\delta\psi}, \tag{A.7}$$

$$\begin{aligned}\frac{\partial\psi}{\partial X}\dot{X} + \frac{\partial\psi}{\partial\dot{X}}\ddot{X} + \frac{\partial\psi}{\partial\ddot{X}}\dddot{X} = &-\frac{\delta H}{\delta\phi} - \beta\left(\frac{\partial\phi}{\partial X}\dot{X} + \frac{\partial\phi}{\partial\dot{X}}\ddot{X}\right) \\ &-\frac{\partial\widetilde{U}}{\partial\phi}V(x) + f(t) + \eta(x,t).\end{aligned} \tag{A.8}$$

Multiplying Eq. (A.7) by $\frac{\partial\psi}{\partial X}$ and Eq. (A.8) by $\frac{\partial\phi}{\partial X}$, and then subtracting both expressions and integrating we arrive at the following equation

$$N\dddot{X} + M\ddot{X} = -\beta C_1\dot{X} - \beta C_2\ddot{X} + F^{ac} + F^{stat} + F^{inh} + F^{st}, \tag{A.9}$$

whose values for the coefficients and forces are given by

$$\begin{aligned}
N &= \int_{-\infty}^{\infty} dx \frac{\partial\phi}{\partial X}\frac{\partial\psi}{\partial\ddot{X}}, \qquad F^{ac} = \int_{-\infty}^{\infty} dx\ \ f(t)\frac{\partial\phi}{\partial X}, \\
C_1 &= \int_{-\infty}^{\infty} dx \left(\frac{\partial\phi}{\partial X}\right)^2, \quad F^{inh} = -\int_{-\infty}^{\infty} dx \frac{\partial\widetilde{U}}{\partial\phi}V(x)\frac{\partial\phi}{\partial X}, \\
C_2 &= \int_{-\infty}^{\infty} dx \frac{\partial\phi}{\partial X}\frac{\partial\phi}{\partial\dot{X}}, \qquad F^{st} = \int_{-\infty}^{\infty} dx\ \ \eta(x,t)\frac{\partial\phi}{\partial X}, \\
M &= \int_{-\infty}^{\infty} dx \left(\frac{\partial\psi}{\partial\dot{X}}\frac{\partial\phi}{\partial X} - \frac{\partial\phi}{\partial\dot{X}}\frac{\partial\psi}{\partial X}\right), \\
F^{stat} &= -\int_{-\infty}^{+\infty} dx\ \ \left\{\frac{\delta H}{\delta\phi}\frac{\partial\phi}{\partial X} + \frac{\delta H}{\delta\psi}\frac{\partial\psi}{\partial X}\right\} \\
&= -\int_{-\infty}^{+\infty} dx\ \ \frac{\partial\mathcal{H}}{\partial X} = -\frac{\partial E}{\partial X},
\end{aligned}$$

where E represents the energy of the system, $\mathcal{H}$ is the Hamiltonian density of Eq. (A.4) and F^{stat} is the static force due to the external field, equal to zero for the above Hamiltonian.

Next we consider the sG potential for the system Eqs. (A.1)-(A.2) for which we assume as solution the ansatz

$$\phi(x,t) = \phi^{(0)}[\gamma(x - X(t))] = 4\arctan\left(\exp\left\{\gamma[x - X(t)]\right\}\right), \tag{A.10}$$

where $\phi^{(0)} = 4\arctan\left\{\exp\left[(x - X_0)/l_0\right]\right\}$ is the static kink solution of the sG system, centered in X_0 and of width l_0. Here $\gamma = 1/\sqrt{1 - \dot{X}^2}$ where we have put $l_0 = 1$ for the sG case.

Considering the previous statement for the static force and taking into account $V(x)$ from Eq. (4.2), we obtain

$$\begin{aligned} N &= 0, \qquad F^{ac} = -qf(t), \\ M &= \gamma^3 M_0, \qquad F^{stat} = 0, \\ C_1 &= \gamma M_0, \qquad F^{inh} = -\frac{\partial U}{\partial X}, \\ C_2 &= 0, \end{aligned}$$

where $M_0 = 8$ is the kink mass, $q = 2\pi$ is the topological charge and $U(X, \dot{X})$ given by

$$U(X,\dot{X}) = 2\epsilon \sum_n \sum_{i=1}^{3} \frac{1}{\cosh^2[\gamma(X - x_i - nL)]} \tag{A.11}$$

is the effective potential. In the non-relativistic limit $\dot{X}^2 \ll 1$, $U(X, \dot{X}) \simeq U(X)$.

A representation for the stochastic force F^{st} can be obtained from the calculation of the variance. In the case of additive noise it is allowed to make the following assumption

$$\left\langle \frac{\partial\phi^{(0)}(x,t)}{\partial X}\frac{\partial\phi^{(0)}(x',t')}{\partial X}\ \eta(x,t)\eta(x',t')\right\rangle$$
$$= \frac{\partial\phi^{(0)}(x,t)}{\partial X}\frac{\partial\phi^{(0)}(x',t')}{\partial X}\ \langle\eta(x,t)\eta(x',t')\rangle. \tag{A.12}$$

Hence the correlation function for F^{st} can be written as

$$\langle F^{st}(t)F^{st}(t')\rangle = \int_{-\infty}^{\infty}\int_{-\infty}^{\infty} dxdx' \frac{\partial\phi^{(0)}(x,t)}{\partial X}\frac{\partial\phi^{(0)}(x',t')}{\partial X}\langle\eta(x,t)\eta(x',t')\rangle, \tag{A.13}$$

for which, taking into account the expression (A.2), after some algebra we get

$$\langle F^{st}(t)F^{st}(t')\rangle = 2\beta k_B T\gamma M_0\delta(t-t'), \tag{A.14}$$

i.e., $F^{st}(t)$ is a white noise with kink diffusion constant

$$D_K = \gamma M_0 D.$$

As a consequence we obtain a non-additive noise term due to the factor $\gamma(\dot{X})$, i.e, we arrive at a problem with multiplicative noise.

Then the equation of motion (A.9) can be rewritten as

$$\gamma^3 M_0\ddot{X} + \beta\gamma M_0\dot{X} = -qf(t) - \frac{\partial U}{\partial X} + \sqrt{D_K}\ \xi(t) \tag{A.15}$$

with $\langle\xi(t)\rangle = 0$, $\langle\xi(t)\xi(t')\rangle = \delta(t-t')$. The Eq. (A.15) in absence of inhomogeneities and noise agrees with the results presented in [48]. The other

r.h.s. terms that appear in (A.15) are in correspondence with those already obtained in [53, 87] in the presence of impurities (non-relativistic approach) and Gaussian white noise, respectively. The procedure used here is equivalent to the so-called adiabatic approach by using modified conservation laws [56].

A.2 Collective coordinates, second approach

In order to get the CC equations we follow a similar procedure as in the previous section but this time we propose a solution with the form

$$\phi(x,t) = \phi[x - X(t), l(t)], \tag{A.16}$$

$$\psi(x,t) = \psi[x - X(t), l(t), \dot{X}, \dot{l}] \tag{A.17}$$

with $\psi = \dot{\phi}$, which considers the kink width as a new collective variable (see e.g. [47]).

Inserting Eqs. (A.16) and (A.17) in our system Eqs. (A.1)-(A.2) and then multiplying the first equation by $\frac{\partial \psi}{\partial X}$ and the second one by $\frac{\partial \phi}{\partial X}$; subtracting both expression and integrating we arrive at the following equation

$$\begin{aligned} &\int_{-\infty}^{+\infty} dx \frac{\partial \phi}{\partial X}\frac{\partial \psi}{\partial \dot{X}}\ddot{X} + \int_{-\infty}^{+\infty} dx[\phi,\psi]\dot{l} + \int_{-\infty}^{+\infty} dx \frac{\partial \phi}{\partial X}\frac{\partial \psi}{\partial \dot{l}}\ddot{l} \\ -F^{stat} &= \int_{-\infty}^{+\infty} dx \;\; F(x,t,\phi,\phi_t,...)\frac{\partial \phi}{\partial X} \end{aligned} \tag{A.18}$$

with $F(x,t,\phi,\phi_t,...) = -\beta\dot{\phi} - \frac{\partial \widetilde{U}}{\partial \phi}V(x) + f(t) + \eta(x,t)$, and

$$[\phi,\psi]=\frac{\partial\phi}{\partial X}\frac{\partial\psi}{\partial l}-\frac{\partial\phi}{\partial l}\frac{\partial\psi}{\partial X}, \tag{A.19}$$

$$\begin{aligned} F^{stat} &= -\int_{-\infty}^{+\infty}dx\ \left\{\frac{\delta H}{\delta\phi}\frac{\partial\phi}{\partial X}+\frac{\delta H}{\delta\psi}\frac{\partial\psi}{\partial X}\right\} \\ &= -\int_{-\infty}^{+\infty}dx\ \frac{\partial\mathcal{H}}{\partial X}, \end{aligned} \tag{A.20}$$

where $\mathcal{H}$ is the Hamiltonian density of Eq. (A.4) for which, as was seen before, a null value for F^{stat} is obtained.

Repeating the same procedure, but now with $\frac{\partial\psi}{\partial l}$ and $\frac{\partial\phi}{\partial l}$, we get the expression

$$\begin{aligned} &\int_{-\infty}^{+\infty}dx[\psi,\phi]\dot{X}+\int_{-\infty}^{+\infty}dx\frac{\partial\phi}{\partial l}\frac{\partial\psi}{\partial\dot{X}}\ddot{X}+\int_{-\infty}^{+\infty}dx\frac{\partial\phi}{\partial l}\frac{\partial\psi}{\partial\dot{l}}\ddot{l} \\ &-K^{int}=\int_{-\infty}^{+\infty}dx\ F(x,t,\phi,\phi_t,...)\frac{\partial\phi}{\partial l}. \end{aligned} \tag{A.21}$$

Following Rice [88] for the particular case of sG

$$\phi(x,t)=\phi^{(0)}[x-X(t),l(t)]=4\arctan\left(\exp\left[\frac{x-X(t)}{l(t)}\right]\right), \tag{A.22}$$

Eq. (A.18) becomes

$$M_0l_0\frac{\ddot{X}}{l}+\beta M_0l_0\frac{\dot{X}}{l}-M_0l_0\frac{\dot{X}\dot{l}}{l^2}=F^{ac}+F^{inh}+F^{st} \tag{A.23}$$

with

$$F^{ac} = \int_{-\infty}^{\infty} dx \;\; f(t)\frac{\partial \phi^{(0)}}{\partial X} = -2\pi f(t) = -qf(t), \tag{A.24}$$

$$F^{inh} = -\int_{-\infty}^{\infty} dx \;\; \sin(\phi^{(0)})V(x)\frac{\partial \phi^{(0)}}{\partial X} = -\frac{\partial U}{\partial X}, \tag{A.25}$$

$$F^{st} = \int_{-\infty}^{\infty} dx \;\; \eta(x,t)\frac{\partial \phi^{(0)}}{\partial X}, \tag{A.26}$$

and

$$U(X,l) = 2\epsilon \sum_{n}\sum_{i=1}^{3} \frac{1}{\cosh^2[(X - x_i - nL)/l]}. \tag{A.27}$$

On the other hand, Eq. (A.21) is transformed into

$$\alpha M_0 l_0 \frac{\ddot{l}}{l} + \beta\alpha M_0 l_0 \frac{\dot{l}}{l} + M_0 l_0 \frac{\dot{X}^2}{l^2} = K^{int}(l,\dot{l},\dot{X}) + K^{inh} + K^{st} \tag{A.28}$$

with

$$K^{inh} = -\int_{-\infty}^{\infty} dx \;\; \sin(\phi^{(0)})V(x)\frac{\partial \phi^{(0)}}{\partial l} = -\frac{\partial U}{\partial l}, \tag{A.29}$$

$$K^{st} = \int_{-\infty}^{\infty} dx \;\; \eta(x,t)\frac{\partial \phi^{(0)}}{\partial l}, \tag{A.30}$$

$$K^{int}(l,\dot{l},\dot{X}) = -\int_{-\infty}^{+\infty} dx \frac{\partial \mathcal{H}}{\partial l} = -\frac{\partial E}{\partial l}, \tag{A.31}$$

where $\alpha = \pi^2/12$, $M_0 = 8$, $l_0 = 1$ and

$$E = \frac{1}{2}\frac{l_0}{l} M_0 \dot{X}^2 + \frac{1}{2}\frac{l_0}{l}\alpha M_0 \dot{l}^2 + \frac{1}{2} M_0 \left(\frac{l_0}{l} + \frac{l}{l_0}\right). \tag{A.32}$$

As in the previous section we use the variances of the stochastic forces in order to obtain approximate expressions for them. Taking the assumption given by the expression (A.12) we find for (A.26) the correlation function

$$\begin{aligned}
&\langle F^{st}(t)F^{st}(t')\rangle \\
&= \int_{-\infty}^{\infty}\int_{-\infty}^{\infty} dxdx' \frac{\partial\phi^{(0)}(x,t)}{\partial X}\frac{\partial\phi^{(0)}(x',t')}{\partial X}\langle\eta(x,t)\eta(x',t')\rangle \\
&= D\delta(t-t')\int_{-\infty}^{\infty} dx \left(\frac{\partial\phi^{(0)}}{\partial X}\right)^2 = D\delta(t-t')\frac{l_0}{l}M_0. \qquad \text{(A.33)}
\end{aligned}$$

In what follows similar expressions to the Eq. (A.12) valid for additive noise are used in order to calculate other correlation functions like

$$\begin{aligned}
&\langle K^{st}(t)K^{st}(t')\rangle \\
&= \int_{-\infty}^{\infty}\int_{-\infty}^{\infty} dxdx' \frac{\partial\phi^{(0)}(x,t)}{\partial l}\frac{\partial\phi^{(0)}(x',t')}{\partial l}\langle\eta(x,t)\eta(x',t')\rangle \\
&= D\delta(t-t')\int_{-\infty}^{\infty} dx \left(\frac{\partial\phi^{(0)}}{\partial l}\right)^2 = D\delta(t-t')\frac{l_0}{l}\alpha M_0,
\end{aligned} \qquad \text{(A.34)}$$

and

$$\begin{aligned}
&\langle F^{st}(t)K^{st}(t')\rangle \\
&= \int_{-\infty}^{\infty}\int_{-\infty}^{\infty} dxdx' \frac{\partial\phi^{(0)}(x,t)}{\partial X}\frac{\partial\phi^{(0)}(x',t')}{\partial l}\langle\eta(x,t)\eta(x',t')\rangle \\
&= D\delta(t-t')\int_{-\infty}^{\infty} dx \ \frac{\partial\phi^{(0)}}{\partial X}\frac{\partial\phi^{(0)}}{\partial l} = 0. \qquad \text{(A.35)}
\end{aligned}$$

From the delta-function correlation for the stochastic forces the absence of cross-correlation is obvious.

Finally, collecting all the previous results we can rewrite Eqs. (A.23),

(A.28) as follows

$$M_0 l_0 \frac{\ddot{X}}{l} + \beta M_0 l_0 \frac{\dot{X}}{l} - M_0 l_0 \frac{\dot{X}\dot{l}}{l^2} = -\frac{\partial U}{\partial X} - q f(t) + \sqrt{\frac{D M_0 l_0}{l}}\ \xi_1(t), \tag{A.36}$$

$$\alpha M_0 l_0 \frac{\ddot{l}}{l} + \beta\alpha M_0 l_0 \frac{\dot{l}}{l} + M_0 l_0 \frac{\dot{X}^2}{l^2} = -\frac{\partial U}{\partial l} + K^{int}(l, \dot{l}, \dot{X}) + \sqrt{\frac{D\alpha M_0 l_0}{l}}\ \xi_2(t) \tag{A.37}$$

with $\langle \xi_i(t) \rangle = 0$, $\langle \xi_i(t)\xi_j(t') \rangle = \delta_{ij}\delta(t - t')$, for $i, j = 1, 2$.
A feature of particular interest in these new equations is the presence of stochastic forces which are of the multiplicative white noise type dependent on the kink width variable.

The method described here using the technique of projection is equivalent to the variational calculations of the momentum and the energy of the system for perturbed nonlinear Klein-Gordon systems of the form of Eqs. (A.1) and (A.2) and with a Hamiltonian of the form of Eq. (A.4) (see [47] for details). Another procedure and derivation has been recently presented in [86].

Now let us analyze the particular case when there are no stochastic forces present in the system. Following the same notation as in [47], and using definition $P(t) = M_0 l_0 \dot{X}/l(t)$ for the momentum, our equations transform into

$$\frac{dP}{dt} + \beta P = -\frac{\partial U}{\partial X} - q f(t), \tag{A.38}$$

$$\alpha[\dot{l}^2 - 2l\ddot{l} - 2\beta l\dot{l}] = \frac{l^2}{l_0^2}\left[1 + \frac{P^2}{M_0^2}\right] - 1 + \frac{2l^2}{M_0 l_0}\frac{\partial U}{\partial l}, \tag{A.39}$$

When the inhomogeneities are absent we get then

$$\frac{dP}{dt} = -\beta P - qf(t), \tag{A.40}$$

$$\alpha[\dot{l}^2 - 2l\ddot{l} - 2\beta l\dot{l}] = \frac{l^2}{l_0^2}\left[1 + \frac{P^2}{M_0^2}\right] - 1. \tag{A.41}$$

The coupling in this case between both equations is only through the expression for the momentum. The CC equations for the ϕ^4 model present the same form as those appearing above with the respective effective parameters of the ϕ^4 system [50].

Appendix B

Numerical schemes and integration procedures

There are different procedures and schemes of integration. The choice of the numerical procedure for the integration depends on the stability, convergence of the numerical method, type of the equation, integration time, among other factors. In case of partial differential equations the boundary conditions and also the length of the system become important. The methods used for solving these equations are of finite difference. Therefore the integration is determined by the mesh size and of the form of the scheme. The stability of the numerical method depends on the relation between the spatial and temporal steps for a specific scheme. Consequently, some schemes of integration are more robust than others under changes of the mesh size. The methods of integration for solving such schemes are classified in implicit and explicit ones. Usually, the implicit methods are more robust against instabilities for a wide range of the mesh size because of the scheme. Among the implicit

schemes, we highlight the Strauss-Vázquez scheme [89]. This is a well known scheme, generally used for problems which involve the integration of NKG systems.

B.1 Strauss-Vázquez scheme and some modifications

Next we consider the original Strauss-Vázquez integration scheme

$$\frac{\phi_l(t+\Delta t)-2\phi_l(t)+\phi_l(t-\Delta t)}{\Delta t^2}+\frac{\phi_{l+1}(t)-2\phi_l(t)+\phi_{l-1}(t)}{\Delta x^2}+ \\ +\frac{U[\phi_l(t+\Delta t)]-U[\phi_l(t-\Delta t)]}{\phi_l(t+\Delta t)-\phi_l(t-\Delta t)}=0. \quad \text{(B.1)}$$

This system have the advantage to conserve the energy. On the other hand, its stability and convergence have been proven [89].

Here l is the spatial grid index. U is the potential for the corresponding NKG system. From previous equation the values for $\phi_l(t)$ and $\phi_l(t-\Delta t)$ can be deduced from the initial conditions of the kink profile. Therefore the integration reduces to finding the values $\phi_l(t+\Delta t)$. In order to determine the values $\phi_l(t+\Delta t)$ one can use the Newton-Raphson, the secant method, or another method for finding roots [90].

However, the original Strauss-Vázquez scheme does not consider the presence of perturbations. Therefore for our purpose a more general formulation of the Strauss-Vázquez scheme is required.

We take for the integration of the Eq. (4.1), the simplest modified Strauss-Vázquez scheme

$$\frac{\phi_l(t+\Delta t)-2\phi_l(t)+\phi_l(t-\Delta t)}{\Delta t^2}+\frac{\phi_{l+1}(t)-2\phi_l(t)+\phi_{l-1}(t)}{\Delta x^2} + \frac{U[\phi_l(t+\Delta t)]-U[\phi_l(t-\Delta t)]}{\phi_l(t+\Delta t)-\phi_l(t-\Delta t)}+\beta\frac{\phi_l(t+\Delta t)-\phi_l(t-\Delta t)}{2\Delta t}+F(t)=0, \tag{B.2}$$

where β is the damping coefficient and $F(t)$ is equivalent to $-f(t)$ in our formulation. A more sophisticated scheme with a generalized expression for the external force $F(t)$ which include parametric and stochastic forces can be found in [91].

Concretely speaking, we use this implicit scheme since it is very robust against instabilities for different mesh sizes. However, explicit schemes are usually faster than the implicit ones and much of the time are used. In our case we have used a fourth-order Runge-Kutta method [90] in order to verify the numerical results obtained with the Strauss-Vázquez scheme.

B.2 Integration of nonlinear Klein-Gordon systems with delta functions as perturbations.

In this section we proceed to the calculus of the partial differential equation in presence of point-like inhomogeneities, which are in our formulation represented by delta functions.

We derive the form for the spatial part of the numerical scheme in presence of delta-like functions using the method of finite elements. We take as an example the sG model. Notwithstanding, it can be used as general procedure for other models.

In order to integrate the sG equation, perturbed by a delta function

$$\phi_{tt} = \phi_{xx} - \sin(\phi)[1 + Q\delta(x-a)], \tag{B.3}$$

it is necessary to split the interval of integration in two parts.
Namely, an interval which contains the point a and another without the point a where the delta function vanishes.
By convenience we integrate in a neighborhood of a, namely in the interval $(a-h, a+h)$ where h represents a small value

$$\int_{a-h}^{a+h} dx \;\; \phi_{tt} = \int_{a-h}^{a+h} dx \;\; \phi_{xx} - \int_{a-h}^{a+h} dx \;\; \sin(\phi)[1 + Q\delta(x-a)]. \tag{B.4}$$

Using the properties of the delta functions the previous equation then becomes

$$\int_{a-h}^{a+h} dx \;\; \phi_{tt} = \phi_x|_{a+h} - \phi_x|_{a-h} - \int_{a-h}^{a+h} dx \;\; \sin(\phi) - Q\sin[\phi(a,t)]. \tag{B.5}$$

Taking into account that h is assumed to be very small, the integrals of the latter expression are reduced to

$$\int_{a-h}^{a+h} dx \;\; \sin(\phi) \approx \sin[\phi(a,t)] \;\; 2h$$

and

$$\int_{a-h}^{a+h} dx \;\; \phi_{tt} \approx \phi_{tt}|_a \;\; 2h.$$

Accordingly the expression (B.4) can be rewritten as

$$\phi_{tt}|_a = \frac{\phi_x|_{a+h} - \phi_x|_{a-h}}{2h} - \sin[\phi(a,t)] - \frac{Q}{2h}\sin[\phi(a,t)], \tag{B.6}$$

where the first r.h.s term represent the second order spatial derivative.
According to this definition we express the first order derivative functions as

$$\phi_x|_{a+h} = \frac{\phi|_{a+2h} - \phi|_a}{2h},$$
$$\phi_x|_{a-h} = \frac{\phi|_a - \phi|_{a-2h}}{2h}.$$

Therefore the second order spatial derivative can be expressed as

$$\frac{\phi_x|_{a+h} - \phi_x|_{a-h}}{2h} = \frac{\phi|_{a+2h} - 2\phi|_a - \phi|_{a-2h}}{4h^2}. \tag{B.7}$$

Applying the transformation $2h \to \Delta x$ we rewrite Eq. (B.6) as

$$\phi_{tt}|_a = \frac{\phi|_{a+\Delta x} - 2\phi|_a + \phi|_{a-\Delta x}}{\Delta x^2} - \left(\sin[\phi(a,t)] + \frac{Q}{\Delta x}\sin[\phi(a,t)]\right). \tag{B.8}$$

For the interval $O = \{x \in (-\infty, h-a]; [h+a, \infty)\}$, where the delta function vanishes, the equation simply results in

$$\phi_{tt}|_x = \frac{\phi|_{x+\Delta x} - 2\phi|_x + \phi|_{x-\Delta x}}{\Delta x^2} - \sin[\phi(x,t)] \qquad \forall x \in O. \tag{B.9}$$

We can then rewrite Eq. (B.3) concisely as

$$\phi_{tt}|_x = \mathcal{L}\phi(x,t) - \sin[\phi(x,t)]\,[1 + Q\ \ \vartheta(x-a)]\,, \tag{B.10}$$

where $\mathcal{L}\phi(x,t) = \frac{\phi|_{x+\Delta x} - 2\phi|_x + \phi|_{x-\Delta x}}{\Delta x^2}$ is the discrete Laplacian and the function $\vartheta(x-a)$ is defined as

$$\vartheta(x-a) \equiv \begin{cases} 1/\Delta x, & |x-a| < \Delta x/2 \\ 0, & \text{otherwise,} \end{cases}$$

which corresponds to the discrete representation for the delta function [92, 93].

Different methods can be implemented for the integration of the latter equation. One can use implicit methods similar to in the previous section with the Strauss-Vázquez scheme. In this case taking into account the expression for the scheme (B.2) and considering in addition the presence of an array of inhomogeneties we obtain

$$\frac{\phi_l(t+\Delta t)-2\phi_l(t)+\phi_l(t-\Delta t)}{\Delta t^2}+\frac{\phi_{l+1}(t)-2\phi_l(t)+\phi_{l-1}(t)}{\Delta x^2}+ \\ +\frac{U[\phi_l(t+\Delta t)]-U[\phi_l(t-\Delta t)]}{\phi_l(t+\Delta t)-\phi_l(t-\Delta t)}\left[1+Q\sum_i \vartheta(l\Delta x-x_i)\right]+ \\ +\beta\frac{\phi_l(t+\Delta t)-\phi_l(t-\Delta t)}{2\Delta t}+F(t)=0, \tag{B.11}$$

where x_i corresponds to the points where the inhomogeneities are located and l denote the number of points in the grid for the spatial dimension as before. For this problem the four-order Runge-Kutta fails because of the presence of irregular functions like delta functions. As alternative one can use a modified Runge-Kutta integrator. We have used the Heun method (see next section) in order to verify our numerical results.

B.3 Numerical solution of stochastic differential equations

For our purpose we start with a set of coupled differential equations in the generalize Langevin form

$$\frac{dA_i}{dt}=q_i([A],t)+\sum_j g_{ij}([A],t)\xi_j(t), \tag{B.12}$$

where $[A] \equiv (A_1, \ldots, A_N)$ and g_{ij} denote the coefficients of the matrix

$$\mathbf{G} = \begin{pmatrix} g_{11} & g_{12} & \cdots \\ g_{21} & g_{22} & \cdots \\ \vdots & \vdots & \ddots \end{pmatrix}.$$

Let us consider a physical system with a set of independent stochastic white noise processes, i.e., certain functions $\xi_i(t)$ so that $\langle \xi_i(t) \rangle = 0$, $\langle \xi_i(t)\xi_j(t') \rangle = \delta_{ij}\delta(t-t')$, for $i, j = 1, ..N$.
We can solve the above stochastic differential equations by using the Heun method [70]. The main reason for the use of the Heun method is because we are dealing with highly irregular and therefore not differentiable functions. This is the case of the white-noise term where we have nothing but a series of delta functions spread over the full interval of integration.

Let us make the analysis of the system (B.12) for the simplest case, i.e., for one variable

$$\frac{dA}{dt} = q(t, A) + g(t, A)\xi(t). \tag{B.13}$$

After implementing the Heun algorithm for the previous equation we obtain the reformulation in finite differentials

$$\begin{aligned} \widetilde{A}(t + \Delta t) &= A(t) + \Delta t \;\; q(t, A(t)) + \Delta t^{1/2} \;\; u(t) g(t, A(t)) \qquad \text{(B.14)} \\ A(t + h) &= A(t) + \frac{\Delta t}{2} \left[q(t, A(t)) + q(t + \Delta t, \widetilde{A}(t + \Delta t)) \right] \\ &\quad + \frac{\Delta t^{1/2} u(t)}{2} \left[g(t, A(t)) + g(t + \Delta t, \widetilde{A}(t + \Delta t) \right], \end{aligned}$$

where $u(t)$ is a set of random numbers with a Gaussian distribution with mean zero and variance one. Following the previous procedure we rewrite

the equations (A.36)-(A.37) as

$$\frac{dA_1}{dt} = A_2 \tag{B.15}$$

$$\frac{dA_2}{dt} = -\beta A_2 + \frac{A_2 A_4}{A_3} + \frac{A_3}{M_0 l_0}\left[-\frac{\partial U}{\partial A_1} - qf(t)\right] + \sqrt{\frac{DA_3}{M_0 l_0}}\ \xi_1(t) \tag{B.16}$$

$$\frac{dA_3}{dt} = A_4 \tag{B.17}$$

$$\frac{dA_4}{dt} = -\beta A_4 - \frac{A_2^2}{\alpha A_3} - \frac{A_3}{\alpha M_0 l_0}\frac{\partial U}{\partial A_3} + \frac{A_3}{\alpha M_0 l_0}K^{int}(A_2, A_3, A_4) + \sqrt{\frac{DA_3}{\alpha M_0 l_0}}\ \xi_2(t). \tag{B.18}$$

This set of coupled differential equations take the form in the matrix notation

$$\frac{d\mathbf{A}}{dt} = \mathbf{q}(t,[A]) + \begin{pmatrix} 0 & 0 & 0 & 0 \\ 0 & \sqrt{D_1}\sqrt{A_3} & 0 & 0 \\ 0 & 0 & 0 & 0 \\ 0 & 0 & 0 & \sqrt{D_2}\sqrt{A_3} \end{pmatrix} \begin{pmatrix} \widetilde{\xi}_1 \\ \widetilde{\xi}_2 \\ \widetilde{\xi}_3 \\ \widetilde{\xi}_4 \end{pmatrix}, \tag{B.19}$$

where $\mathbf{A}^T = (A_1, A_2, A_3, A_4)$, $\mathbf{q}(t,[A])$ is the vector formed by the $q_i(t,[A])$ terms, corresponding to the noiseless part of the respective equations (B.15)-(B.18); $D_1 = \alpha D_2 = \frac{D}{M_0 l_0}$, and $\widetilde{\xi}_2 = \xi_1$, $\widetilde{\xi}_4 = \xi_2$. Notice in the previous Eq. (B.19) that only appear diagonal terms depending on the variable A_3. This results from the fact that no cross-correlation function was obtained from the collective variable equations. The details can be seen in the appendix A. Following the Heun method of one variable and taking into account that we have only diagonal terms, the system of equations (B.19) reduces to the

discrete numerical scheme

$$\begin{aligned}
\widetilde{A}_i(t+\Delta t) &= A_i(t) + \Delta t \;\; q_i(t,[A](t)) + \Delta t^{1/2} \;\; u_i(t) g_i(t, A_3(t)) \\
A_i(t+h) &= A_i(t) + \frac{\Delta t}{2}\left[q_i(t,[A](t)) + q_i(t+\Delta t, \widetilde{[A]}(t+\Delta t))\right] \\
&\quad + \frac{\Delta t^{1/2} u_i(t)}{2}\left[g_i(t, A_3(t)) + g_i(t+\Delta t, \widetilde{A}_3(t+\Delta t))\right]
\end{aligned}$$

where $\widetilde{[A]}(t+\Delta t) \equiv (\widetilde{A}_1(t+\Delta t), \widetilde{A}_2(t+\Delta t), \ldots)$ and $u_i(t)$ are a set of independent Gaussian random variables that satisfy the following relations

$$\begin{aligned}
\langle u_i(t) \rangle = 0, \qquad \langle u_i(t) u_j(t) \rangle = \delta_{ij} \\
\langle u_i(t) u_j(t') \rangle = 0, \qquad t \neq t'
\end{aligned}$$

which are generated by the Box-Müller-Wiegner algorithm.
For the integration of the partial differential equation similar equations can be deduced using the Heun method, like the following

$$\widetilde{\phi}_l(t+\Delta t) = \phi_l(t) + \Delta t \;\; \psi_l(t), \tag{B.20}$$

$$\begin{aligned}
\widetilde{\psi}_l(t+\Delta t) &= \psi_l(t) + \Delta t \left\{ \mathcal{L}\phi_l(t) - \sin[\phi_l(t)] \left[1 + Q \sum_i \vartheta(l\Delta x - x_i) \right] \right. \\
&\quad \left. - \beta \psi_l(t) + F(t) \right\} + \sqrt{D} \sqrt{\frac{\Delta t}{\Delta x}} \;\; u_l(t),
\end{aligned} \tag{B.21}$$

$$\phi_l(t+\Delta t) = \phi_l(t) + \frac{\Delta t}{2}\left[\psi_l(t) + \widetilde{\psi}_l(t+\Delta t)\right], \tag{B.22}$$

$$\begin{aligned}\psi_l(t+\Delta t) = \psi_l(t) + \frac{\Delta t}{2}\Bigg\{ & \mathcal{L}\phi_l(t) + \mathcal{L}\widetilde{\phi}_l(t+\Delta t) - \beta[\psi_l(t) + \widetilde{\psi}_l(t+\Delta t)] \\ & -(\sin[\phi_l(t)] + \sin[\widetilde{\phi}_l(t+\Delta t)])\left[1 + Q\sum_i \vartheta(l\Delta x - x_i)\right] + \\ & +F(t) + F(t+\Delta t)\Bigg\} + \sqrt{D}\sqrt{\frac{\Delta t}{\Delta x}}\ u_l(t),\end{aligned} \tag{B.23}$$

where l are the nodes of the grid for the spatial dimension. u_l are a set of independent Gaussian random numbers generated for each node of the grid in every step of time. These were generated using the Box-Müller-Wiegner algorithm.

Here as before the Heun method is suitable for the integration since for this system we have delta functions spread over the interval of the integration and also along the spatial coordinate. One can use an implicit method with the Strauss-Vázquez scheme but it has the disadvantage that it take great amount of time for the integration of stochastic partial differential equations. This is because the calculus is made on the average over many realizations.

Bibliography

[1] P. Hänggi, R. Bartussek: In *Nonlinear Physics of Complex Systems*, ed. by J. Parisi, S.C. Müller, W. Zimmermann Lecture notes in Physics Vol. 476 (Springer, Berlin, Heidelberg, New York 1996) pp. 294-308.

[2] P. Reimann, Phys. Rep. **361**, 57 (2002).

[3] B. Alberts, A. Johnson, J. Lewis, M. Raff, K. Roberts and P. Walker, *Molecular biology of the cell* (Garland, New York, 2002).

[4] J. Maddox, Nature, **365**, 203 (1993); **368**, 287 (1994); F. Jülicher and J. Prost, Rev. Mod. Phys. **69**, 1269 (1997).

[5] R.K. Dodd, J.C. Eilbeck, J.D. Gibbon, and H.C. Morris, *Solitons and Nonlinear Waves* (Academic Press, London, 1982).

[6] A. Scott, *Nonlinear Science: Emergence & Dynamics of Coherent Structures* (Oxford, 1999).

[7] H. Linke, W. Sheng, A. Löfgren, H. Xu, P. Omling and P.E. Lindelof, Eurpphys. Lett. **43**, 341 (1998); H. Linke, T.E. Humphrey, A. Löfgren, A.O. Sushkov, R. Newbury, R.P. Taylor and P. Omling, Science **286**, 2314 (1999).

[8] J.B. Majer, J. Peguiron, M. Grifoni, M. Tusveld and J. E. Mooij, Phys. Rev. Lett. **90**, 056802 (2003).

[9] A. Sánchez and A.R. Bishop, SIAM Review **40**, 579 (1998).

[10] L. Morales-Molina, N.R. Quintero, F.G. Mertens and A. Sánchez, Phys. Rev. Lett. **91**, 234102 (2003).

[11] L. Morales-Molina, F.G. Mertens and A. Sánchez, Eur. Phys. J. B **37**, 79 (2004).

[12] R.P. Feynman, R.B. Leighton, and M. Sands, *The Feynman Lectures on Physics* (Addison Wesley, Reading, MA, 1996), Vol.1, chap. 46.

[13] J.M. Parrondo and P. Español, Am. J. Phys. **64**, 1125 (1996).

[14] O. Magnasco, Phys. Rev. Lett., **71**, 1477 (1993).

[15] R. Bartussek, P. Hänggi and J.G. Kissner, Europhys. Lett. **28**, 459 (1994).

[16] T.E. Dialynas, K. Lindenberg and G.P. Tsironis, Phys. Rev. E. **56**, 3976 (1997).

[17] P. Reimann and P. Hänggi, Appl. Physics A **75**, 169 (2002).

[18] P. Reimann, R. Bartussek, R. Haüsler, P. Hänggi, Phys. Lett. A **215**, 26 (1996).

[19] J.M.R. Parrondo, J.M. Blanco, F.J. Cao and R. Brito, Europhys. Lett. **43**, 248 (1998).

[20] R.D. Astumian and P. Hänggi, Physics Today **55** (11), 33 (2002).

[21] S. Leibler, Nature **370**, 412 (1994).

[22] T.A. Duke and R.H. Austin, Phys. Rev. Lett. **80** 1552 (1998).

[23] I. Derényi and R. D. Astumian, Phys. Rev. E **58**, 7781 (1998).

[24] F. Marchesoni, Phys. Rev. Lett. **77**, 2364 (1996).

[25] A.V. Savin, G.P. Tsironis and A.V. Zolotaryuk, Phys. Lett. A **229**, 279 (1997); Phys. Rev. E **56**, 2457 (1997).

[26] M. Salerno and N.R. Quintero, Phys. Rev. E. **65**, 025602, (2002); N.R. Quintero, B. Sánchez-Rey and M. Salerno, e-print 0405023.

[27] G. Carapella, Phys. Rev. B **63**, 054515 (2001); G. Carapella and G. Costabile, Phys. Rev. Lett. **87**, 077002 (2001).

[28] F. Falo, P.J. Martínez, J.J. Mazo and S. Cilla, Europhys. Lett. **45**, 700 (1999).

[29] F. Falo, P.J. Martínez, J.J. Mazo, T.P. Orlando and E. Trías, Appl. Phys. A **75**, 263 (2002).

[30] E. Trías, J.J. Mazo, F. Falo, T.P. Orlando, Phys. Rev. E **61**, 2257 (2000).

[31] S. Flach, Y. Zolotaryuk, A.E. Miroshnichenko and M.V. Fistul, Phys. Rev. Lett. **88**, 184101 (2002);

[32] M. Salerno and Y. Zolotaryuk, Phys. Rev. E **65**, 056603 (2002).

[33] A. Ustinov, C. Coqui, A. Kemp, Y. Zolotaryuk, and M. Salerno, Phys. Rev. Lett. **93** 087001 (2004).

[34] J. Rousselet, L. Salome, A. Ajdari and Jacques Prost, Nature **370**, 446 (1994).

[35] A.P. Davis, Nature **401**, 120 (1999).

[36] W.D. Volkmuth and R.H. Austin, Nature **358**, 600 (1992).

[37] I. Zapata, J. Luczka, F. Sols and P. Hänggi, Phys. Rev. Lett. **77**, 2292 (1996).

[38] A. Sterck, S. Weiss and D. Koelle, Appl. Phys. A **75**, 253 (2002).

[39] C.S. Lee, B. Jankó, I. Deremyi and A.-L. Barabasi, Nature **400**, 337 (1999).

[40] J.E. Villegas, S. Savel'ev, F. Nori, E.M. Gonzalez, J.V. Anguita, R. García, J.L. Vicent, Science **302**, 1188 (2003).

[41] B.Y. Zhu, L. Van Look, F. Marchesoni, V.V. Moshchalkov and F. Nori, Physica E **18**, 322 (2003); B.Y. Zhu , F. Marchesoni and F. Nori, *ibid.* **18**, 318 (2003).

[42] R.D. Astumian, Science **276**, 917 (1997).

[43] S. Flach, O. Yevtushenko and Y. Zolotaryuk, Phys. Rev. Lett. **84**, 2358 (2000).

[44] I. Goychuk and P. Hänggi, J. Phys. Chem. B **105**, 6642 (2001).

[45] N.R. Quintero, A. Sánchez, Phys. Lett. A **247**, 161 (1998).

[46] N.R. Quintero, A. Sánchez, Eur. Phys. J. B **6**, 133 (1998).

[47] N.R. Quintero, A. Sánchez and F.G. Mertens, Phys. Rev. E **62**, 5695 (2000).

[48] N.R. Quintero, A. Sánchez and F.G. Mertens, Phys. Rev. Lett. **84**, 871 (2000).

[49] A. Sánchez, A.R. Bishop and F. Domínguez-Adame, Phys. Rev. E **49**, 4603 (1994).

[50] N.R. Quintero, Ph.D thesis, Universidad Carlos III de Madrid (In spanish) (2000).

[51] M.V. Satarić, J.A. Tuszyński and R.B Żakula, Phys. Rev. E **48**, 589 (1993); M.V. Satarić and J.A. Tuszyński, *ibid.* **67**, 011901 (2003).

[52] Yu.S. Kivshar Z. Fei and L. Vázquez, Phys. Rev. Lett. **67**, 1177 (1991); Z. Fei, Yu.S. Kivshar and L. Vázquez Phys. Rev. A **46**, 5214 (1992).

[53] S. Gredeskul, Yu.S. Kivshar, L.K. Maslov, A. Sánchez and L.Vázquez, Phys. Rev. A. **45**, 8867 (1992).

[54] Yu.S. Kivshar, A. Sánchez, O. Chubykalo, A.M. Kosevich and L.Vázquez, J. Phys. A: Math. Gen. **25**, 5711 (1992).

[55] D.W. McLaughlin and A.C. Scott, Phys. Rev. A. **18**, 1652 (1978).

[56] Yu.S. Kivshar and B. Malomed, Rev. Mod. Phys. **61**, 763, (1989).

[57] A.A. Golubov, A.V. Ustinov and I.L. Serpuchenko, Phys. Lett. A **130**, 107 (1988); A.A. Golubov, I.L. Serpuchenko, and A.V. Ustinov, Sov. Phys. JETP **67**, 1256 (1988).

[58] M. Aldana-González, G. Cocho, H. Larrade, G. Martinez-Mekler, J. Theor. Biol. **220**, 27 (2003).

[59] P. Jung, J.G. Kissner and P. Hänggi, Phys. Rev. Lett. **76**, 3436 (1996); J.L. Mateos, *ibid.* **84**, 258 (2000).

[60] R. D. Vale and R. A. Milligan, Science **288**, 88 (2000).

[61] S. Cilla and L.M. Floría, Physica D **113**, 157 (1998).

[62] D. Dan, A. M. Jayannavar and G. I. Menon, Physica A **318**, 40 (2003).

[63] H.Y. Wang and J.D. Bao, Physica A **337**, 13 (2004).

[64] F. Marchesoni , B.Y. Zhu and F. Nori, Physica A **325**, 78 (2003).

[65] M. Barbi, M. Salerno, Phys. Rev. E **62**, 1988 (2000); **63**, 066212 (2001).

[66] M.O. Magnasco, Phys. Rev. Lett. **71**, 1477 (1993)

[67] C.R. Doering, W. Horshtemke and J. Riordan, Phys. Rev. Lett.**72**, 2984 (1994).

[68] M.M. Millonas and M. I. Dykman, Phys. Lett. A **185**, 65 (1994).

[69] I. Derenyi and T. Vicsek, Phys. Rev. Lett. **75**, 374 (1995).

[70] Sotchastic effects in Physical Systems by M. San Miguel and R. Toral, *in Instabilities and Nonequilibrium Structures V*, ed. by E. Tirapegui and W. Zeller (Kluwer, Dordrecht, 1997).

[71] S. Cilla, Ph.D. thesis, Universidad de Zaragoza (In Spanish) (2000).

[72] D. Koelle, R. Kleiner, F. Ludwig, E. Dantsker, and J. Clarke, Rev. Mod. Phys. **71**, 631 (1999).

[73] P. Hänggi, P. Talkner and M. Borkovec, Rev. Mod. Phys. **62** 251 (1990).

[74] D. Dziarmaga and W. Zakrzewski, Phys. Lett. A **251**, 193 (1999).

[75] N.R. Quintero, A. Sánchez and F.G. Mertens, Phys. Rev. E **60**, 222 (1999); Eur. Phys. J. B **16**, 361 (2000).

[76] F. Marchesoni, Phys. Rev. E **56**, 2492 (1997).

[77] S. Savele'v, F. Marchesoni, P. Hänggi and F. Nori, Europhys. Lett. **67**, 179 (2004).

[78] O.M. Braun Yu.S. Kivshar and M. Kosevich, J. Phys. C **21**, 3881 (1988).

[79] Yu.S. Kivshar and B.A. Malomed, Phys. Rev. B **37**, 9325 (1988).

[80] F. Marchesoni, Phys. Lett. A **115**, 29 (1986).

[81] C. Marquet, A. Buguin, L. Talini, and P. Silberzan, Phys. Rev. Lett. **88**, 168301 (2002).

[82] D. van der Meer, P. Reimann, K. van der Weele, and D. Lohse, Phys. Rev. Lett. **92**, 184301 (2004).

[83] G. Tsiavaliaris, S. Fujita-Backer, and D. J. Manstein, Nature **427**, 558 (2004).

[84] O.M. Braun, Yu.S. Kivshar, Phys. Rep. **306**, 1 (1998).

[85] F. G. Mertens, H.-J. Schnitzer and A. R. Bishop, Phys. Rev. B **56**, 2510 (1997).

[86] N.R. Quintero and E. Zamora-Sillero, Physica D **197**, 63 (2004).

[87] E. Joergensen, V.P. Koshelets, R. Monaco, J. Mygind and M.R. Samuelsen, Phys. Rev. Lett. **49**, 1093 (1982); D.J. Bergman, E. Ben-Jacob, Y. Imry and K. Maki, Phys. Rev. A **27**, 3345 (1983).

[88] M.J. Rice and E.J. Mele, Solid State Commun. **35**, 487 (1980); M. Salerno and A.C. Scott Phys. Rev. B **26**, 2474 (1982); M.J. Rice, *ibid.* **28**, 3587 (1983).

[89] W.A. Strauss and L. Vázquez, J. Comput. Phys. **28**, 271 (1978).

[90] W.H. Press, S.A. Teukolsky, W.T. Vetterling, B.P. Flannery, *Numerical Recipes in FORTRAN*, 2nd edn. (Cambridge University Press, Cambridge, 1992).

[91] P.J. Pascual and L. Vázquez, Phys. Rev. B **32** 8305 (1985).

[92] S. Gasiorowicz, *Quantum physics* (John Wiley & Sons, 1974).

[93] I.M. Gel'fand and G.E. Shilov, *Generalized Functions* (Academic Press, New York and London, 1964).

Ackwnoledgments

First, I would like to express my deep gratitude to my supervisor (doctor vater) Prof. Franz Mertens for giving to me this wonderful opportunity, for his total support and comprehension, for the fruitful and stimulating discussions about physics and for his patient way in correcting my English. I will be forever in debt to him. Vielen dank!.

A very special thanks to Angel Sanchez for his support and continuous encouragement. Without his help I would probably be lost. Muchísimas gracias.

I also wish to give special thanks to Niurka Quintero and Edward Arevalo. To Niurka I have to thank for her assistance from the very beginning until the last days. A great part of my work is a result of our fruitful collaboration. Also for everything that I could learn from her. For her friendship. Infinitas gracias.

To the second person for transmitting me part of his knowledge on Fortran and for having introduced me in the running of programs, for his continuous assistance in the beginning of this work and more importantly for his friendship.

I also wish to thank to my friends in Bayreuth, Christian Brunhuber and Kunle Adegoke for the correction of my thesis. To my friends Christian Schuster, Kunle Adegoke, Christian Brunhuber, Denis Sheka and Oscar for the good times that we spent together in Bayreuth. To my friends Jochen, Juan Pablo Zagorodny and Robert Kuhn for their assistances.

Thanks to our secretary, Sigrid Glass for making things to work out and at the same time the life more pleasant to us. Thanks for her kindness and comprehension. Vielen dank!.

Thanks to those persons non mentioned here, who somehow, maybe by coincidence, I had the opportunity to know and to share.

I will remember all these persons with affection and with the hope that we will meet again somewhere else in a near future.

This thesis is dedicated to my family in Cuba.